nagra

ARBEITSBERICHT NAB 24-24

Thermo-hydraulic Modelling of the Temperature Distribution in the Siting Regions JO, NL and ZNO

November 2024

Nagra | National Cooperative for the Disposal of Radioactive Waste
Hardstrasse 73 | 5430 Wettingen | Switzerland
+41 56 437 11 11 | info@nagra.ch | nagra.ch

nagra

ARBEITSBERICHT NAB 24-24

Thermo-hydraulic Modelling of the Temperature Distribution in the Siting Regions JO, NL and ZNO

November 2024

KEYWORDS
Repository-induced effects, temperature distribution, JO, NL, ZNO, storyboard, deep geological repository, L/ILW, HLW

Nagra | **National Cooperative for the Disposal of Radioactive Waste**
Hardstrasse 73 | 5430 Wettingen | Switzerland
+41 56 437 11 11 | info@nagra.ch | nagra.ch

Abstract

In Stage 3 of the Sectoral Plan for Deep Geological Repositories in Switzerland (SGT) (BFE 2008), the three candidate siting regions Jura Ost (JO), Nördlich Lägern (NL) and Zürich Nordost (ZNO) were examined in detail. The broadened site-specific database formed the basis to select the siting region NL for a repository for disposal of SF/HLW and L/ILW for which the general license application will be prepared (Nagra 2025b). The arguments for site selection were reported in Nagra (2025a), encompassing the results of the qualitative assessment of the 13 SGT criteria and quantitative assessment of the site specific repository projects (Nagra 2024h). The thermal and hydraulic conditions in the three siting regions formed an essential part of the geoscientific data base, which fed into the site selection process.

A traceable workflow was followed for the assessment of the thermal-hydraulic conditions in the candidate siting regions, comprising the compilation of available geothermal information at the regional scale, modelling of the thermo-hydraulic conditions at the repository sites and the derivation of the inputs required for the safety analyses. This report documents the pursued assessment workflow and provides:

- an overview of the existing geoscientific data base at regional and local scale (geological, hydrogeological and geothermal setting of the siting regions; data base of geothermal properties)
- a description of the model portfolio implemented for the thermo-hydraulic simulations
- an estimation of ambient host-rock temperatures under consideration of the site-specific combined hydrogeological and geothermal conditions
- an evaluation of heat flow associated with the repository structures and the relevant impact on hydraulic conditions and groundwater gradients

Table of Contents

List of Tables

List of Figures

List of Acronyms

AOI	Area of interest
BOZ1, BOZ2	Boreholes Bözberg 1 and 2 in the siting region JO drilled in the context of the TBO campaign
BUL1, BAC1, STA2, STA3	Boreholes Bülach 1, Bachs 1, Stadel-2and Stadel-3 in the siting region NL drilled in the context of the TBO campaign
ENSI	Swiss Federal Nuclear Safety Inspectorate
HLW	High level waste
JO	Siting Region Jura Ost
L/ILW	Low- and intermediate-level waste
LokMOD	Geological layer models derived from seismic interpretations and documented in NAB 24-10
Mont Terri URL	Mont Terri Underground Rock Laboratory
NAB	Nagra Work Report
NL	Siting region Nördlich Lägern
PA	Performance Assessment
RBG	Rahmenbewilligungsgesuch (License Application)
RIN	Borehole Riniken, drilled in the context of the crystalline programme
SA	Safety Assessment
SGT	Sectoral Plan for Deep Geological Repositories
TBO	Tiefbohrprogramm (site investigation programme)
ZNO	Siting region Zürich Nordost

1 Introduction

1.1 Background

The procedure for selecting the sites for the deep geological repositories in Switzerland (BFE 2008) has been specified in the concept part of the Sectoral Plan for Deep Geological Repositories (SGT). The SGT concept foresees separate repositories for low- and intermediate-level waste (L/ILW) and for Spent Fuel (SF) and High-Level Waste (HLW)[1]. The site selection procedure has been realised in three stages. In the final Stage 3, the three candidate siting regions Jura Ost (JO), Nördlich Lägern (NL) and Zürich Nordost (ZNO) were examined in detail and, where necessary, supplementary geological investigations have been performed (see Nagra 2025a). With the completion of the sectoral plan process, Nagra will submit a general license application (Rahmenbewilligungsgesuch - RBG) at the end of 2024 to define the repository site, the repository type and the main features of the project.

Following the sectoral plan, Nagra announced in autumn 2022 a project for a deep geological repository in NL to be prepared for licence application. The arguments for site selection are reported in Nagra (2025a), encompassing the results of (i) the delineation of the favourable areas for the HLW- and L/ILW repository in the three siting regions (Nagra 2024a) and (ii) the qualitative assessment of the 13 SGT criteria and quantitative assessment of the site specific repository projects (Nagra 2024h). The safety case for a deep geological repository in NL is detailed in Nagra (2024f), based on model-supported performance assessment (Nagra 2024j) and numerical analyses of radionuclide transport in the repository near-field (Nagra 2024i). The thermal and hydraulic conditions in the three siting regions are forming an essential part of the scientific data base, which feeds into the site selection process and into the safety case. Previous modelling studies related to the thermo-hydraulic conditions in the three siting regions are reported in Papafotiou & Senger (2014), Papafotiou et al. (2014) and Senger & Papafotiou (2013).

1.2 Objectives

The assessment of the thermal-hydraulic conditions in the deep underground of the potential siting regions encompasses several steps ranging from the compilation of available geothermal information to model calibrations, comparisons between different model approaches and finally simulation of different scenarios that are required by the provisional safety analyses. The objectives of this report are the following:

- overview of the existing geoscientific data base at regional and local scale (geological, hydrogeological and geothermal setting of the siting regions; data base of geothermal properties)
- description of the model portfolio implemented for the thermo-hydraulic simulations
- estimation of ambient host-rock temperatures under consideration of the site-specific combined hydrogeological and geothermal conditions
- evaluation of the impact of hydraulic conditions and ambient groundwater gradients prevailing in the siting regions on heat flow

[1] The two repositories are to be implemented at different sites or at the same site (combined repository). Guidelines of the regulator for the realisation of a combined repository are given in ENSI (2018).

1.3 Report outline

The chapters of this report are structured as follows:

- Chapter 2 describes the geological, hydrogeological and geothermal setting of the three siting regions in a wider geological context, referring to the state of knowledge as reported in the geological synthesis (Nagra 2024c).
- Chapters 3 to 5 present the thermo-hydraulic conditions in the siting regions JO, NL and ZNO, derived from site scale modelling. The model portfolio is described and the calibration procedures for modelling the measured temperature profiles in the TBO boreholes are discussed in detail. For each siting region, vertical profiles of calculated temperature through the center of the HLW- and L/ILW-repository are provided.
- Finally, Chapter 6 summarises the modelling results.

2 Geological, hydrogeological and geothermal setting

The geological, hydrogeological and geothermal conditions in the 3 siting regions Jura Ost, Nördlich Lägern and Zürich Nordost have been investigated intensively during the last two decades. Recent extensions of the geoscientific data base at regional scale have been gained in the context of Nagra's site investigation programme with 3-D seismics in each of the 3 siting regions and a total of 9 deep investigation boreholes (Nagra 2024c – Chapter 3). This chapter summarises the geoscientific findings with focus on the geothermal setting in the siting regions.

The regional geological setting, including the tectonic conditions and the lithostratigraphic layer sequence is detailed in Section 2.1. Local scale hydrogeology with the major hydrogeological units is given in Section 2.2. The geothermal conditions at regional scale are presented in Section 2.3.

2.1 Geological background

Well-established geological knowledge complemented by dedicated site investigation programmes provide a sound basis for reconstructing the geological evolution of Northern Switzerland and adjacent areas (Nagra 2024c – Chapter 3). The area of interest encompasses central Northern Switzerland, delimited by the Black Forest Massif in the north, the Hegau – Bodensee Graben in the northeast, the Upper Rhine Graben in the west and the Jura Fold-and-Thrust Belt and the northern alpine Molasse basin in the south (Fig. 2-1, Fig. 2-2). An ENE-WSW-striking Permocarboniferous Graben crosses the whole study area, including the JO and NL siting regions. The trough is filled with coarse- to fine-grained siliciclastic, partly organic-rich sediments (coal). Sediments of Carboniferous to Permian age.

The lower Mesozoic units (Muschelkalk) overlying the crystalline basement and the fill of the Permocarbonifersous Graben are dominted by siliciclastic, evaporitic and calcareous sediments. These rocks are overlain by mostly argillaceous and calcareous sediments of Liassic and Early and Middle Jurassic age (Lias, Dogger). The overlying Late Jurassic sediments (Malm) are dominated by limestones and marls. The uppermost sediments of the Malm includes mostly filled karst features resulting from a long time of subaerial exposure. These units are directly overlain by medium to fine grained Paleogene and Neogene Molasse sediments. The top of the Molasse deposits represents another important unconformity, which is overlain by Quaternary sediments, including unconsolidated fluvial and glacial sediments including gravels, sands, tills and fine-grained lacustrine sediments.

The three siting regions Jura Ost (JO), Nördlich Lägern (NL) and Zürich Nordost (ZNO) are located within the northern Alpine foreland of central Northern Switzerland. The tectonic setting is of interest for hydrogeological simulations because faults that have developed during the different tectonic stages may change the regional and local hydrogeological setting, depending on their conductivity. In the following, the main fault systems of the different tectonic units (see Fig. 2-2) are shortly described.

The most important tectonic features include:

- The WSW-ENE-oriented faults related to the Permocarboniferous Trough, which were repeatedly reactivated.
- The Jura-Fold-and-Thrust belt, which decreases in shortening from west to east and thus had to largest influence on the JO site. During the Jura deformation the compressive deformation preferentially localised along existing fault zones including the faults related to the Konstanz-Frick Trough.

- The eastern part of the study area is influenced by the formation of the NW-SE-striking Hegau-Bodensee Graben.

The position of the siting regions relative to this element strongly influenced the fault pattern (Nagra 2024c).

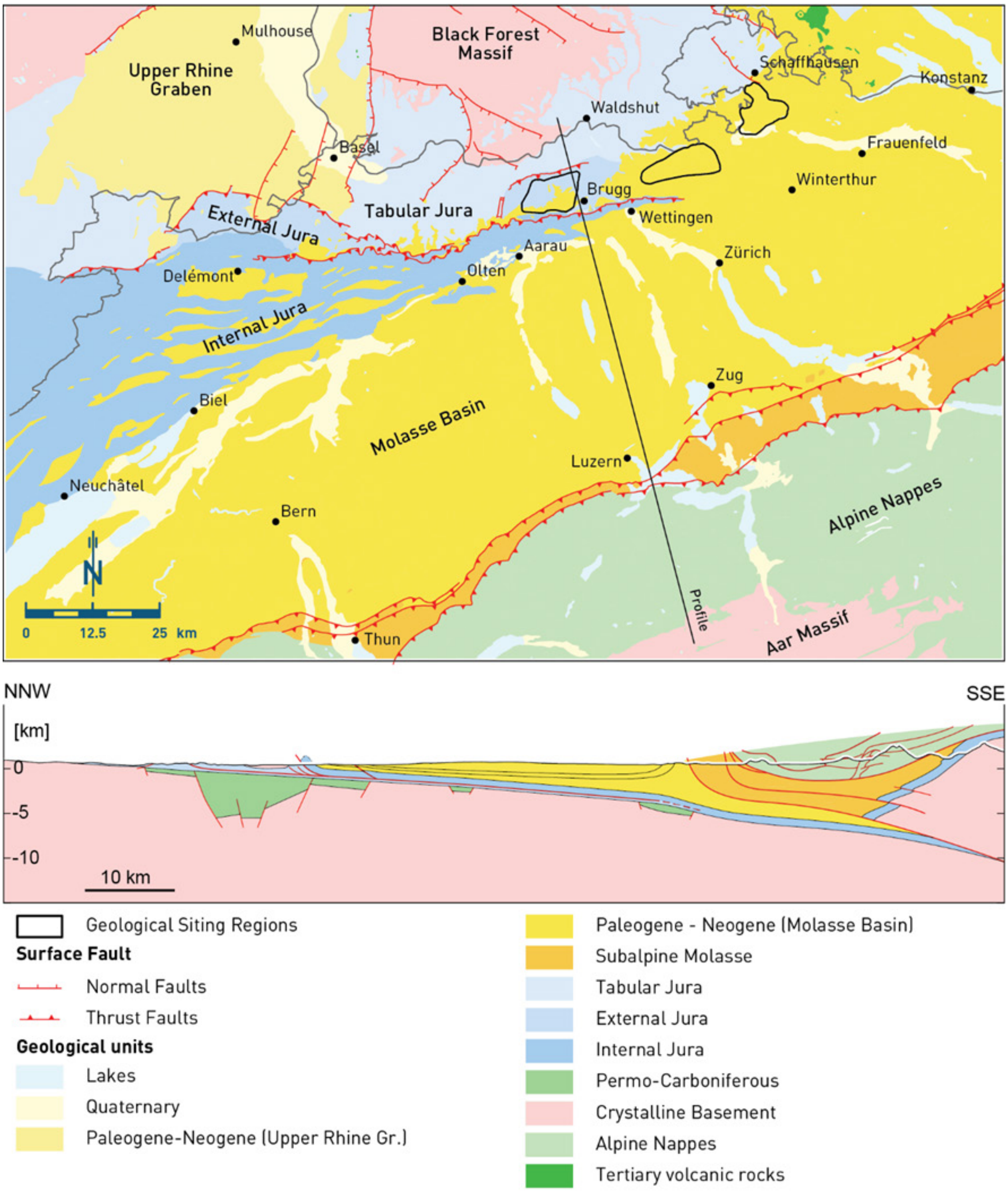

Fig. 2-1: Simplified tectono-geological map with a profile of Switzerland
From Nagra (2024c)

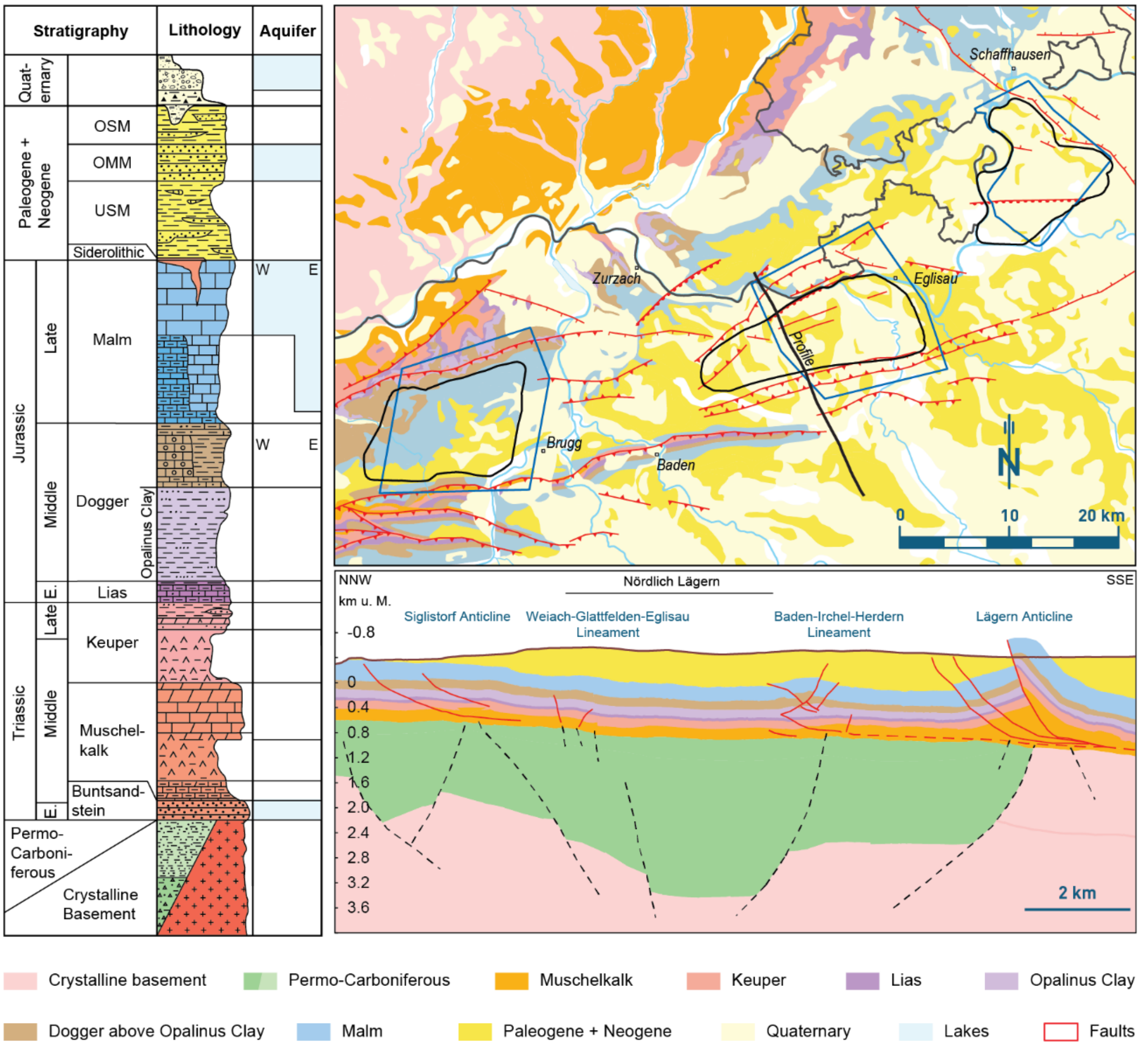

Fig. 2-2: Stratigraphic column, geological map and profile of Northern Switzerland

From Nagra (2024c)

2.2 Hydrogeological setting

The hydrological conditions at regional scale are controlled by the Lake Constance and the rivers Rhine, Aare, Reuss, Limmat, Thur, Töss and Wutach and their respective tributaries. These rivers and the lake constitute the main discharge systems for the aquifers in central Northern Switzerland. The area of interest includes parts of the Molasse basin and the most important discharge and recharge locations for the main regional aquifers.

Owing mainly to earlier investigation programmes of Nagra in Northern Switzerland, the regional hydrostratigraphy is well established and was updated with the new data (Fig. 2-3). The units are divided into regional and local aquifers separated by aquitards. The regional aquifers refer to the thick and brittle carbonate rocks, namely the Malm aquifer, Hauptrogenstein aquifer (JO and the area to the west) and Muschelkalk aquifer. These aquifers are termed regional because of their comparably uniform properties in Northern Switzerland. The units in between of these regional aquifers are mostly aquitards rich in clay minerals with the most obvious exception referring to the local Keuper aquifer which are discussed in more detail in Nagra (2024c) and in Nagra (2024b).

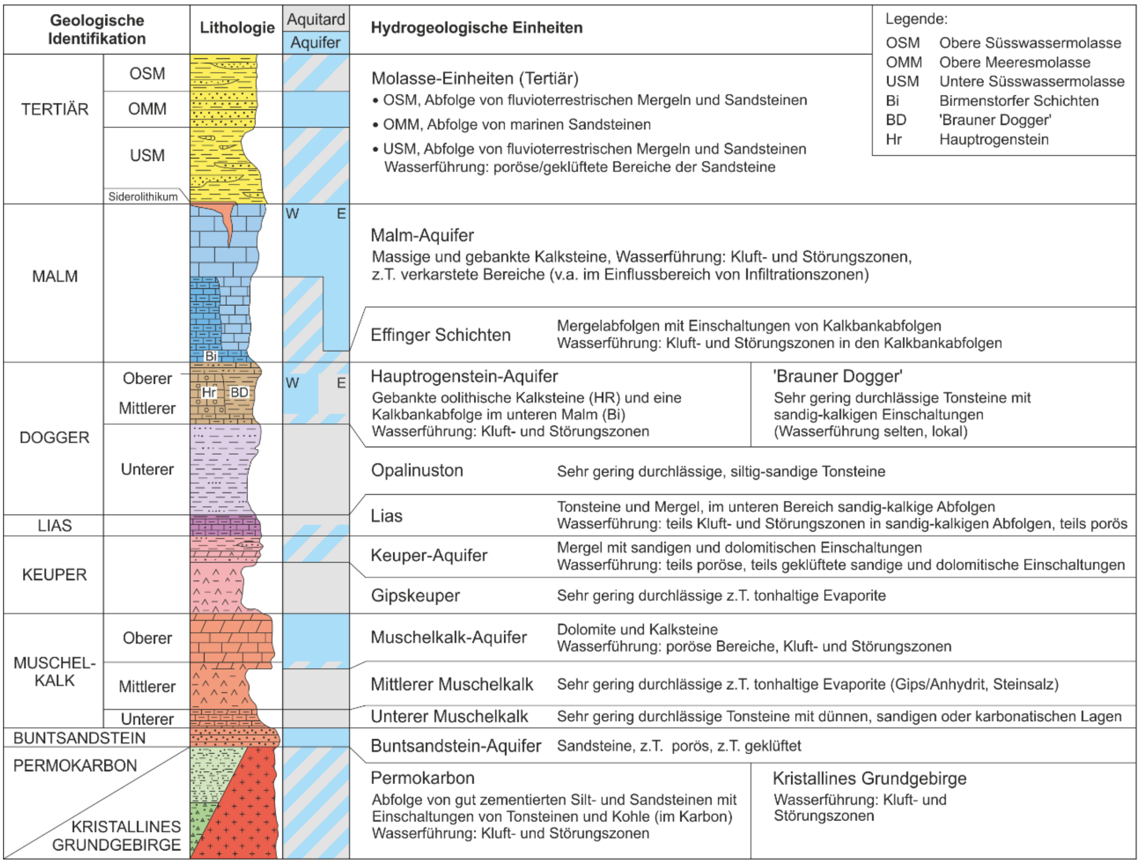

Fig. 2-3: Hydrostratigraphic profile representing the hydrogeological conditions in the 3 siting areas

Nagra (2024c)

2.3 Geothermal setting and thermal rock properties

Predictions of the thermo-hydraulic evolution in the three siting regions JO, NL and ZNO require knowledge of the current geothermal conditions at regional scale. These are determined by regional heat flow and the way heat is conducted and perturbed in the hydrogeological setting. Regional heat flow maps of the Swiss Molasse Basin date back to the late 1990s and have been updated in recent years as a contribution to Switzerland's desired energy transition (Fig. 2-4).

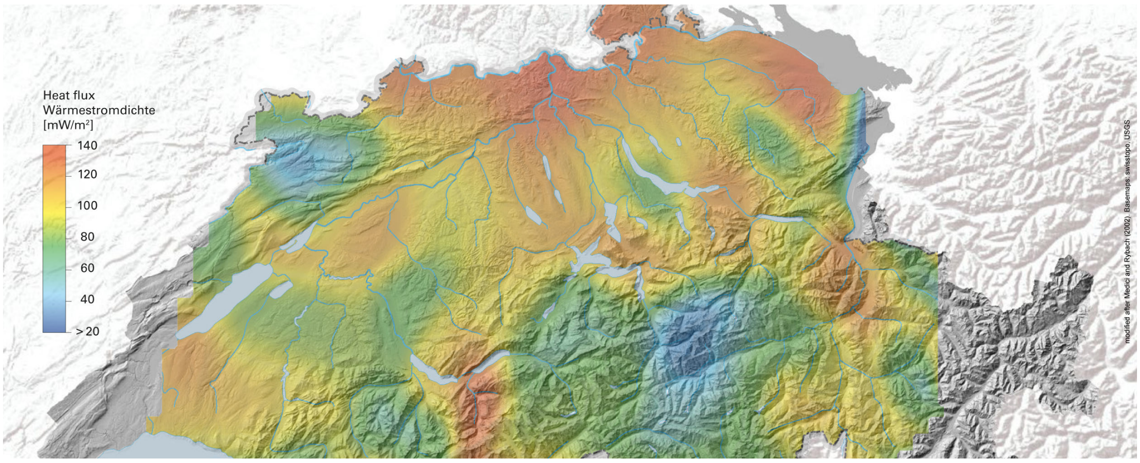

Fig. 2-4: Regional heat flow maps of the Swiss Molasse Basin

https://georessourcen.ethz.ch

Heat originates from basal heat flow through the base rock, as well as from emissions of radiogenic heat from the rocks themselves. Consequently, heat is transmitted by means of conduction and convection through the saturated geologic formations. The geothermal setting is thus determined on one hand by the ability of the saturated rocks to store and transfer thermal energy and on the other hand by hydraulic gradients associated with groundwater flow that may perturb heat flow patterns. The thermal properties used to describe transfer and storage of heat in rock formations are typically the rock heat conductivity and the specific heat capacity. In the context of modelling heat transport processes, the distribution of these factors determines temperature gradients and temperature-depth profiles in the subsurface that can be used to calibrate and verify numerical models.

2.3.1 Sources of heat

The main source of heat energy in the subsurface is basal heat flow that in general originates from the basement underlying the sedimentary rocks and is transported upward towards the land surface.

The magnitude of this heat flux is typically estimated by inverse modelling of heat transport calibrating to measurements of temperature and rock thermal properties obtained in deep boreholes. Such analyses have been carried out for some of Nagra's investigation boreholes (i.e., Weiach, see Nagra 1989). Kohl (2010) and Schill et al. (2011) provide maps of heat flow at the surface. Although some deviations may occur i.e., through heat flux perturbations due to groundwater flow or heterogeneities, it is assumed that subsurface heat flow measurements groundwater monitoring boreholes and shallow geothermal energy systems (up to 400 m bg) provide an estimate of the heat flow at the base of the Mesozoic sedimentary sequence. Additional considerations related to this uncertainty will be presented in the subsequent paragraphs.

In addition to the basal heat flow, natural radiogenic heat production contributes to the amount of heat stored and transferred in the rock formations. Schärli & Kohl (2002) estimated the amount of heat produced by the sedimentary formations and the crystalline basement based on Gamma-Spectrometer logs in the Weiach and Böttstein boreholes (Fig. 2-5). The average heat production rate for the sedimentary geological formations (Quaternary, Tertiary, Malm, Dogger, Lias, Keuper and Muschelkalk) was estimated to be 0.5 µW/m³. For the Permocarbon and the crystalline basement, the average heat production rate was 2.5 µW/m³.

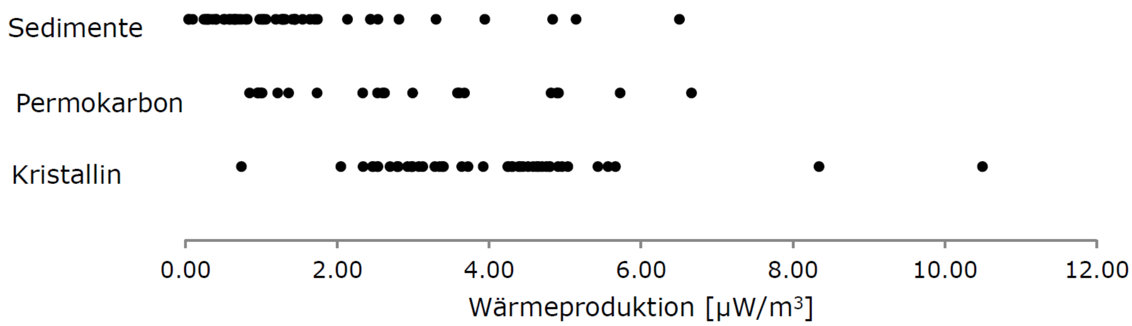

Fig. 2-5: Heat production rates measured in Weiach and Böttstein

See also Papafotiou et al. (2014)

2.3.2 Thermal properties – experimental database from core samples

Thermal conductivity and specific heat capacity are the key rock properties which control temperature distribution in the deep geological underground of the siting regions. The thermal rock properties can be measured in geotechnical laboratories with dedicated test programmes on core samples.

Measurements of thermal conductivity have been carried out in different lithologies from several deep boreholes in the context of Nagra's site investigation programme. Measurements of thermal conductivity for the boreholes Benken (Opalinus Clay only, Nagra 2001) and Weiach (the full Mesozoic sedimentary sequence, Nagra 1989) have been determined with the "divided bar" method (Gutzeit et al. 1982). In the recently drilled boreholes Stadel-3 (STA3), Trüllikon 1 (TRU1) and Bözberg 1 (BOZ1), thermal conductivity and heat capacity have been determined for different lithologies of the Mesozoic sequence using the transient cylindrical probe method (Schärli & Rybach 2001). Complementary measurements of thermal conductivity on Opalinus Clay samples from Mont Terri, Bülach BUL1-1 and Trüllikon TRU1-1 at ambient and elevated temperatures were carried out by Seiphoori (2022). The results confirm the expected dependency of thermal conductivity and heat capacity on lithology where marely lithologies have the lowest thermal conductivity which increases towards more calcitic, dolomitic and finally anhydritic rocks (see Fig. 2-6).

Clay-rich rocks, like the Opalinus Clay, show a sometimes pronounced anisotropy of thermal conductivity where thermal conductivity parallel to bedding is in the range of 2.5 W/(m·K) while normal to bedding it is in the range of 1 - 1.8 W/(m·K), resulting in an anisotropy factor of up to 2 (see Fig. 2-7).

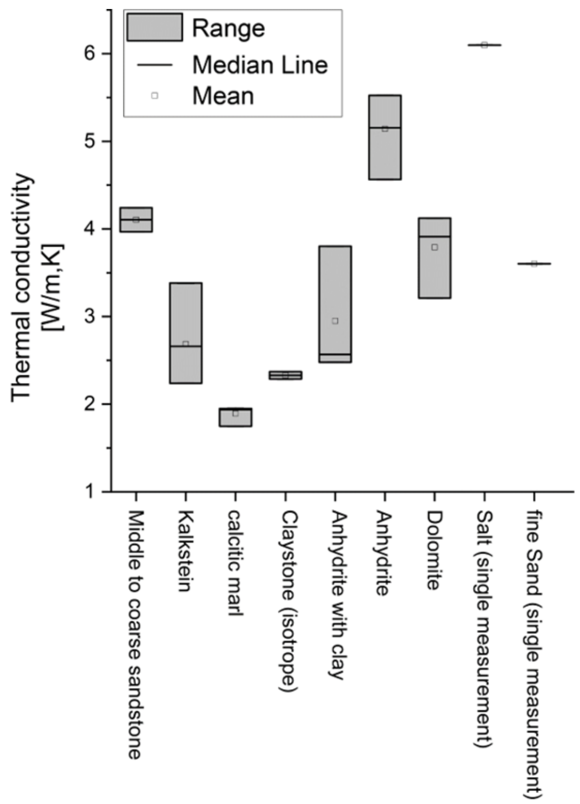

Fig. 2-6: Measured thermal conductivities of the boreholes Benken (BEN), Weiach (WEI), Trüllikon 1 (TRU1), Stadel-3 (STA3) and Bözberg (BOZ1)

Data provided in Appendix A in tabular form. Note that the anisotropic values measured in the Opalinus Clay are not included in the category Claystone.

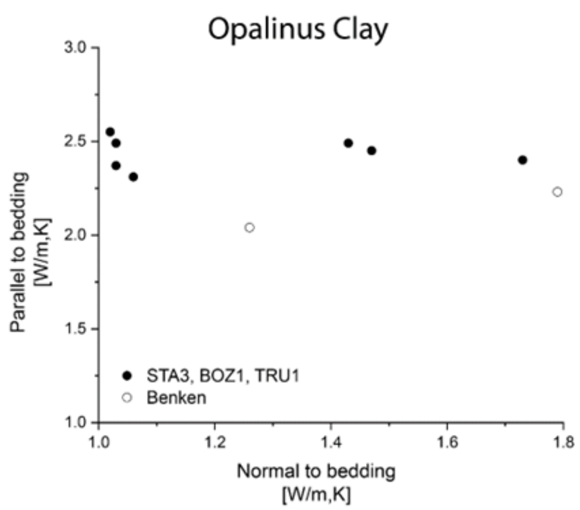

Fig. 2-7: Anisotropy of thermal conductivity in the Opalinus Clay sequence

Data provided in Appendix A in tabular form.

A plot of the thermal conductivities measured in the Mesozoic sequence is given in Fig. 2-8. While some lithostratigraphic units show a well-defined thermal conductivity (e.g. the Malm and Lias), other lithostratigraphic units show a large spread reflecting the heterogeneous lithologies of these units on a large scale.

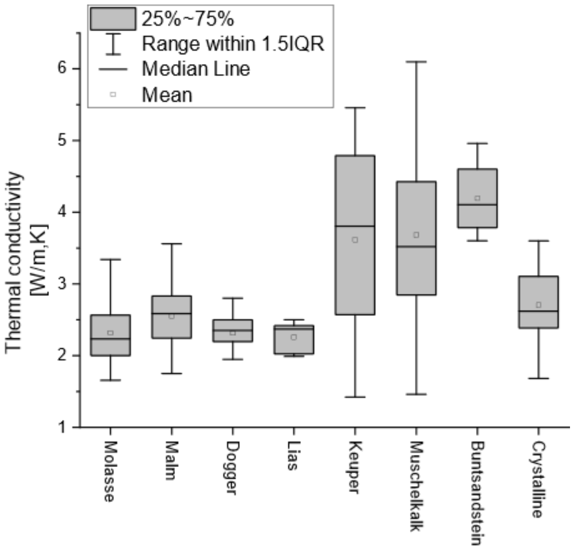

Fig. 2-8: Range of thermal conductivities of the Mesozoic sequence

Data provided in Appendix A in tabular form. Please note that the Dogger includes the host rocks of the Opalinus Clay which has not been included here because of the pronounced anisotropy.

The heterogeneous lithostratigraphic units show successions of sand-, carbonate- and clay-rich layers, sometimes including anhydritic layers or even salt. The measured thermal conductivities hence are a mix of the lithology-depend thermal conductivities.

Complementary measurements on Opalinus Clay samples at ambient and at elevated temperatures by Seiphoori (2022) were conducted with a TCi analyser (C – Therm Technologies, Canada) in combination with a cylindrical pressure cell, developed to ensure that the material remains under confined conditions during heating and measurements and also to minimise the evaporation at elevated temperatures (Fig. 2-9). The measurements indicate for a temperature range between 20 and 120 °C that thermal conductivity does not depend significantly on absolute temperature.

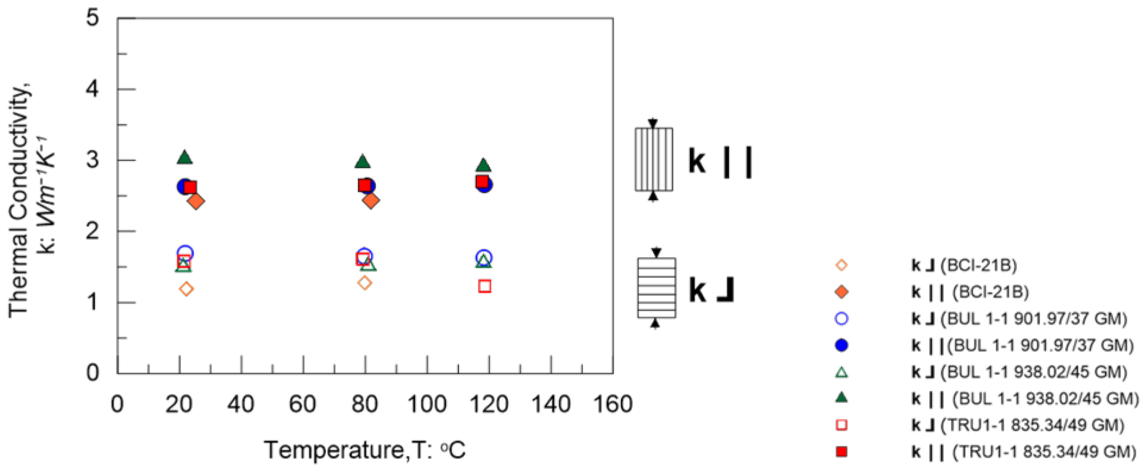

Fig. 2-9: Thermal conductivity Opalinus Clay samples from different depth versus temperature

The ratio of k|| to k˩ falls in the range of 1.55 – 2.19 W/(m·K), considering all tested materials (from Seiphoori 2022).

The specific heat capacity of the rocks ranges between 700 to 900 J/(kg·K). It is dependent on porosity, applied pressure and temperature and hence, in a geological context, is also depth dependent. However, the measurements performed here show no clear evidence of either so the depth/temperature/pressure range encountered in the boreholes only has a negligible effect. Also, no clear distinction of specific heat capacity with lithologies can be determined.

2.3.3 Temperature logs from TBO boreholes

The reliability of thermal conductivity measurements on core samples is often affected by artefacts associated with the recovery and preparation of the core samples.

Temperature profiles measured in the boreholes can be compared with heat transport models and used for calibrating uncertain parameters such as thermal rock properties and base rock heat flow. Such calibrations were performed for thermal conductivity of the hydrogeological units considered in the three siting regions JO, NL and ZNO.

For JO model, temperature logging data from two boreholes are used. They correspond to boreholes BOZ1 and BOZ2. These data are shown on Fig. 2-10. After completion of the drilling and testing campaign, borehole BOZ1 was equipped with a long-term monitoring system, which allows monitoring of long-term trends of temperature profiles (Nagra 2024c). Worth mentioning that the initial temperature profiles measured with the long-term monitoring system matched well with the logging data.

For NL model, three borehole temperature data are used that are data correspond to boreholes BUL1, STA2, and STA3. These data are depicted on Fig. 2-11 below. After completion of the drilling and testing campaign, borehole STA3 was equipped with a long-term monitoring system, which allows monitoring of long-term trends of temperature profiles (Nagra 2024c). The initial temperature profiles measured with the long-term monitoring system matched well with the logging data.

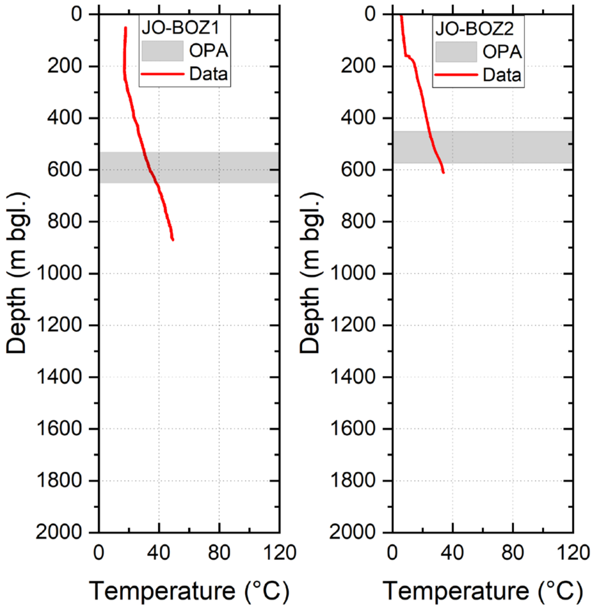

Fig. 2-10: Siting region JO: post completion temperature logs in boreholes BOZ1 and BOZ2

Opalinus Clay formation gray shaded.

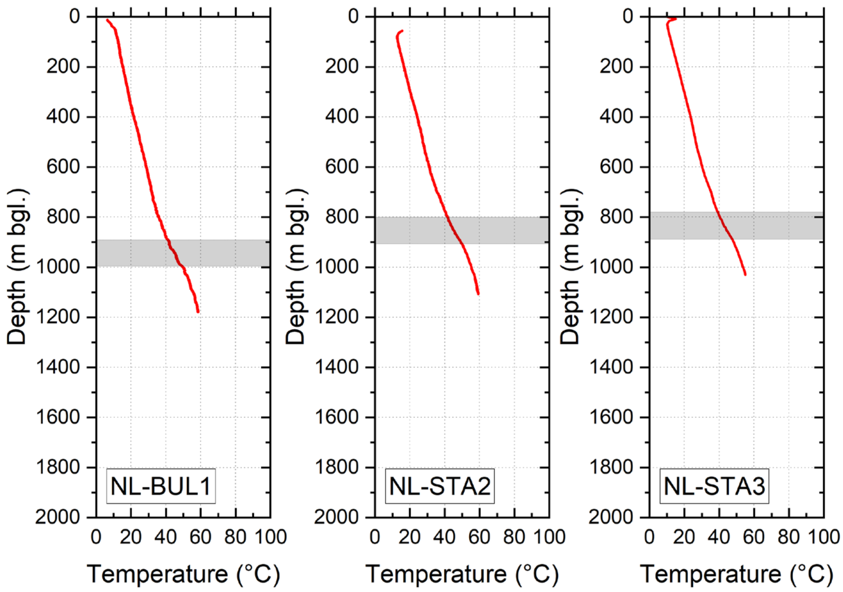

Fig. 2-11: Siting region NL: post completion temperature logs in boreholes BUL1, STA2 and STA3

Opalinus Clay formation gray shaded.

For ZNO model, borehole temperature data obtained from three boreholes are used that are BEN, MAR1 and TRU1. These data are shown on Fig. 2-12. After completion of the drilling and testing campaign, borehole MAR1 was equipped with a long-term monitoring system, which allows monitoring of long-term trends of temperature profiles (Nagra 2024c). The long-term monitoring system matched well with the logging data.

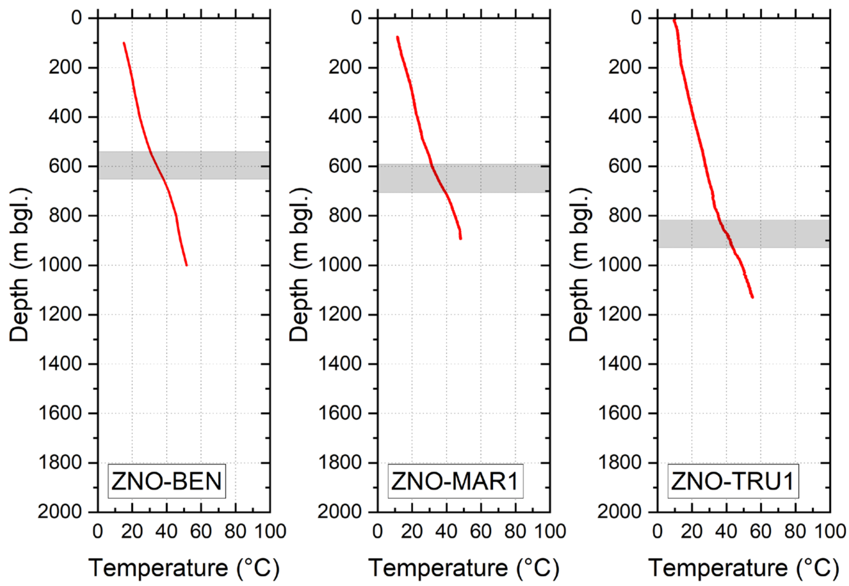

Fig. 2-12: Siting region ZNO: post completion temperature logs in boreholes BEN, MAR1 and MAR2

Opalinus Clay formation gray shaded.

The observed temperature data for each site shown above are used in the framework of an inverse modelling procedure to calibrate the heat conductivity value for each geological formation.

3 Thermo-hydraulic conditions in the siting region JO

The geological interpretations of 3-D seismics in the siting region JO are reported in Nagra (2024b), forming the basis for the geological layer model LocMOD-V1-JO. The decision has been taken to develop the site-specific repository projects JO-HLW and JO-L/ILW with reference to the geological layer stack, described in Nagra (2024b). Moreover, to ensure a consistent geometric representation of the site-specific repository projects in Performance Assessment (PA) and Safety Assessment (SA), all assessment models are referring to the same version of the geological layer model LocMOD-V1-JO.

A portfolio of numerical PA models was elaborated in the context of the site selection process for assessment of the proposed HLW and L/ILW repository configuration in the siting area JO comprising:

- a thermo-hydraulic 3-D model of the entire primary investigation perimeter on a footprint area of around 5 × 7 km^2
- 3-D repository nearfield models, containing the proposed HLW repository and the L/ILW repository on a footprint area of around 3 × 3 km^2
- several vertical cross sections through the disposal fields of repository projects for HLW and L/ILW in the siting region JO

This report addressed the temperature distribution in the Mesozoic layer stack at the scale of the primary investigation perimeter. Section 3.1 presents the model set-up, including model geometry, property assignment, initial conditions and boundary conditions. Model calibrations with the temperature profiles from the deep investigation boreholes BOZ1-1 and BOZ2-1 are described in Section 3.2. The results of the TH-calculations at site scale are discussed in Section 3.3, including an assessment of the impact of thermal history on the recent temperature distribution at site scale. Eventually, Section 3.4 gives a survey of the vertical temperature profiles at the center of the HLW and the L/ILW repository in the siting region JO.

3.1 3-D model of the siting region JO

3.1.1 Seismic surfaces

In total, 14 surfaces ("flying carpets") were used to set-up the portfolio of numerical PA models for Jura Ost (JO). Names and identifies of the surfaces are summarized in Tab. 3-1. The first set of surfaces provided (LocMod2023_V1_JO_pointset_data_50x50_2023.06.23_cam) covers the area of seismic interpretation. Compared to the proposed locations of the L/ILW and HLW repository for the siting region JO, these surfaces do not fully cover the L/ILW repository in the eastern model domain. In order to cover the entire area needed for the simulation of temperature distribution in the siting area, the surfaces had to be extended by approximately 500 m to the east (Fig. 3-1). Note, that the result outside the seismic interpreted horizons (blue polygon) has no seismic or geological "back-up interpretation". It is based only on the convergent algorithm that was used and therefore a simple mathematical abstraction, but it should follow the best trend possible of the original layer surface in the western vicinities.

Tab. 3-1: Seismic surfaces

(2023.07.12 LocMod2023_V1 JO Extended Surfaces, point-set data 50x50) provided by Nagra for JO

Description	**Filename**	**First row X**[1]	**First row Y**[1]	**First row Z**[1]
Top Hauptrogenstein	LocMod2023_v1_50x50_JO_159.8_Oxf_300_extended_eroded_rebuilt_2023_07_11_cam	649881.56	257978.93	392.54
Near Top Gerstenhübel Bd.	LocMod2023_v1_50x50_JO_159.8_Oxf_700_2023_07_11_cam_Extrapolate within boundary_extended_more			296.64
Top Wutach Fm.	LocMod2023_v1_50x50_JO_159.8_Oxf_975_2023_07_11_cam_Extrapolate within boundary_extended_more			199.70
Top Passwang Fm.	LocMod2023_v1_50x50_JO_168.2_Baj_100_2023_07_11_cam_Extrapolate within boundary_extended_more			130.09
Intra Passwang Fm.	LocMod2023_v1_50x50_JO_168.2_Baj_200_2023_07_11_cam_Extrapolate within boundary_extended_more			102.18
Top OPA	LocMod2023_v1_50x50_JO_170.9_Aal_300_2023_07_11_cam_Extrapolate within boundary_extended_more			69.58
Top Lias	LocMod2023_v1_50x50_JO_174.7_Toa_100_2023_07_11_cam_Extrapolate within boundary_extended_more			-61.64
Top Frick Mb.	LocMod2023_v1_50x50_JO_192.9_Sin_100_2023_07_11_cam_Extrapolate within boundary_extended_more			-79.73
Top Beggingen Mb.	LocMod2023_v1_50x50_JO_192.9_Sin_200_2023_07_11_cam_Extrapolate within boundary_extended_more			-89.06
Top Gansingen Mb.	LocMod2023_v1_50x50_JO_227_Car_100_2023_07_11_cam_Extrapolate within boundary_extended_more			-113.91
Top Bänkerjoch Fm.	LocMod2023_v1_50x50_JO_227_Car_300_2023_07_11_cam_Extrapolate within boundary_extended_more			-133.65
Intra Bänkerjoch Fm.	LocMod2023_v1_50x50_JO_237_Lad_200_2023_07_11_cam_Extrapolate within boundary_extended_more			-220.29
Top Muschelkalk	LocMod2023_v1_50x50_JO_237_Lad_400_2023_07_11_cam_Extrapolate within boundary_extended_more			-231.67
Bottom Mesozoikum	LocMod2023_v1_50x50_JO_251.9_Per_100_2023_07_11_cam_Extrapolate within boundary_extended_more			-423.77
Ground Level[2]	dhm25_jo.xyz	641011.50	269986.50	590.5960

[1] Corresponds to the first line found in the ASCII file (may differ from the lowest X/Y/Z values).
[2] Surface file communicated separately to the 2023Mod package.

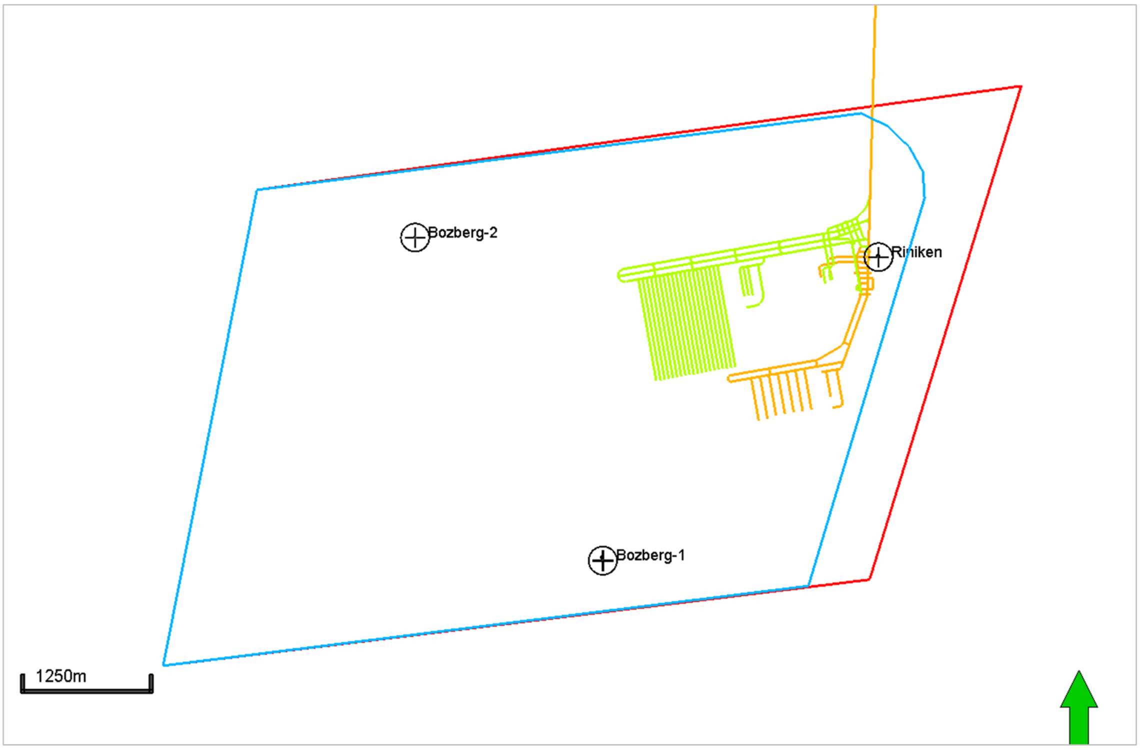

Fig. 3-1: Area of interest (AOI) for JO provided by Nagra

Blue polygon: area of seismic interpretation. Red polygon: extended surface area for TH-model

3.1.2 Geometric model set-up (base model)

The 3D base model area comprises the whole stratigraphic surfaces provided by Nagra (Nagra 2024b) with boreholes Riniken (RIN), Bözberg-1 (BOZ1), and Bözberg-2 (BOZ2) including the extension to the east. In the horizontal direction, the model is discretized by 100 ×100 m elements as shown in Fig. 3-2. The 2D base models for HLW and I/ILW are placed in the center of the repositories (Fig. 3-2). The cross-section has a length of 2 km in each case with a finer discretization along the slice. The center of each repository area is indicated in Fig. 3-2 (CHAA is the location of the center of HLW repository, and CSMA is the location of the center of L/ILW repository).

In the vertical direction, the surfaces from the seismic interpretation were implemented into a stack of geological formations/facies as illustrated in Fig. 3-3 and shown in Tab. 3-2. In addition to the LocMod2023 surfaces, further formation units are included to extend the model in the vertical direction to avoid any boundary effects on the thermal-hydraulic processes. Quaternary formation on top of Malm is added with a variable thickness which is defined by region between the two surfaces:

- "LocMod2023_v1_50x50_JO_159.8_Oxf_300_extended_eroded_rebuilt_2023_07_11_cam" and
- "dhm25_jo"

There are areas in the west where the dhm25_jo and the Oxf_300 surface coincides, i.e., there is no Quaternary present. The model is extended into the deep earth by another formation layer of 1,029 m thick Permocarbon basement.

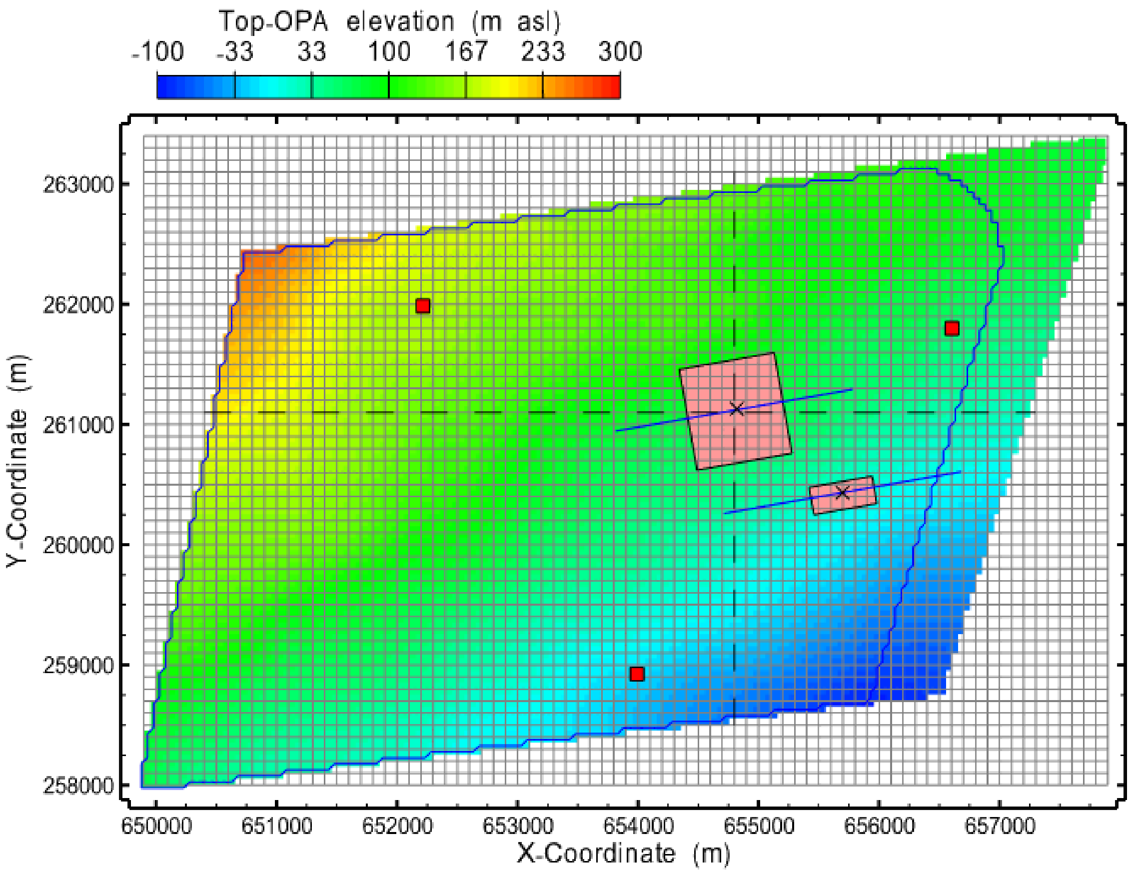

Fig. 3-2: Plan view of the 3D JO base model grid (regular 100 × 100 m grid)

With representation of the extended surface "LocMod2023_v1_50x50_JO_170.9_Aal_300[…]", the area of seismic interpretation (blue polygon), the proposed HLW (red) and L/ILW (magenta) repository, borehole locations Riniken RIN (656604, 261799, 385.07 m asl), Bözberg-1 BOZ1 (653992, 258925, 513 m asl), Bözberg-2 BOZ2 (652216, 261985, 624 m asl), and cross-sections of the 2D base models (HLW and L/ILW). CHLW (654820, 261130, 524 m asl) and CLILW (655698, 260432, 491 m asl) indicate the centers of HLW and L/ILW repository areas.

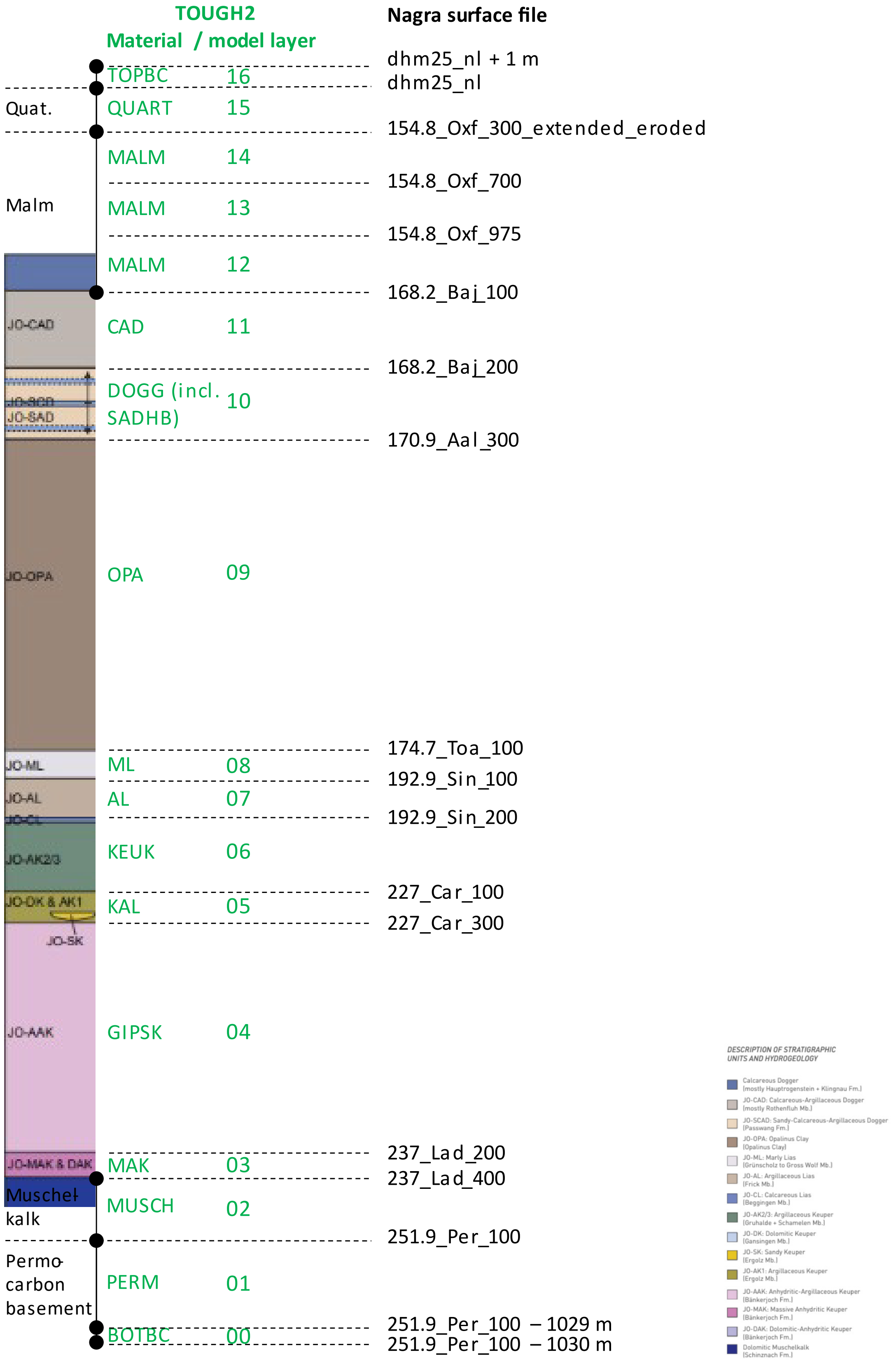

Fig. 3-3: Geological abstraction of stratigraphy for Jura Ost

Modified from Nagra (2024b) and layers implemented in the numerical model.

Tab. 3-2: Vertical discretization of the JO numerical base model

Layer	Stratigraphic units / formation	TOUGH2 Material name	Vertical discretization (layer)
00	Bottom Boundary	BOTBC	1
01	Permocarbon basement	PERM	1
02	Muschelkalk	MUSCH	1
03	Dolomitic-Anhydritic Keuper (DAK) & Massive Anhydritic Keuper (MAK) of Bänkerjoch Formation	MAK	1
04	Anhydritic-Argillaceous Keuper (AAK) of Bänkerjoch Formation	GIPSK	1
05	Argillaceous Keuper (AK1) & Sandy Keuper (SK) & Dolomitic Keuper (JO-DK) of Klettgau Formation	KAL	1
06	Argillaceous Keuper (JO-AK2/3 - of Klettgau and Staffelegg Formation) & Calcareous Lias (CL) of Staffegg Formation	KEUK	1
07	Argillaceous Lias (AL) of the Staffelegg Formation	AL	1
08	Marly Lias (ML) of Staffelegg Formation	ML	1
09a, b	Opalinus Clay (OPA)	OPA	5 (2 for upper and bottom OPA, three 1 m middle layers)
09c		OPAM	
09d, e		OPA	
10	Sandy-Argillaceous Dogger (SAD) & Sandy-Calcareous Dogger (SCD) of Passwang Formation	DOGG	1
11	Calcareous-Argillaceous Dogger (JO-CAD) of Passwang Formation	CAD	1
12	Hauptrogenstein	MALM	3 (4 where Quaternary is not present)
13			
14			
15	Quaternary (QUAT)	QUAT	1
16	Top Boundary (TOP-BC)	TOPBC	1

In the 3D base model, the Opalinus Clay was split into upper and lower OPA by generating a surface at the 50% of the Opalinus Clay thickness calculated as the difference between

- "LocMod2023_v1_50x50_JO_170.9_Aal_300[…]" and
- "LocMod2023_v1_50x50_JO_174.7_Toa_100[…]"

The surface in the middle of OPA is used to generate three additional layers in the middle of the Opalinus Clay. That is, the Opalinus Clay is divided into 5 sub-layers, with three layers of 1 m thickness implemented in the middle, with which the TH-values (i.e., the thermal conductivity) at repository horizon can be precisely obtained.

The Sandy-Argillaceous Dogger (SAD) and Sandy-Calcareous Dogger (SCD) of Passwang Formation above the Opalinus Clay are combined in only one layer. In contrast, three hard-bed layers (SADHB) with a thickness of 3 m each are modeled alternating with the Sandy-Argillaceous Dogger (DOGG) in the 2D base model, resulting in more sub-layers.

Fig. 3-4 shows a cross-section of the 3D JO base model through the proposed HLW repository. A 3D view of the entire model provides Fig. 3-5.

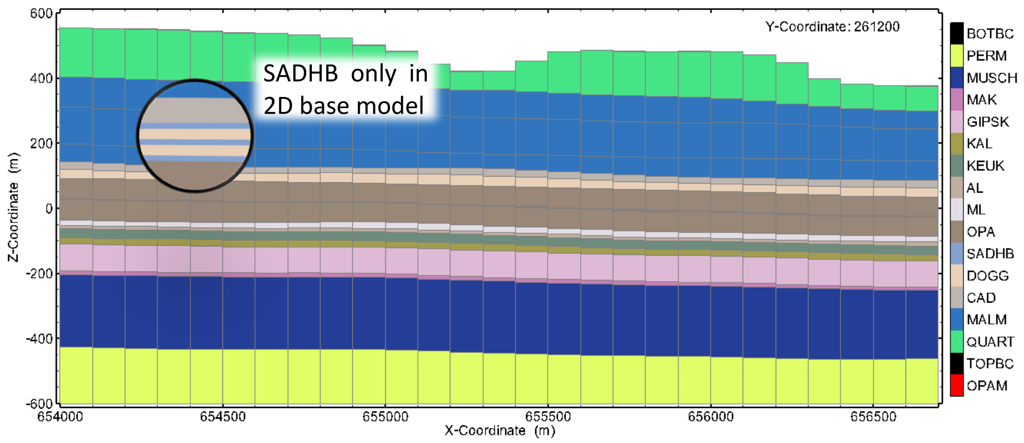

Fig. 3-4: Detail of a cross-section along the coordinate X passing through proposed JO HLW repositoy at Y = 261200

Note: SADHB layers are not present in the 3D base model.

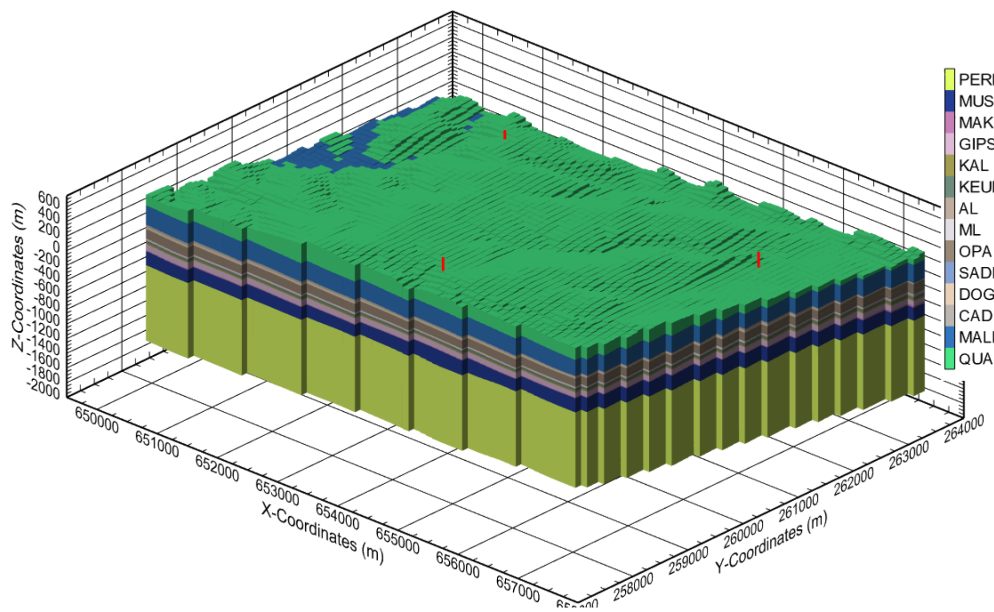

Fig. 3-5: 3D view of the 3D JO base model grid

Borehole locations are shown for Riniken (RIN), Bözberg-1 (BOZ1), and Bözberg-2 (BOZ2).

3.1.3 Thermo-hydraulic model parameters, boundary, and initial conditions

The Opalinus Clay host rock and over- and underlying units are each represented as homogeneous layers with uniform (but possibly anisotropic) thermal-hydraulic properties. The property assignment is largely based on the new reference data sets from Nagra (2024b) . The relevant thermal and flow properties are described in the following. The flow and transport properties are summarized in Tab. 3-3. Parameters of formations / facies, which consist of several litho-stratigraphic units, are calculated as a weighted arithmetic mean for the horizontal permeability and porosity and as a weighted harmonic mean for the vertical permeability. The thickness of the borehole BOZ1 is used for the weighting.

The sandy Keuper unit SK in the Ergholz Member is not included in the calculation of the mean value for the Keuper Aquifer KAL, as the proportion of this unit is not known. Instead, the parameters for SK are listed separately in the table, even if the unit does not exist as a separate unit in the base model.

The succession in the Dogger above the Opalinus Clay is not shown in the 3D base model due to the higher variability. Instead, the mean value for the Dogger unit is calculated under the assumption that three hard-beds (SCD unit) of 3 m thickness are present in the Sandy-Argillaceous Dogger SAD. For the more local 2D models, however, three hard beds (SADHB) are modelled. Therefore, parameters for the SAD and SCD units and the weighted average are listed in the table.

The thermal parameters (mainly the heat conductivity and the specific heat) of each formation are summarized in Tab. 3-4.

The initial conditions essentially correspond to hydrostatic conditions (i.e., pressures are in hydrostatic conditions) and temperature for a geothermal gradient of 0.043 ºC/m. At the top boundary layer land-surface temperature is fixed to 10 ºC and pressures are set to constant atmospheric pressure. At the bottom boundary layer, no-flow condition is assigned, and a constant heat flux of 120 mW/m^2 is assigned corresponding to the reference value of natural thermal flux from the earth (Senger et al. 2014). All lateral boundaries are assumed to be no-flow and adiabatic boundaries.

Tab. 3-3: Flow and transport properties assigned to the stack of geological formations

<table>
<tr><th>Formation / facies</th><th colspan="2">Equivalent lithostratigraphy</th><th colspan="2">$K_{x,y}$ [m²]</th><th colspan="2">K_z [m²]</th><th colspan="2">ϕ [-]</th></tr>
<tr><td>PERM</td><td colspan="2">-</td><td colspan="4"></td><td colspan="2"></td></tr>
<tr><td>Dolomitic Muschelkalk (DM)</td><td colspan="2">DM</td><td colspan="4">4.54E-14</td><td colspan="2"></td></tr>
<tr><td>Anhydritic Keuper (MAK)</td><td colspan="2">MAK & DAK</td><td colspan="4">9.08E-21</td><td colspan="2">0.018</td></tr>
<tr><td>Anhydritic-Argillaceous Keuper (GIPSK)</td><td colspan="2">AAK</td><td colspan="4">9.08E-21</td><td colspan="2">0.094</td></tr>
<tr><td rowspan="2">Keuper Aquifer (KAL)</td><td colspan="2">JO-DK&AK1</td><td colspan="2">3.03E-14</td><td colspan="2">2.72E-20</td><td colspan="2">0.114</td></tr>
<tr><td colspan="2">SK[1]</td><td colspan="4">9.08E-15</td><td colspan="2">nan</td></tr>
<tr><td>Calcareous Lias, Argillaceous Keuper (KEUK)</td><td colspan="2">CL&JO-AK2/3</td><td colspan="2">1.96E-20</td><td colspan="2">2.08E-21</td><td colspan="2">0.122</td></tr>
<tr><td>Argillaceous Lias (AL)</td><td colspan="2">AL</td><td colspan="2">9.08E-21</td><td colspan="2">1.82E-21</td><td colspan="2">0.081</td></tr>
<tr><td>Marly Lias (ML)</td><td colspan="2">ML</td><td colspan="4">4.54E-21</td><td colspan="2">0.074</td></tr>
<tr><td>Opalinus Clay (OPA)</td><td colspan="2">OPA</td><td colspan="2">4.54E-21</td><td colspan="2">9.08E-22</td><td colspan="2">0.120</td></tr>
<tr><td>Sandy-Argillaceous Dogger (DOGG)</td><td>SAD</td><td rowspan="2">SAD & SCD</td><td>9.08E-21</td><td rowspan="2">7.08E-21</td><td>1.82E-21</td><td rowspan="2">2.47E-21</td><td>0.097</td><td rowspan="2">0.078</td></tr>
<tr><td>Sandy-Calcareous Dogger (SADHB)</td><td>SCD</td><td>4.54E-21</td><td>4.54E-21</td><td>0.054</td></tr>
<tr><td>Calcareous-Argillaceous Dogger (CAD)</td><td colspan="2">JO-CAD</td><td colspan="4">4.54E-21</td><td colspan="2">0.084</td></tr>
<tr><td>MALM</td><td colspan="2">JO-CD (Malm aquifer)</td><td colspan="4">4.54E-16</td><td colspan="2"></td></tr>
<tr><td>TERT</td><td colspan="2">-</td><td colspan="4"></td><td colspan="2"></td></tr>
</table>

[1] Unit neglected in some models

Tab. 3-4: Reference values of heat conductivity and specific heat values assigned to the stack of geological formations for the JO model

Layer	Formation	Heat conductivity [W/m˚C]	Specific heat [J/kg ˚C]
00	BOTBC	2.58	995.0
01	PERM	2.58	995.0
02	MUSCH	4.021	905.5
03	MAK	4.021	905.5
04	GIPSK	2.143	995.0
05	KAL	2.143	995.0
06	KEUK	2.143	995.0
07	AL	2.143	995.0
08	ML	2.143	995.0
09	OPA	1.55	946.5
10	DOGG	2.203	995.0
11	CAD	2.203	995.0
12 – 14	MALM	3.211	905.5
15	QUAT	3.0	995.0
16	TOPBC	3.0	995.0

3.2 Modelling workflow

The simulations of heat flow through the stack of geological formations presented in this section are performed using the EOS1 module of iTOUGH2 v7.1 (Finsterle et al. 2017). The modelling workflow is outlined in Section 3.3.1 and the inverse model is described in Section 3.3.2. The results from the numerical simulations are presented in Section 3.4.

3.2.1 Approach

The objective is to use temperature data in order to estimate the heat conductivity of each formation layer using an inverse modelling workflow. Note that there is no available data for borehole RIN, therefore only data from boreholes BOZ1 and BOZ2 are used (see Fig. 2-10).

The modelling workflow is set up with a forward simulation using the initial estimates of thermal conductivity presented in Tab. 3-3 to compare the simulated and measured temperature profiles at each borehole. The simulation is initiated with a linear temperature profile and runs for a hypothetical period of 1 Mio. years in order to obtain a temperature profile as close to steady-state as possible. Fig. 3-6 shows the temperature profiles associated with the two boreholes after 1 Mio. years. As can be observed the simulated temperature profiles generated using the initial estimates of heat conductivities are already close to the observed data with slightly higher temperatures compared to the measured data through borehole BOZ2.

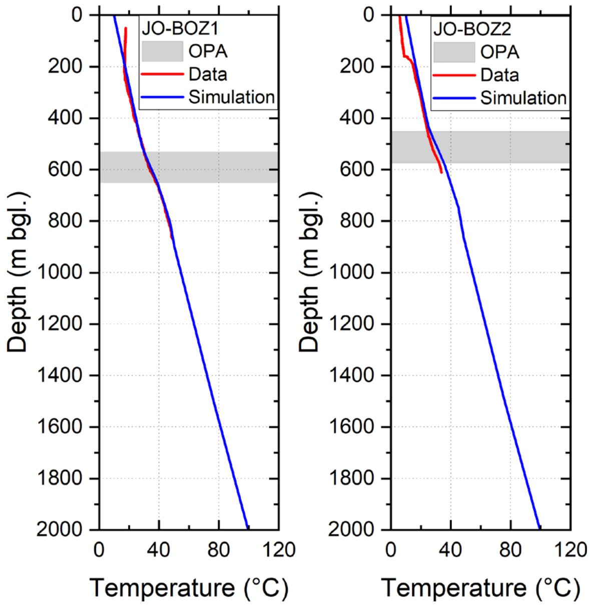

Fig. 3-6: Siting region JO: Comparison between measured temperatures and simulated temperatures in the quasi-steady state

using the initial estimates for heat conductivities at boreholes BOZ1 and BOZ2, respectively.

3.2.2 Inverse model

Inverse computations were performed using iTOUGH2 to improve the fit between simulated and measured temperature profiles. The inverse calculations aim to identify the optimal set of heat conductivity values that minimizes the differences between calculated and measured temperatures. The model involves 15 heat conductivity values to be estimated as shown in Tab. 3-4. Heat conductivity values of formations BOTBC and TOPBC were excluded from the inverse procedure to reduce the number of parameters to be estimated. Moreover, the heat conductivity of formation PERM was also excluded as no temperature data are available along this layer. In addition, it is assumed that the sets of formations (MUSCH and MAK), (GIPSK, KAL, KEUK, AL, and ML), (SADHB and DOGG), and (MALM and CAD) have each the same heat conductivity value. Therefore, in total there are six parameters to be estimated as shown in Tab. 3-4. It is important to mention that only observed temperature data below 200 m are taken into account in the inverse procedure (data above 200 m depth are ignored as they look like artifacts).

The key elements of an inverse modeling in iTOUGH2 are: (1) a simulation program to model flow and transport in the hydrogeologic system, here the thermal model (forward model), (2) the objective function which measures the misfit between the model output and the data, (3) the minimization algorithm which reduces the objective function by automatically updating parameter values, and (4) the error analysis which allows one to judge the quality of the estimates. The iTOUGH2 code estimates elements of a parameter vector (vector of heat conductivities of each formation) based on (temperature) observations by minimizing an objective function which is a function of the residual vector (here, the vector of squared differences between calculated and measured temperatures). The code offers a number of different minimization algorithms, the Levenberg-Marquardt modification of the Gauss-Newton algorithm is found to be a rather general and robust procedure for iteratively updating the parameter vector. By default, iTOUGH2 uses the Levenberg-Marquardt minimization algorithm, which is a modification of the Gauss-Newton algorithm.

In this report, the default minimization algorithm is used. Several preliminary test cases have been carried out in order to efficiently obtain the optimal parameters set (the best estimate set). These preliminary tests aimed to properly select the numerical parameters used by the algorithm, mainly the number of optimization iterations, the relative error, and the parameter bandwidth intervals. The numerical parameters were set to their default values.

3.3 Discussion of the results

The heat conductivity values presented in Tab. Tab. 3-4are used as initial guess for the inverse procedure. These values are also presented in Tab. 3-5 which shows also the lower and upper limits of heat conductivity of each formation. The low (resp. upper) limit of heat conductivity of each formation is assumed to be equal to the reference value minus 1.5 W/m˚C (resp. plus 1.5 W/m˚C), except for the upper limit of parameter n° 1 (i.e., MUSCH and MAK) which is allowed to exceed the initial value by 2.5 W/mK. Indeed, preliminary numerical experiments have shown that the estimated value of parameter n° 1 often reaches its upper limit. The lower and upper limits of heat conductivity of each formation are presented in Tab. 3-5.

Tab. 3-5: Initial, best estimate, lower and upper limit values of heat conductivity

Parameter number	**Layer**	**Formation**	**Initial estimate heat conductivity** [W/m˚C]	**Best estimate heat conductivity** [W/m˚C]	**Heat conductivity lower limit** [W/m˚C]	**Heat conductivity upper limit** [W/m˚C]
1	02 – 03	MUSCH MAK	4.021	2.79	2.521	6.521
2	04 – 08	GIPSK KAL KEUK AL ML	2.143	1.71	0.643	3.643
3	09	OPA	1.55	1.81	0.05	3.05
4	10	DOGG (incl. SADHB)	2.203	1.73	0.703	3.703
5	11 – 14	CAD MALM	3.211	3.81	1.711	4.711
6	15	QUAT	3.0	3.05	1.5	4.5

Tab. 3-5 shows also the results of the inverse calculations (column: best estimate). This best estimate set of heat conductivity values is then used as input for a forward calculation in order to obtain the temperature prediction associated with the optimal set of heat conductivity values.

3.3.1 Calibrated temperature profiles at TBO boreholes

Fig. 3-7 shows the comparison between measured and simulated temperatures associated with the 2 boreholes BOZ1 and BOZ2, respectively, using the best estimate heat conductivity values. The figure shows that the fitted set of heat conductivity significantly improved the results.

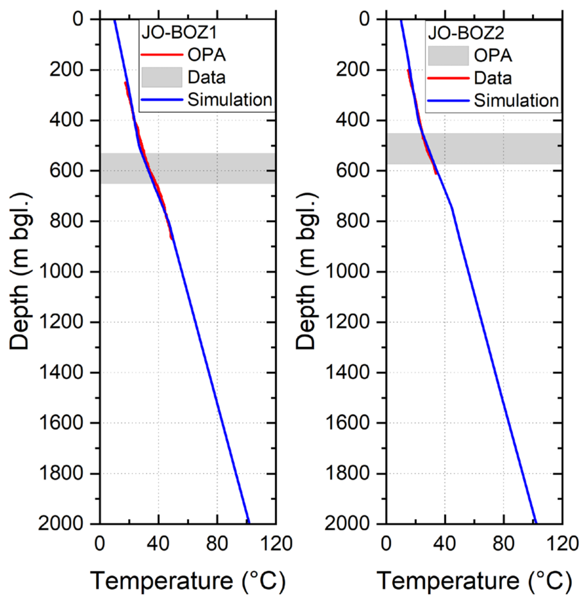

Fig. 3-7: Siting region JO: Comparison between measured temperatures and simulated temperatures using the best estimate heat conductivity values at boreholes BOZ1 and BOZ2, respectively

3.3.2 Temperature profiles through the center of HLW and L/ILW repositories

The best estimate set of heat conductivities is used to compute the 1-D temperature evolution through the center of HLW and L/ILW repositories (see Fig. 3-1). Fig. 3-8 depicts the simulated temperature profile at the center of each repository area along the vertical directions. The maximal temperature at the bottom of the model reaches about 100 °C for both locations. This corresponds to a thermal gradient of about 0.045 ºC/m.

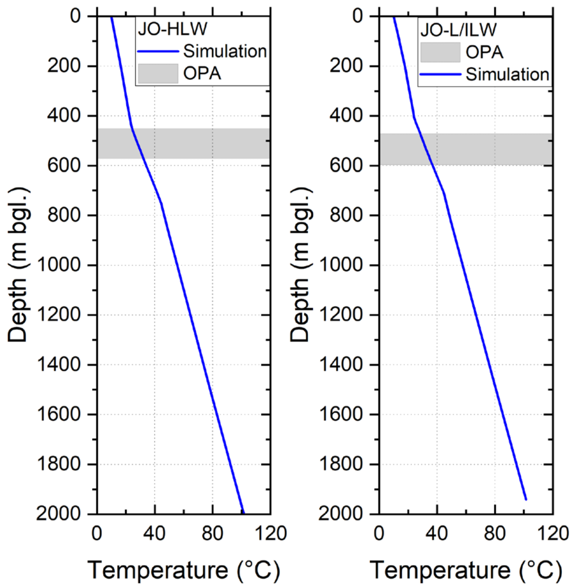

Fig. 3-8: Siting region JO: Temperatures profiles through the centers HLW and L/LW repositories along the vertical axis obtained using the best estimate set of heat conductivities

Coordinates of repository (center of HLW-tunnel): 654820, 261130, -12 m asl / 512 m bg; L/ILW (center of L/ILW cavern): 655698, 260432, -45 m asl / 536 m bg).

3.3.3 Cross-sections of temperature distributions

Fig. 3-9 and Fig. 3-10 show cross-sections of temperature distributions spanning the JO local model in the south-north (SN) and west-east (WE) directions, respectively. The plots show isolines spanning parallel to the surface elevation, indicating that surface morphology affects the temperature distribution even in the deeper parts of the model (i.e., 450 m below ground surface in cross-section WE). Along the SN, temperatures in the Opalinus Clay vary from 21 °C to 35 °C depending on the formation depth. Along the WE cross-section, the Opalinus Clay dips gently eastward, resulting in formation temperatures ranging between 26 °C and 35 °C.

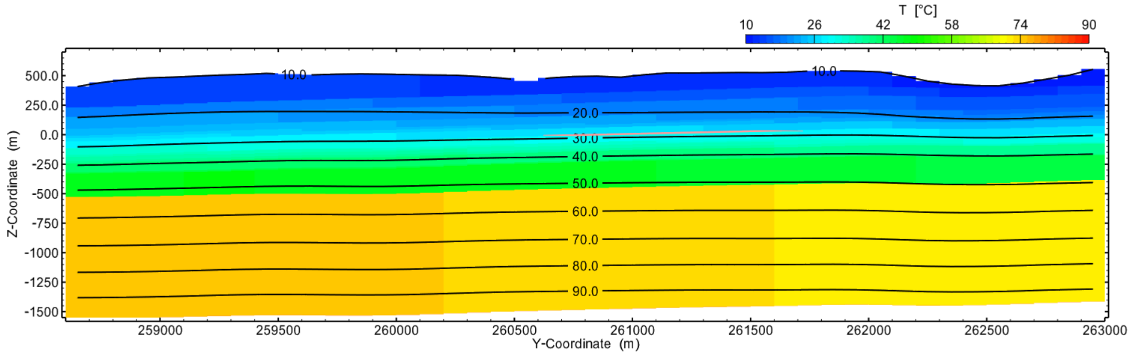

Fig. 3-9: Siting region JO: Cross-sectional temperature distribution in the South-North (SN) direction (through the center of the HLW repository)

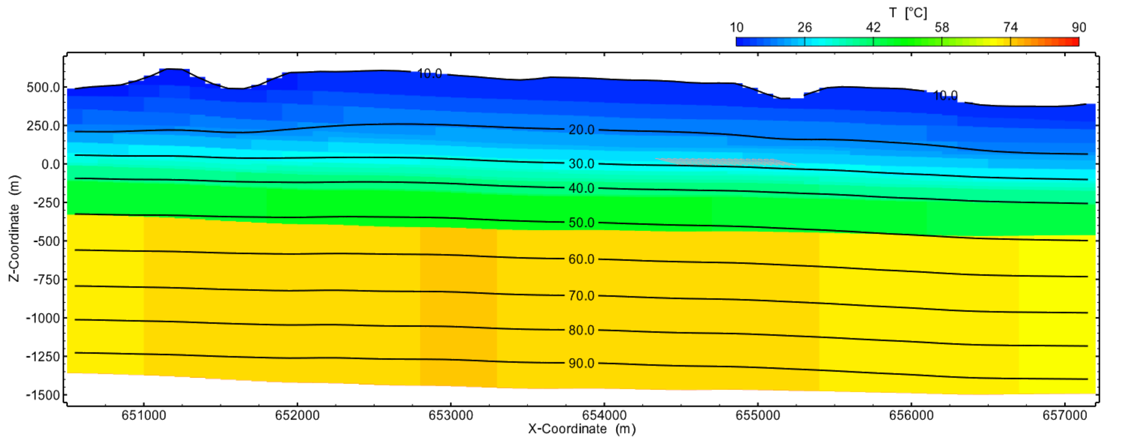

Fig. 3-10: Siting region JO: Cross-sectional temperature distribution in the West-East (WE) direction (through the center of the HLW repository)

4 Thermo-hydraulic conditions in the siting region NL

The geological interpretations of 3-D seismics in the siting region NL are reported in Nagra (2024b), forming the basis for the geological layer model LocMOD-V1-NL. The digital surfaces of version V1 of the geological layer model NL were used for the elaboration of the 3-D model of a deep geological repository in NL with the repository fields NL-HLW and NL-L/ILW. Moreover, to ensure a consistent geometric representation of the site-specific repository projects in Performance Assessment (PA) and Safety Assessment (SA), all assessment models are referring to the same version of the geological layer model LocMOD-V1-NL.

A portfolio of numerical PA models was elaborated in the context of the site selection process for assessment of the proposed HLW and L/ILW repository fields in the siting area NL comprising:

- a thermo-hydraulic 3-D model of the entire primary investigation perimeter on a footprint area of around $4 \times 10\ km^2$
- 3-D repository nearfield models, containing the proposed HLW repository and the L/ILW repository on a footprint area of around $3 \times 3\ km^2$
- several vertical cross sections through the disposal fields of repository projects for HLW and L/ILW in the siting region NL

This report addressed the temperature distribution in the Mesozoic layer stack at the scale of the primary investigation perimeter. Section 4.1 presents the model set-up, including model geometry, property assignment, initial conditions and boundary conditions. Model calibrations with the temperature profiles from the deep investigation boreholes BUL1, STA2 and STA3 are described in Section 4.2. The results of the TH-calculations at site scale are discussed in Section 4.3, including an assessment of the impact of thermal history on the recent temperature distribution at site scale. Eventually, Section 4.4 gives a survey of the vertical temperature profiles at the center of the HLW and the L/ILW repository fields in the siting region NL.

4.1 3-D model of the siting region NL

4.1.1 Seismic surfaces

In total, 20 surfaces ("flying carpets") have been provided by Nagra for Nördlich Lägern (NL) for the modelling scope described in this report. These are summarized in Tab. 4-1. The surfaces will are reported in Nagra (2024b).

Tab. 4-1: Seismic surfaces (2023Mod_NL_pointset_data_50x50) provided by Nagra for NL

Description	Filename	First row X[1]	First row Y[1]	First row Z[1]
Top Malm	2023Mod_50x50_NL_149.2_Kim_100_Base_Cenozoic_2023_05_02_cam			-34.27
Middle Malm	2023Mod_50x50_NL_149.2_Kim_700_nTop_Villigen_Fm_2023_05_02_cam			-151.74
Bottom Malm	LocMod2023_v1_50x50_NL_154.8_Oxf_300_nTop_Wildegg_Fm_2023_05_12_cam			-209.11
Near Top Gerstenhübel Bd.	LocMod2023_v1_50x50_NL_154.8_Oxf_700_nTop_Gerstenhuebel_Bd_2023_05_25_cam			-236.69
Near Base Gerstenhübel Bd.	LocMod2023_v1_50x50_NL_154.8_Oxf_750_Intra_Wildegg_Fm_2023_05_12_cam			-241.74
Top Wutach Fm.	2023Mod_50x50_NL_154.8_Oxf_975_Top_Dogger_Gr_2023_05_02_cam			-310.22
Top "Herrenwis Unit"	2023Mod_50x50_NL_168.2_Baj_200_Top_Herrenwis_Unit_eq_2023_05_02_cam			-373.04
Top Wedelsand-stein Fm.	2023Mod_50x50_NL_168.2_Baj_300_Base_Herrenwis_Unit_eq_2023_05_02_cam	675274.72	263749.80	-373.04
Not used	LocMod2023_v1_50x50_NL_168.2_Baj_400_Intra_Wedelsandstein_Fm_2023_05_25_cam			-378.96
Top OPA	2023Mod_50x50_NL_170.9_Aal_300_Top_Opalinus_Clay_2023_05_02_cam			-389.06
Top Lias	2023Mod_50x50_NL_174.7_Toa_100_Top_Lias_Gr_2023_05_02_cam			-495.16
Top Frick Mb.	LocMod2023_v1_50x50_NL_192.9_Sin_100_Top_Frick_Mb_2023_05_25_cam			-507.17
Top Beggingen Mb.	LocMod2023_v1_50x50_NL_192.9_Sin_200_Top_Beggingen_Mb_2023_05_12_cam			-528.12
Top Seebi Mb.	LocMod2023_v1_50x50_NL_208.5_Nor_100_Top_Seebi_Mb_2023_05_25_cam			-554.27
Top Gansingen Mb.	LocMod2023_v1_50x50_NL_227_Car_100_Top_Gansingen_Mb_2023_05_12_cam			-563.62

Tab. 4-1: Cont.

Description	Filename	First row X[1]	First row Y[1]	First row Z[1]
Top Bänkerjoch Fm.	2023Mod_50x50_NL_227_Car_300_Top_Baenkerjoch_Fm_2023_05_02_cam			-572.79
Intra Bänkerjoch Fm.	LocMod2023_v1_50x50_NL_237_Lad_200_Intra_Baenkerjoch_Fm_2023_05_25_cam	675274.72	263749.80	-636.88
Top Muschelkalk	2023Mod_50x50_NL_237_Lad_400_Top_Muschelkalk_Gr_2023_05_02_cam			-651.16
Bottom Mesozoikum	2023Mod_50x50_NL_251.9_Per_100_Base_Mesozoic_2023_05_02_cam			-860.84
Ground Level[2]	dhm25_nl.xyz	664000.0	276000.0	350.097

1 Corresponds to the first line found in the ASCII file (may differ from the lowest X/Y/Z values).
2 Surface file communicated separately to the 2023Mod package.

4.1.2 Geometric model set-up (base model)

The 3D model area envelopes the proposed repository and a maximum of the stratigraphic surfaces provided by Nagra (see Nagra 2024b), with boreholes Stadel-2-1 (STA2), Stadel-3-1 (STA3), and Bülach-1-1 (BUL). Boreholes Bachs-1-1 (BAC1) and Weiach (WEI) are in the vicinity of the model on the west and north, respectively. In the horizontal direction, the model is discretized by 100 × 100 m elements as shown in Fig. 4-1. The 2D base models for HLW and I/ILW are placed in the center of the repositories (Fig. 4-1). The cross-section has a length of 2 km in each case. The center of each repository area is indicated in Fig. 4-2 (CHAA is the location of the center of HLW repository, and CSMA is the location of the center of L/ILW repository).

In the vertical direction, the surfaces from the seismic interpretation were implemented into a stack of geological formations/facies as illustrated in Fig. 4-2 and shown in Tab. 4-2. In addition to the LocMod2023 surfaces, further formation units are included to extend the model in the vertical direction to avoid any boundary effects on the thermal-hydraulic processes. Tertiary/Quartz formation on top of Malm is added with a variable thickness which is defined by region between the two surfaces 149.2_Kim_100_Base_Cenozoic and dhm25_nl. The model is extended into the deep earth by another formation layer of 1029 m thick Permocarbon basement.

The Opalinus Clay was split into upper and lower OPA by generating a surface at the 50% of the Opalinus Clay thickness calculated as the difference between:

- "2023Mod_50x50_NL_170.9_Aal_300[…]" and
- "2023Mod_50x50_NL_174.7_Toa_100[…]"

The surface in the middle of OPA is used to generate three additional layers in the middle of the Opalinus Clay. That is, the Opalinus Clay is divided into 5 sub-layers, with three layers of 1 m thickness implemented in the middle, with which the TH-values (i.e., the thermal conductivity) at repository horizon can be precisely obtained.

In the 3D base model, the Sandy-Argillaceous Dogger (SAD) and Sandy-Calcareous Dogger (SCD) of Wedelsandstein Formation above the Opalinus Clay are combined in only one layer. In contrast, three hard-bed layers (SAD-HB) with a thickness of 3 m each are modeled alternating with the Sandy-Argillaceous Dogger (DOGG) in the 2D base model, resulting in a total of 5 sub-layers.

The «Herrenwis Unit» is differentiated into three different units (GDS 3.1 AN23-0230). In the eastern part of Nördlich Lägern (boreholes Stadel-3-1 and Bülach-1-1) the stratigraphic unit Calcareous Dogger NLE-CD occurs, towards the west (boreholes Stadel-2-1, Weiach) the Calcareous Dogger NLW-CD, and even further towards the west the stratigraphic unit Argillaceous Dogger NL-ARD (borehole Bachs-1-1). In the model, the «Herrenwis Unit» is divided into two parts, with HERRE standing for NLE-CD and HERRW for NLW-CD. The third unit NL-ARD is neglected due to its low thickness and its marginal location. The division of the «Herrenwis Unit» into a western (HERRW) and an eastern part (HERRE) in the model area is shown in Fig. 4-3. Fig. 4-4shows the transition from HERRW to HERRE in a detailed cross-section of the 3D model through the location of borehole Stadel-3-1. A 3D view of the entire model can be seen in Fig. 4-5.

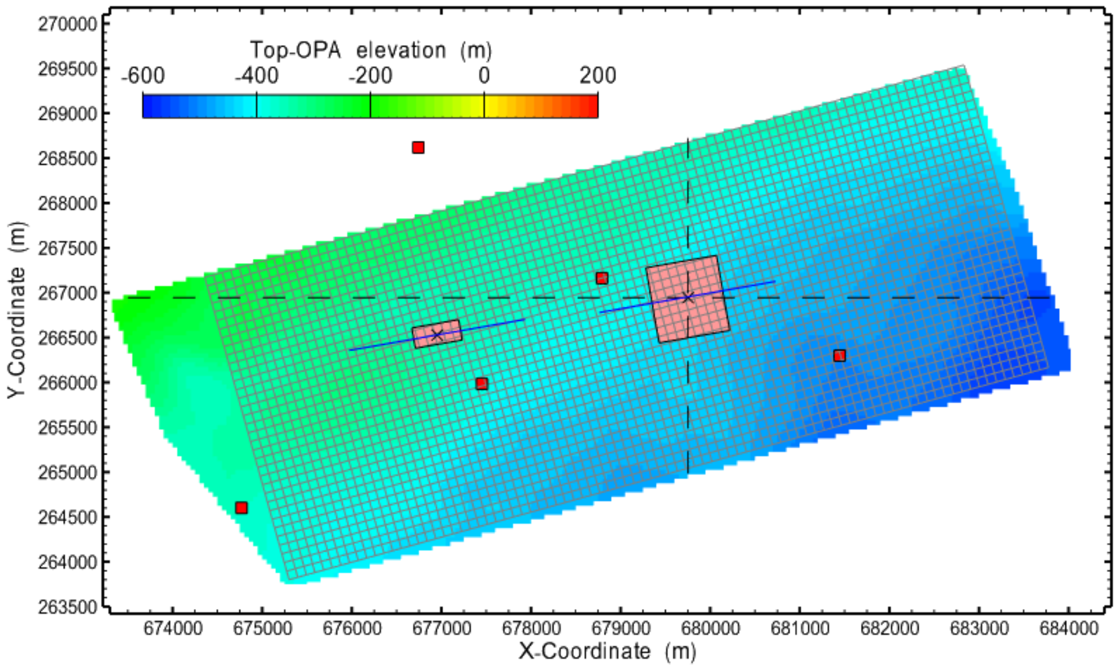

Fig. 4-1: Plan view of the 3D NL base model grid (regular 100 × 100 m grid)

With representation of the OPA surface "2023Mod_50x50_NL_170.9_Aal_300[…]", the proposed repository, borehole locations Weiach WEI (676744, 268618, 368.66 m asl), Stadel-2-1 STA2 (677453, 265982, 417 m asl), Stadel-3-1 STA3 (678793, 267162, 407 m asl), Bülach-1-1 BUL (681446, 266298, 389.62 m asl), Bachs-1-1 BAC1 (674769, 264601), and cross-sections of the 2D base models (HLW and L/ILW). CHLW (679753, 266945, 448m asl) and CLILW (: 676953, 266528, 436 m asl) indicate the centers of HLW and L/ILW repository areas.

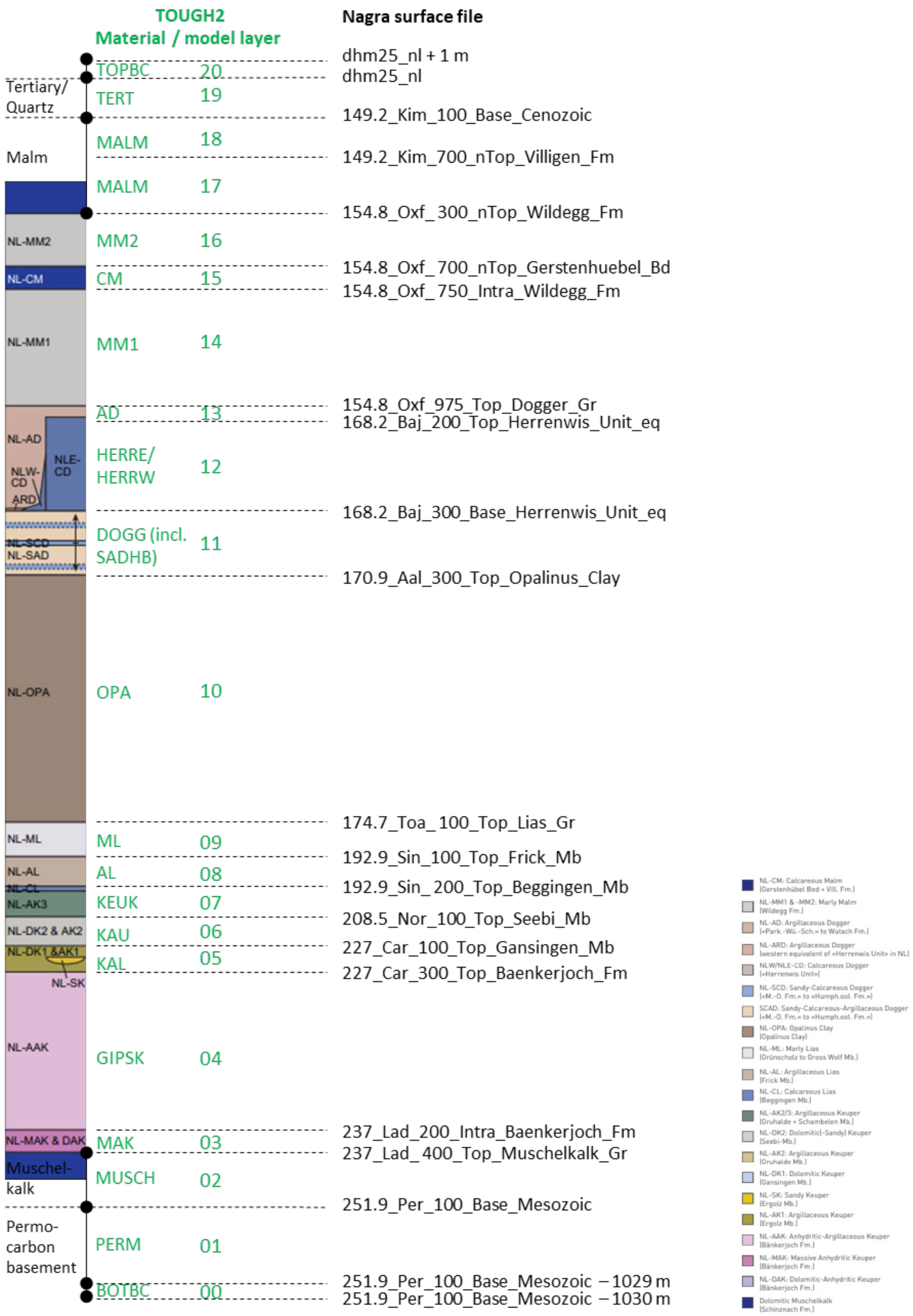

Fig. 4-2: Geological abstraction of stratigraphy for Nördlich Lägern

Modified from Nagra (2024b) and layers implemented in the numerical model.

Tab. 4-2: Vertical distretization of the NL base model

Layer	Stratigraphic units / formation	TOUGH2 Material name	Vertical discretization (layer)
00	Bottom Boundary	BOTBC	1
01	Permocarbon basement	PERM	1
02	Muschelkalk	MUSCH	1
03	Dolomitic-Anhydritic Keuper (DAK) & Massive Anhydritic Keuper (MAK) of Bänkerjoch Formation	MAK	1
04	Anhydritic-Argillaceous Keuper (AAK) of Bänkerjoch Formation	GIPSK	1
05	Argillaceous Keuper (AK1) & Sandy Keuper (SK) both Ergolz Member of the Klettgau Formation & Dolomitic Keuper (NL-DK1 - Gansingen Member)	KAL	1
06	Argillaceous Keuper (NL-AK2 - "lower" Gruhalde Member) & Dolomitic Keuper (NL-DK2 - Seebi Member) &	KAU	1
07	Argillaceous Keuper (NL-AK3 - "upper" Gruhalde Member and Schambelen Member of the Staffegg Formation) & Calcareous Lias (CL - Beggingen Member) of the Staffegg Formation	KEUK	1
08	Argillaceous Lias (AL – Frick Member) of the Staffelegg Formation	AL	1
09	Marly Lias (ML) of the Staffelegg Formation	ML	1
10a, b	Opalinus Clay (OPA)	OPA	5 (2 for upper and bottom OPA, three 1-m middle layers)
10c		OPAM	
10d, e		OPA	
11	Sandy-Argillaceous Dogger (SAD) & Sandy-Calcareous Dogger (SCD) of Wedelsandstein Formation	DOGG	1
12	Herrenwis unit: in the eastern part (boreholes Stadel-3-1 and Bülach-1-1) Calcareous Dogger (NLE-CD), towards the west (boreholes Stadel-2-1, Weiach) the NLE-CD is neighbored by the stratigraphic unit Calcareous Dogger (NLW-CD)	HERRE/HERRW	1
13	Argillaceous Dogger (AD)	AD	1 (2 where Herrenwis is not present)
14	Marly Malm (NL-MM1)	MM1	1
15	Calcareous Malm (NL-CM - Gerstenhübel Beds)	CM	1
16	Marly Malm (NL-MM2)	MM2	1

Tab. 4-2: Cont.

Layer	Stratigraphic units / formation	TOUGH2 Material name	Vertical discretization (layer)
17	Malm	MALM	2
18			
19	Tertiary (TERT) / Quartz (QUAT)	TERT	1
20	Top Boundary (TOP-BC)	TOPBC	1

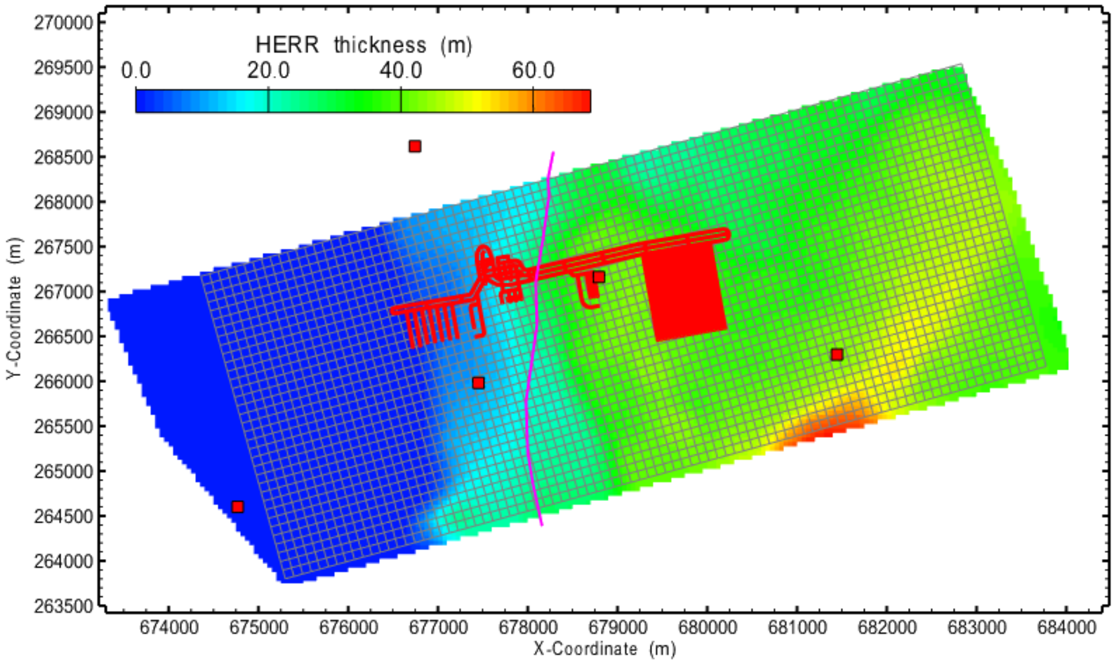

Fig. 4-3: Division of the «Herrenwis Unit» into western (HERRW) and eastern parts (HERRE) in the model area

Plan view of the thickness between surfaces 168.2_Baj_200_Top_Herrenwis_Unit and 168.2_Baj_300_Base_Herrenwis_Unit, the proposed repository, and borehole locations Weiach, Stadel-2-1, Stadel-3-1, Bülach-1-1, and Bachs-1-1.

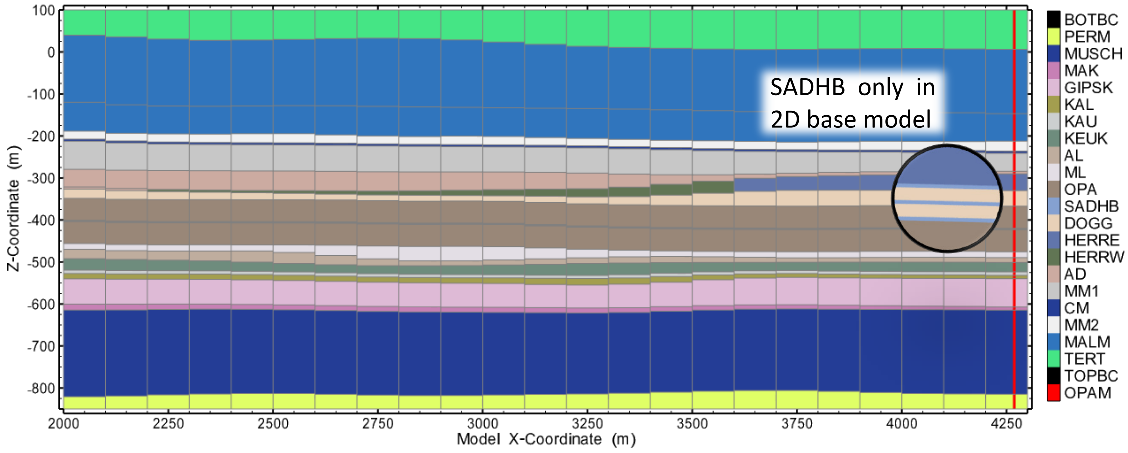

Fig. 4-4: Detail of a cross-section of the NL model along the model coordinate X passing through the borehole Stadel-3-1

Note: SADHB layers are not present in the 3D base model.

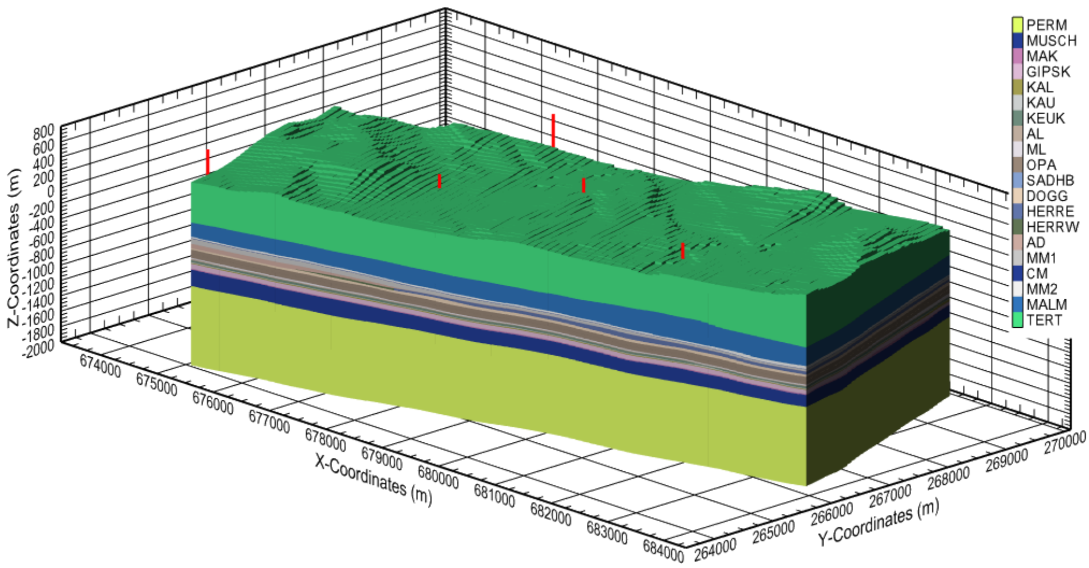

Fig. 4-5: 3D view of the NL base model grid. Borehole locations are shown for Weiach, Stadel-2-1, Stadel-3-1, Bülach-1-1, and Bachs-1-1

4.1.3 Thermo-hydraulic model parameters, boundary, and initial conditions

The Opalinus Clay host rock and over- and underlying units are each represented as homogeneous layers with uniform (but possibly anisotropic) thermal-hydraulic properties. The property assignment is largely based on the new reference data sets from GDS-3.1. The relevant thermal and flow properties are described in the following. The flow and transport properties are summarized in Tab. 4-3. Parameters of formations/facies, which consist of several litho-stratigraphic units, are calculated as a weighted arithmetic mean for the horizontal permeability and porosity and as a weighted harmonic mean for the vertical permeability. The thickness of the borehole STA3-1 is used for the weighting.

The sandy Keuper unit SK in the Ergholz Member is not included in the calculation of the mean value for the Keuper Aquifer KAL, as the proportion of this unit is not known. Instead, the parameters for SK are listed separately in the table, even if the unit does not exist as a separate unit in the base model.

The succession in the Dogger above the Opalinus Clay is not shown in the 3D base model due to the higher variability. Instead, the mean value for the Dogger unit is calculated under the assumption that three hard-beds (SCD unit) of 3 m thickness are present in the Sandy-Argillaceous Dogger SAD. For the more local 2D models, however, three hard beds (SADHB) are modelled. Therefore, parameters for the SAD and SCD units and the weighted average are listed in the table.

The thermal parameters (mainly the heat conductivity and the specific heat) of each formation are summarized in Tab. 4-4.

The initial conditions essentially correspond to hydrostatic conditions (i.e., pressures are in hydrostatic conditions) and temperature for a geothermal gradient of 0.043 ºC/m. At the top boundary layer land-surface temperature is fixed to 10 ºC and pressures are set to constant atmosphere pressure. An alternative scenario is also explored where the temperature at the top is not fixed. In this case, the initial temperature distribution assumes a temperature of 10 °C at an elevation offset of 410 m, while maintaining the same geothermal gradient of 0.043 ºC/m. At the bottom boundary layer, no flow condition is assigned, and a constant heat flux of 120 mW/m^2 is assigned corresponding to the reference value of natural thermal flux from the earth (Senger et al. 2014). All lateral boundaries are assumed to be no-flow and adiabatic boundaries.

Tab. 4-3: Flow and transport properties assigned to the stack of geological formations

<table>
<tr><th>Formation / facies</th><th colspan="2">Equivalent lithostratigraphy</th><th colspan="2">$K_{x,y}$ [m^2]</th><th colspan="2">K_z [m^2]</th><th colspan="2">ϕ [-]</th></tr>
<tr><td>PERM</td><td colspan="2">-</td><td colspan="4"></td><td colspan="2"></td></tr>
<tr><td>Dolomitic Muschelkalk (DM)</td><td colspan="2">DM</td><td colspan="4">4.54E-14</td><td colspan="2"></td></tr>
<tr><td>Anhydritic Keuper (MAK)</td><td colspan="2">MAK & DAK</td><td colspan="4">9.08E-21</td><td colspan="2">0.017</td></tr>
<tr><td>Anhydritic-Argillaceous Keuper (GIPSK)</td><td colspan="2">AAK</td><td colspan="4">9.08E-21</td><td colspan="2">0.091</td></tr>
<tr><td rowspan="2">Lower Keuper Aquifer (KAL)</td><td colspan="2">DK1&AK1</td><td colspan="2">9.08E-20</td><td colspan="2">2.24E-20</td><td colspan="2">0.121</td></tr>
<tr><td colspan="2">SK[1]</td><td colspan="4">9.08E-15</td><td colspan="2">0.144</td></tr>
<tr><td>Upper Keuper Aquifer (KAU)</td><td colspan="2">DK2&AK2</td><td colspan="2">7.21E-20</td><td colspan="2">7.43E-21</td><td colspan="2">0.087</td></tr>
<tr><td>Calcareous Lias, Argillaceous Keuper (KEUK)</td><td colspan="2">CL&AK3</td><td colspan="2">1.89E-20</td><td colspan="2">2.06E-21</td><td colspan="2">0.108</td></tr>
<tr><td>Argillaceous Lias (AL)</td><td colspan="2">AL</td><td colspan="2">9.08E-21</td><td colspan="2">1.82E-21</td><td colspan="2">0.083</td></tr>
<tr><td>Marly Lias (ML)</td><td colspan="2">ML</td><td colspan="4">4.54E-21</td><td colspan="2">0.075</td></tr>
<tr><td>Opalinus Clay (OPA)</td><td colspan="2">OPA</td><td colspan="2">4.54E-21</td><td colspan="2">9.08E-22</td><td colspan="2">0.115</td></tr>
<tr><td>Sandy-Argillaceous Dogger (DOGG)</td><td>SAD</td><td rowspan="2">SAD & SCD</td><td>9.08E-21</td><td rowspan="2">7.72E-21</td><td>1.82E-21</td><td rowspan="2">2.22E-21</td><td>0.123</td><td rowspan="2">0.123</td></tr>
<tr><td>Sandy-Calcareous Dogger (SAD-HB)</td><td>SCD</td><td>4.54E-21</td><td>4.54E-21</td><td>0.123</td></tr>
<tr><td>Calcareous Dogger (HERRE)</td><td colspan="2">E-CD</td><td colspan="4">9.08E-20</td><td colspan="2">0.026</td></tr>
<tr><td>Calcareous Dogger (HERRW)</td><td colspan="2">W-CD</td><td colspan="4">9.08E-20</td><td colspan="2">0.043</td></tr>
<tr><td>Argillaceous Dogger (AD)</td><td colspan="2">AD</td><td colspan="2">9.08E-21</td><td colspan="2">1.82E-21</td><td colspan="2">0.120</td></tr>
<tr><td>Marly Malm (MM1)</td><td colspan="2">MM1</td><td colspan="2">9.08E-20</td><td colspan="2">1.82E-20</td><td colspan="2">0.074</td></tr>
<tr><td>Calcareous Malm (CM)</td><td colspan="2">CM (Gerstenhübel Beds)</td><td colspan="4">9.08E-20</td><td colspan="2">0.030</td></tr>
<tr><td>Marly Malm (MM2)</td><td colspan="2">MM2</td><td colspan="2">9.08E-20</td><td colspan="2">1.82E-20</td><td colspan="2">0.063</td></tr>
<tr><td>MALM</td><td colspan="2">CM (Malm aquifer)</td><td colspan="4">9.08E-17</td><td colspan="2"></td></tr>
<tr><td>TERT</td><td colspan="2">-</td><td colspan="4"></td><td colspan="2"></td></tr>
</table>

[1] Unit neglected in some models

Tab. 4-4: Reference values of heat conductivity and specific heat values assigned to the stack of geological formations for the NL model

Layer	**Formation**	**Heat conductivity** [W/m˚C]	**Specific heat** [J/kg ˚C]
00	BOTBC	2.58	995.0
01	PERM	2.58	995.0
02	MUSCH	4.021	905.5
03	MAK	4.021	905.5
04	GIPSK	2.143	995.0
05	KAL	2.143	995.0
06	KAU	2.143	995.0
07	KEUK	2.143	995.0
08	AL	2.143	995.0
09	ML	2.143	995.0
10	OPA	1.55	946.5
11	DOGG	2.203	995.0
12	HERRE/HERRW	3.211	905.5
13	AD	3.211	905.5
14	MM1	3.211	905.5
15	CM	3.211	905.5
16	MM2	3.211	905.5
17-18	MALM	3.211	905.5
19	TERT	3.0	995.0
20	TOPBC	3.0	995.0

4.2 Modelling workflow

The simulations of heat flow through the stack of geological formations presented in this section are performed using the EOS1 module of iTOUGH2 v7.1 (Finsterle et al. 2017). The modelling workflow is outlined in Section 4.3.1 and the inverse model is described in Section 4.3.2. The results from the numerical simulations are presented in Section 4.4.

4.2.1 Approach

The objective is to use temperature data in order to estimate the heat conductivity of each formation layer using an inverse modelling workflow. Note that there is no available data for boreholes BAC1 and WEI, therefore only data for boreholes BUL1, STA2 and STA3 are used (see Fig. 2-11).

The modelling workflow is set up with a forward simulation using the initial estimates of thermal conductivity presented in Tab. 4-4 to compare the simulated and measured temperature profiles at each borehole. The simulation is initiated with a linear temperature profile and runs for 1 Mio. years in order to obtain a temperature profile as close to steady-state as possible. Fig. 4-6 shows the temperature profiles associated with the three boreholes after 1 Mio. years. As can be observed the temperature profiles generated using the initial estimates of heat conductivities are already in good agreement with the observed data. A slightly higher temperatures can be observed. These results can be improved further using the inverse procedure presented below.

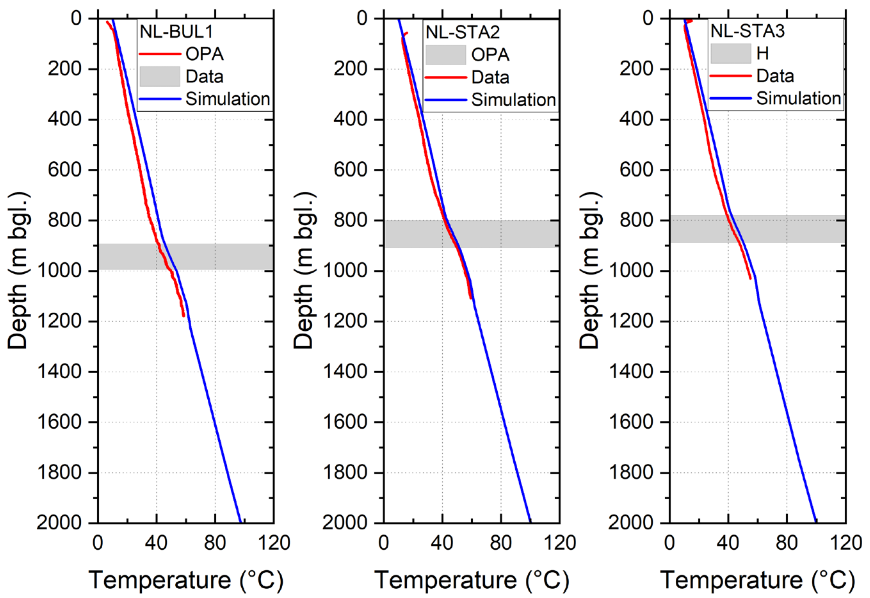

Fig. 4-6: Siting region NL: Comparison between measured temperatures and simulated temperatures at 1 Mio. years using the initial estimates for heat conductivities at boreholes BUL1, STA2 and STA3, respectively

4.2.2 Inverse model

To improve the fit between simulated and measured temperature profiles, inverse computations have been performed using iTOUGH2. The inverse calculations aim to identify the optimal set of heat conductivity values that minimizes the differences between calculated and measured temperatures. The model involves 21 heat conductivity values to be estimated as shown in Tab. 4-4. To reduce the number of parameters to be estimated, heat conductivity values of formations BOTBC and TOPBC are excluded from the inverse procedure. Moreover, the heat conductivity of formation PERM is also excluded as no temperature data are available along this layer. In addition, it is assumed that the sets of formations (MUSCH and MAK), (GIPSK, KAL, KAU, KEUK, AL, and ML), and (HERRE/HERRW, AD, MM1, CM, MM2, and MALM) have each the same heat conductivity value. Therefore, in total there are six parameters to be estimated as shown in Tab. 4-5.

The key elements of an inverse modelling in iTOUGH2 are: (1) a simulation program to model flow and transport in the hydrogeologic system, here the thermal model (forward model), (2) the objective function which measures the misfit between the model output and the data, (3) the minimization algorithm which reduces the objective function by automatically updating parameter values, and (4) the error analysis which allows one to judge the quality of the estimates. The iTOUGH2 code estimates elements of a parameter vector (vector of heat conductivities of each formation) based on (temperature) observations by minimizing an objective function which is a function of the residual vector (here, the vector of squared differences between calculated and measured temperatures). The code offers a number of different minimization algorithms, the Levenberg-Marquardt modification of the Gauss-Newton algorithm is found to be a rather general and robust procedure for iteratively updating the parameter vector. By default, iTOUGH2 uses the Levenberg-Marquardt minimization algorithm, which is a modification of the Gauss-Newton algorithm.

In this report, the default minimization algorithm is used. Several preliminary test cases have been carried out in order to efficiently obtain the optimal parameters set (the best estimate set). These preliminary tests aimed to properly select the numerical parameters used by the algorithm, mainly the number of optimization iterations, the relative error, and the parameter bandwidth intervals. The numerical parameters were set to their default values.

4.3 Discussion of the results

The heat conductivity values presented in Tab. 4-4 are used as initial guess for the inverse procedure. These values are also presented in Tab. 4-5 which shows also the lower and upper limits of heat conductivity of each formation. The low (resp. upper) limit of heat conductivity of each formation is assumed to be equal to the reference value minus 1.5 (resp. plus 1.5), except for the upper limit of parameter n° 1 (i.e. MUSCH and MAK) which is allowed to exceed the initial value by 2.5 W/m˚C as preliminary numerical experiments have shown that the estimated value of parameter n° 1 often reaches its upper limit. The lower and upper limits of heat conductivity for both scenarios, normal scenario with fixed temperature at the top and the alternative scenario of each formation are presented in Tab. 4-5. Tab. 4-5 shows the results of the inverse calculations (columns: best estimate). This best estimate set of heat conductivity values of the normal scenario is then used as input for a forward calculation in order to obtain the temperature prediction associated with the optimal set of heat conductivity values.

4.3.1 Calibrated temperature profiles at TBO boreholes

Fig. 4-7 shows the comparison between measured and simulated temperatures associated with the 3 boreholes BUL1, STA2 and STA3, respectively, using the best estimate heat conductivity values. The figure shows that the fitted set of heat conductivity significantly improved the results. Similar results (not shown here) were also obtained with the alternative scenario.

Tab. 4-5: Initial, best estimate, lower and upper limit values of heat conductivity

Parameter number	**Layer**	**Formation**	**Initial estimate heat conductivity** [W/m˚C]	**Best estimate heat conductivity** [W/m˚C]	**Best estimate head conductivity for alternative scenario** [W/m °C]	**Heat conductivity lower limit** [W/m˚C]	**Heat conductivity upper limit** [W/m˚C]
1	02 – 03	MUSCH MAK	4.021	6.52	6.263	2.521	6.521
2	04 – 09	GIPSK KAL KAU KEUK AL ML	2.143	2.03	1.98	0.643	3.643
3	10	OPA	1.55	1.43	1.4	0.05	3.05
4	11	DOGG	2.203	2.30	2.527	0.703	3.703
5	12 – 18	HERRE/ HERRW AD MM1 CM MM2 MALM	3.211	3.09	2.735	1.711	4.711
6	19	TERT	3.0	3.52	4.267	1.5	4.5

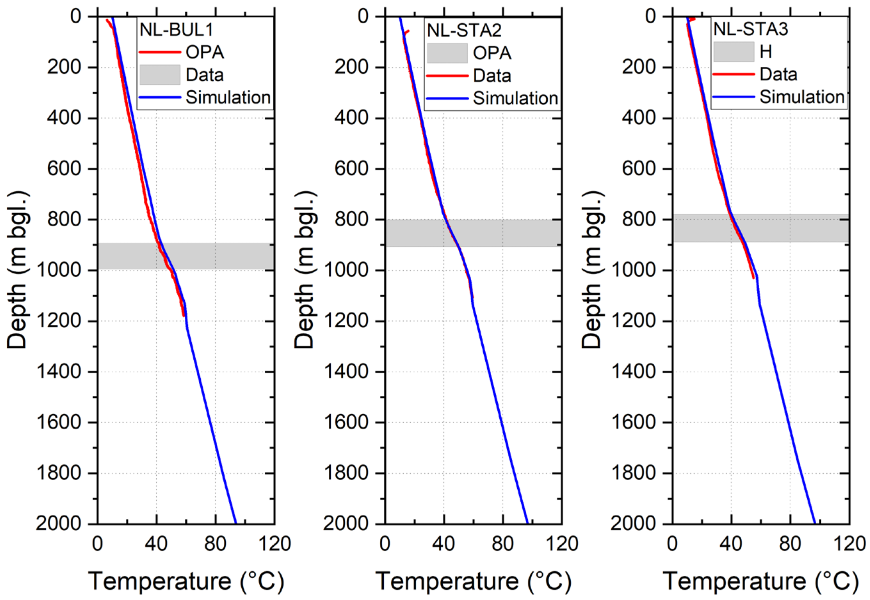

Fig. 4-7: Siting region NL: Comparison between measured temperatures and simulated temperatures using the best estimate heat conductivity values at boreholes BUL1, STA2 and STA3, respectively

4.3.2 Temperature profiles through the center of HLW and L/ILW repositories

The best estimate set of heat conductivities is used to compute the 1-D temperature evolution though the center of HLW and L/ILW as shown in Fig. 4-1. Fig. 4-8 depicts the simulated temperature profile at the center of each repository area along the vertical directions. The maximal temperature at the bottom of the model reaches about 105 °C for both areas, respectively. This corresponds to a thermal gradient of about 0.042 ºC/m.

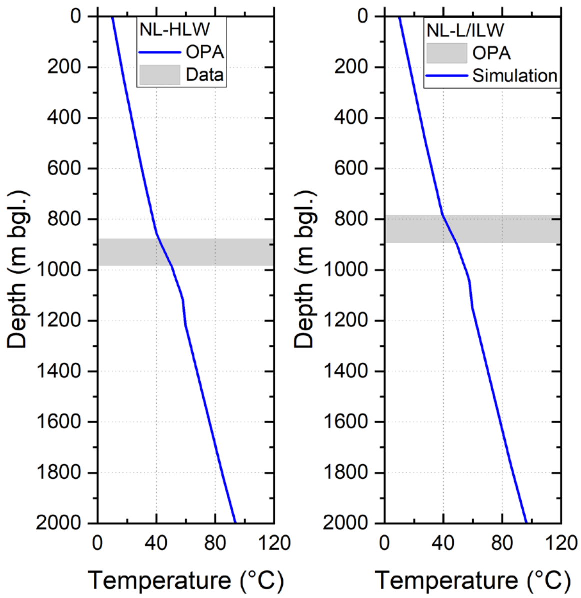

Fig. 4-8: Siting region NL: Temperatures profiles through the centers HLW and L/LW repositories along the vertical axis obtained using the best estimate set of heat conductivities

Depth - HLW (center of the HLW tunnel): -477 m asl / 925 m bg; depth - L/ILW (center of the L/ILW cavern): -403 m asl / 839 m bg.

4.3.3 Cross-sections of temperature distributions

Fig. 4-9 and Fig. 4-10 show cross-sections of temperature distributions spanning the NL local model in the south-north (SN) and west-east (WE) directions, respectively. The plots show isolines spanning parallel to the surface elevation, indicating that surface morphology affects the temperature distribution even in the deeper parts of the model (i.e., 850 m below ground surface in cross-section WE). Along the SN, temperatures in the Opalinus Clay vary from 42 °C to 52 °C depending on the formation depth. Along the WE cross-section, the Opalinus Clay dips gently eastward, resulting in formation temperatures ranging between 44 °C and 51 °C.

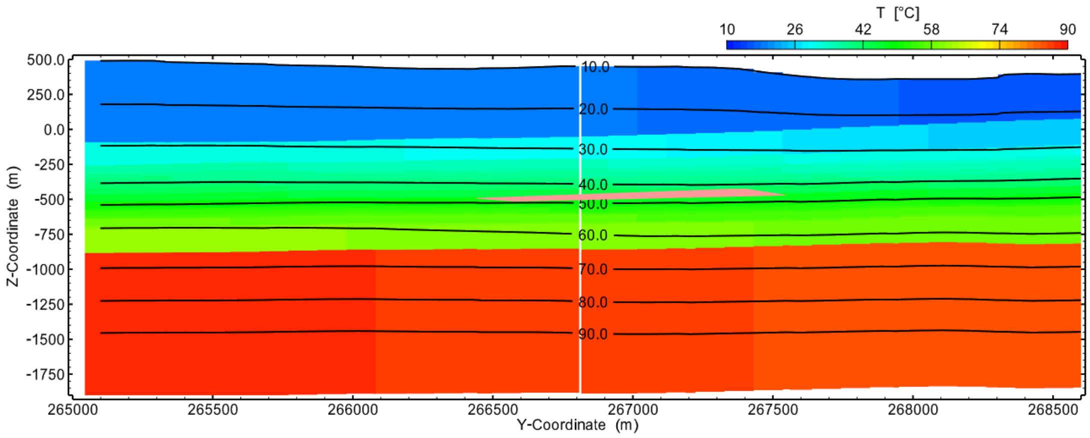

Fig. 4-9: Siting region NL: Cross-sectional temperature distribution in the South-North (SN) direction along X-Coordinate 679753 (Fig. 4-1)

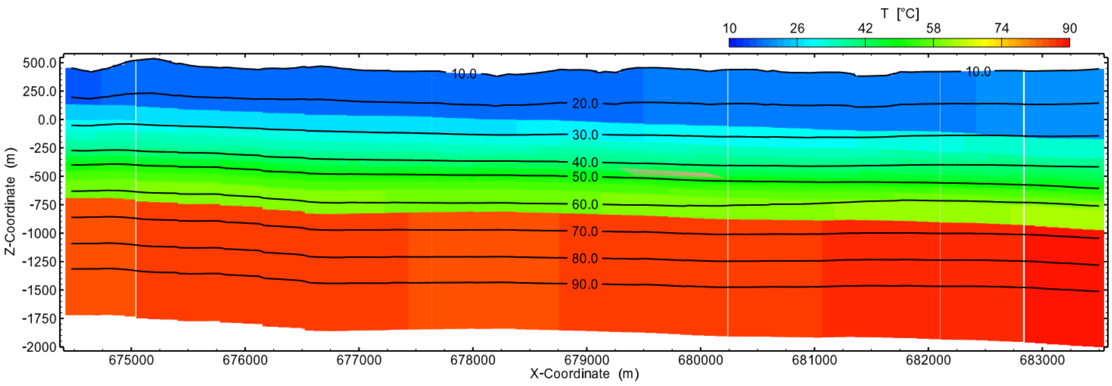

Fig. 4-10: Siting region NL: Cross-sectional temperature distribution in the West-East (WE) direction along Y-Coordinate 266945 (Fig. 4-1)

5 Thermo-hydraulic conditions in ZNO

The geological interpretations of 3-D seismics in the siting region ZNO are reported in Nagra (2024b), forming the basis for the geological layer model LocMOD-V1-ZNO. The decision has been taken to develop the site-specific repository projects ZNO-HLW and ZNO-L/ILW with reference to the geological layer stack, described in Nagra (2024b). Moreover, to ensure a consistent geometric representation of the site-specific repository projects in Performance Assessment (PA) and Safety Assessment (SA), all assessment models are referring to the same version of the geological layer model LocMOD-V1-ZNO.

A portfolio of numerical PA models was elaborated in the context of the site selection process for assessment of the proposed HLW and L/ILW repository configuration in the siting area JO comprising:

- a thermo-hydraulic 3-D model of the entire primary investigation perimeter on a footprint area of around 6 × 3 km^2
- 3-D repository nearfield models, containing the proposed HLW repository and the L/ILW repository on a footprint area of around 3 × 3 km^2
- several vertical cross sections through the disposal fields of repository projects for HLW and L/ILW in the siting region ZNO

This report addressed the temperature distribution in the Mesozoic layer stack at the scale of the primary investigation perimeter. Section 5.1 presents the model set-up, including model geometry, property assignment, initial conditions and boundary conditions. Model calibrations with the temperature profiles from the deep investigation boreholes BOZ1-1 and BOZ2-1 are described in Section 5.2. The results of the TH-calculations at site scale are discussed in Section 5.3, including an assessment of the impact of thermal history on the recent temperature distribution at site scale. Eventually, Section 5.4 gives a survey of the vertical temperature profiles at the center of the HLW and the L/ILW repository in the siting region ZNO.

5.1 3-D model of the siting region ZNO

5.1.1 Seismic surfaces

In total, 15 surfaces ("flying carpets") have been provided by Nagra for Zürich Nord-Ost (ZNO) for the modelling scope described in this report. These are summarized in Tab. 5-1.

Tab. 5-1: Seismic surfaces (2023Mod_ZNO_pointset_data_50x50) provided by Nagra for ZNO

<table>
<tr><th>Description</th><th>Filename</th><th>First row X[1]</th><th>First row Y[1]</th><th>First row Z[1]</th></tr>
<tr><td>Top Malm</td><td>LocMod2023_v1_50x50_ZNO_149.2_Kim_100_2023_06_30_cam</td><td rowspan="15">693113.59</td><td rowspan="15">275523.94</td><td>-24.79</td></tr>
<tr><td>Middle Malm</td><td>LocMod2023_v1_50x50_ZNO_149.2_Kim_700_2023_06_30_cam</td><td>-202.79</td></tr>
<tr><td>Bottom Malm</td><td>LocMod2023_v1_50x50_ZNO_154.8_Oxf_300_2023_06_30_cam</td><td>-266.05</td></tr>
<tr><td>Top Wutach Fm.</td><td>LocMod2023_v1_50x50_ZNO_154.8_Oxf_975_2023_06_30_cam</td><td>-280.42</td></tr>
<tr><td>Intra Humph.oolith Fm.</td><td>LocMod2023_v1_50x50_ZNO_168.2_Baj_200_2023_06_30_cam</td><td>-329.12</td></tr>
<tr><td>Top OPA</td><td>LocMod2023_v1_50x50_ZNO_170.9_Aal_300_2023_06_30_cam</td><td>-363.88</td></tr>
<tr><td>Top Lias</td><td>LocMod2023_v1_50x50_ZNO_174.7_Toa_100_2023_06_30_cam</td><td>-464.32</td></tr>
<tr><td>Top Frick Mb.</td><td>LocMod2023_v1_50x50_ZNO_192.9_Sin_100_2023_06_30_cam</td><td>-485.74</td></tr>
<tr><td>Top Beggingen Mb.</td><td>LocMod2023_v1_50x50_ZNO_192.9_Sin_200_2023_06_30_cam</td><td>-498.49</td></tr>
<tr><td>Top Seebi Mb.</td><td>LocMod2023_v1_50x50_ZNO_208.5_Nor_100_2023_06_30_cam</td><td>-537.35</td></tr>
<tr><td>Top Gansingen Mb.</td><td>LocMod2023_v1_50x50_ZNO_227_Car_100_2023_06_30_cam</td><td>-552.03</td></tr>
<tr><td>Top Bänkerjoch Fm.</td><td>LocMod2023_v1_50x50_ZNO_227_Car_300_2023_06_30_cam</td><td>-557.10</td></tr>
<tr><td>Intra Bänkerjoch Fm.</td><td>LocMod2023_v1_50x50_ZNO_237_Lad_200_2023_06_30_cam</td><td>-616.87</td></tr>
<tr><td>Top Muschelkalk</td><td>LocMod2023_v1_50x50_ZNO_237_Lad_400_2023_06_30_cam</td><td>-634.54</td></tr>
<tr><td>Bottom Mesozoikum</td><td>LocMod2023_v1_50x50_ZNO_251.9_Per_100_2023_06_30_cam</td><td>-819.17</td></tr>
<tr><td>Ground Level[2]</td><td>dhm25_zno.xyz</td><td>681312.50</td><td>284287.50</td><td>467.4990</td></tr>
</table>

1 Corresponds to the first line found in the ASCII file (may differ from the lowest X/Y/Z values).
2 Surface file communicated separately to the 2023Mod package.

5.1.2 Geometric model set-up (base model)

The 3D base model area comprises the whole stratigraphic surfaces provided by Nagra (Nagra 2024b), with boreholes BEN, TRU1, TRU2, TRU3, MAR1, and RHE1. In the horizontal direction, the model is discretized by 100x100 m elements as shown in Fig. 5-1. The 2D base models for HLW and I/ILW are placed in the center of the repositories (Fig. 5-1). The cross-section has a length of 2 km in each case. The center of each repository area is indicated in Fig. 5-2 (C_{HLW} is the location of the center of HLW repository, and $C_{L/ILW}$ is the location of the center of L/ILW repository).

In the vertical direction, the surfaces from the seismic interpretation were implemented into a stack of geological formations/facies as illustrated in Fig. 5-2 and shown in Tab. 5-2. In addition to the LocMod2023 surfaces, further formation units are included to extend the model in the vertical direction to avoid any boundary effects on the thermal-hydraulic processes. Tertiary/ Quaternary formation on top of Malm is added with a variable thickness which is defined by region between the two surfaces 149.2_Kim_100 and dhm25_zno. The model is extended into the deep earth by another formation layer of 8 m thick Buntsandstein and 1,000 m thick Crystalline basement.

The Opalinus Clay was split into upper and lower OPA by generating a surface at the 50% of the Opalinus Clay thickness calculated as the difference between:

- "LocMod2023_v1_50x50_ZNO_170.9_Aal_300[…]" and
- "LocMod2023_v1_50x50_ZNO_174.7_Toa_100[…]"

The surface in the middle of OPA is used to generate three additional layers in the middle of the Opalinus Clay. That is, the Opalinus Clay was divided into 5 sub-layers, with three layers of 1 m thickness implemented in the middle, with which the TH-values (i.e., the thermal conductivity) at repository horizon can be precisely obtained.

In the 3D base model, the Sandy-Argillaceous Dogger (SAD) and Sandy-Calcareous Dogger (SCD) of Passwang Formation above the Opalinus Clay are combined in only one layer. In contrast, three hard-bed layers (SAD-HB) with a thickness of 3 m each are modeled alternating with the Sandy-Argillaceous Dogger (DOGG) in the 2D base model, resulting in a total of 5 sub-layers.

Fig. 5-3 shows a cross-section of the 3D model through the proposed HLW repository. A 3D view of the entire model provides Fig. 5-4.

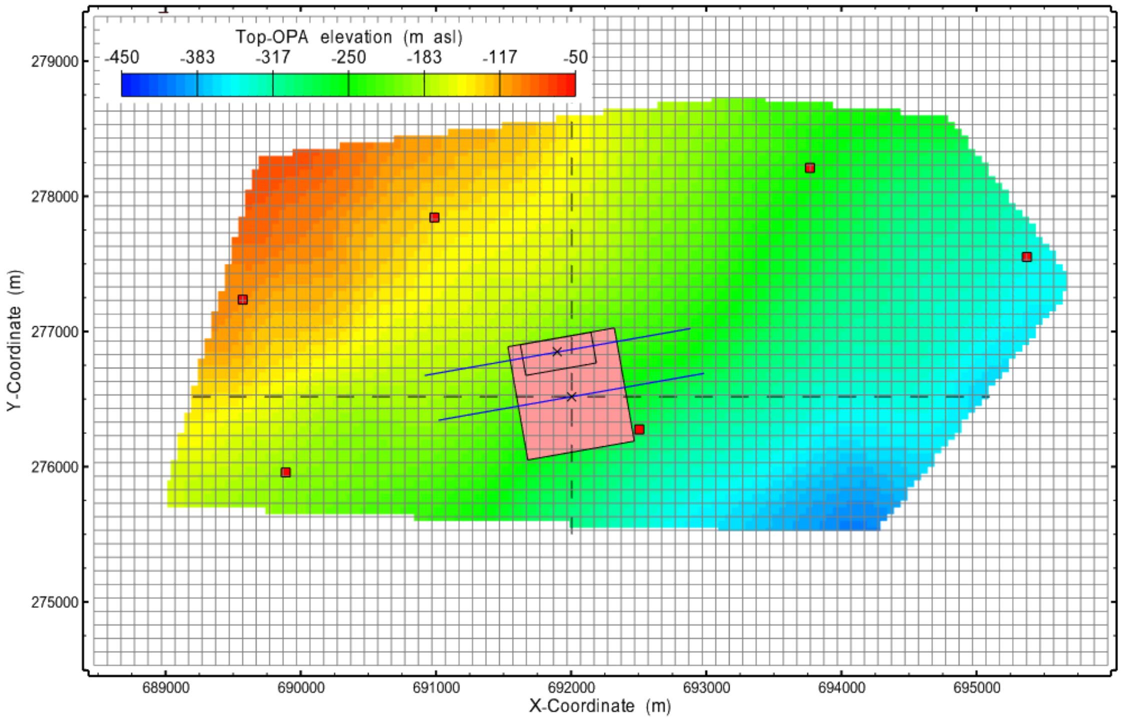

Fig. 5-1: Plan view of the 3D ZNO base model grid (regular 100 × 100 m grid)

With representation of the surface "LocMod2023_v1_50x50_ZNO_170.9_Aal_300[…]", the proposed HLW and L/ILW repository, and borehole locations BEN (690989, 277843), TRU1 (695372, 277551, 475 m), TRU2 (692505, 276276, 418 m), TRU3 (693767, 278210, 509 m), MAR1 (689889, 275957, 400 m), RHE1 (689571, 277235, 387 m), and cross-sections of the 2D base models (HLW and L/ILW). CHLW (692005, 276517, 430 m asl) and CLILW (691897, 276850, 417 m asl) indicate the centers of HLW and L/ILW repository areas.

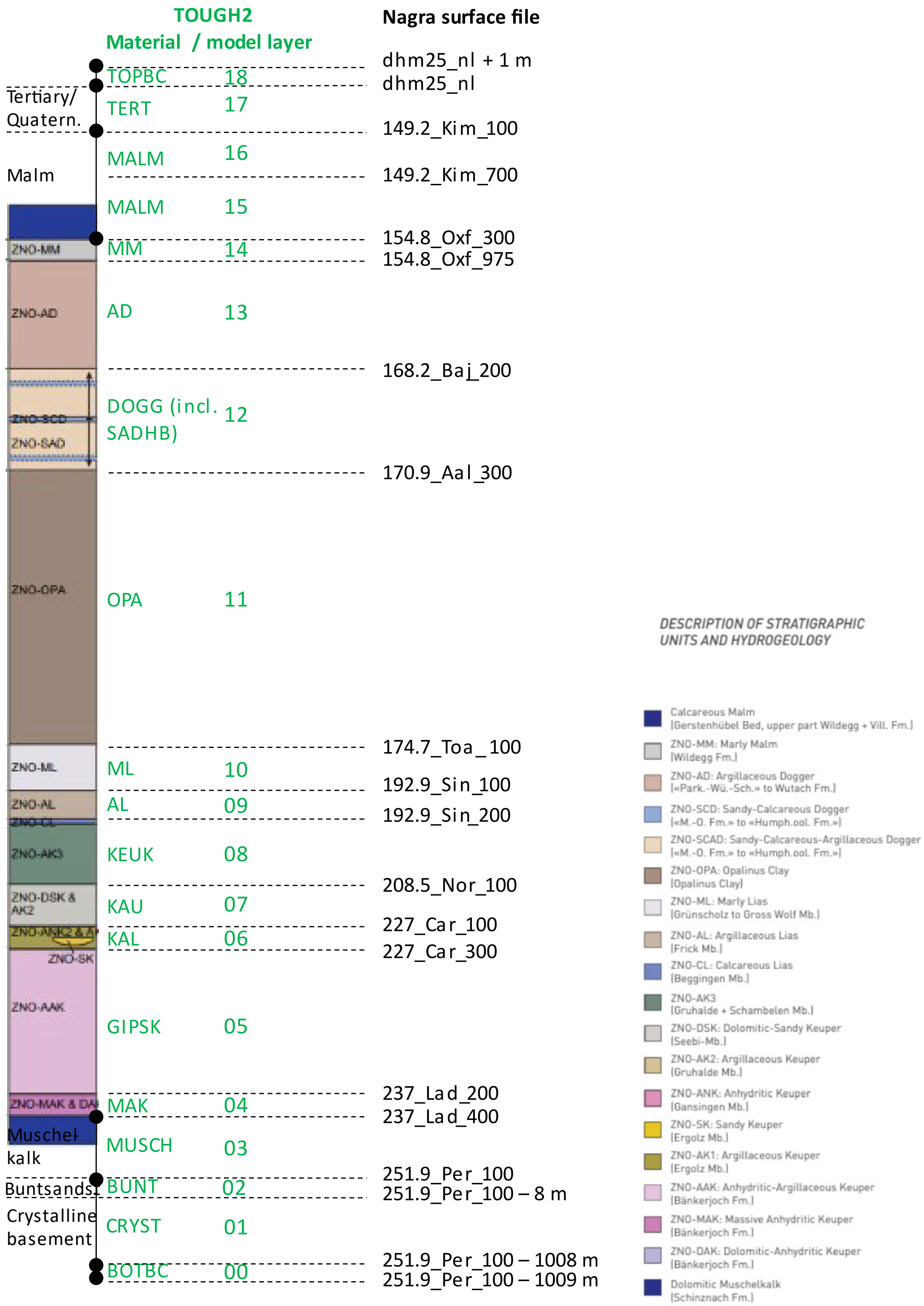

Fig. 5-2: Geological abstraction of stratigraphy for Zürich Nord-Ost

Modified from Nagra (2024b) and layers implemented in the numerical model.

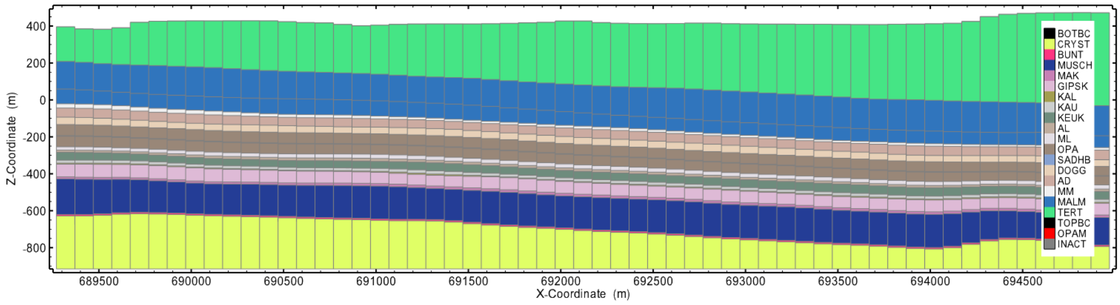

Fig. 5-3: Detail of a cross-section along the coordinate X passing through proposed ZNO repositoy at Y = 27,6517 m

Note: SADHB layers are not present in the 3D base model.

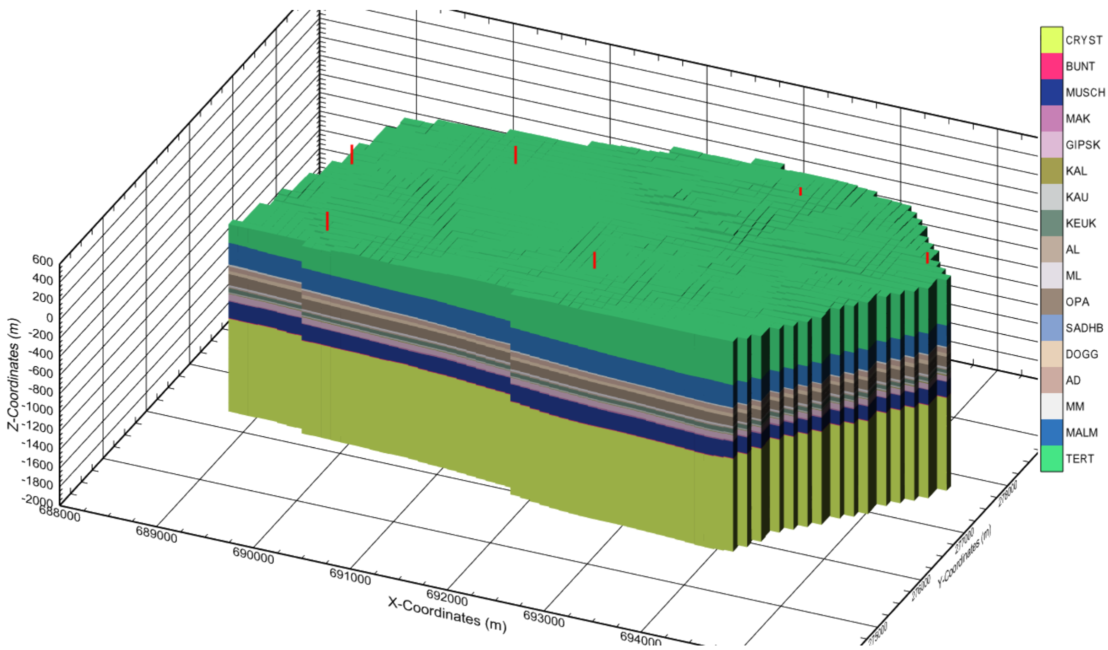

Fig. 5-4: 3D view of the ZNO base model grid. Borehole locations are shown for BEN, TRU1, TRU2, TRU3, MAR1, and RHE1

Tab. 5-2: Vertical distretization of the ZNO numerical model

Layer	Stratigraphic units / Formation	TOUGH2 Material name	Vertical discretization (layer)
00	Bottom Boundary	BOTBC	1
01	Crystaline basement	CRYST	1
02	Buntsandstein	BUNT	1
03	Muschelkalk	MUSCH	1
04	Dolomitic-Anhydritic Keuper (DAK) & Massive Anhydritic Keuper (MAK) of Bänkerjoch Formation	MAK	1
05	Anhydritic-Argillaceous Keuper (AAK) of Bänkerjoch Formation	GIPSK	1
06	Argillaceous Keuper (AK1) & Sandy Keuper (SK) & Anhydritic Keuper (ZNO-ANK) of Klettgau Formation	KAL	1
07	Argillaceous Keuper (ZNO-AK2) & Dolomitic-Sandy Keuper (ZNO-DSK) of Klettgau Formation	KAU	1
08	Argillaceous Keuper (ZNO-AK3) & Calcareous Lias (CL) of Staffegg Formation	KEUK	1
09	Argillaceous Lias (AL – Frick Member) of the Staffelegg Formation	AL	1
10	Marly Lias (ML) of the Staffelegg Formation	ML	1
11a, b	Opalinus Clay (OPA)	OPA	5 (2 for upper and bottom OPA, three 1-m middle layers)
11c		OPAM	
11d, e		OPA	
12	Sandy-Argillaceous Dogger (SAD) & Sandy-Calcareous Dogger (SCD) of Passwang Formation	DOGG	1
13	Argillaceous Dogger (AD)	AD	1
14	Marly Malm (ZNO-MM)	MM	1
15	Malm	MALM	2
16			
17	Tertiary (TERT) / Quartz (QUAT)	TERT	1
18	Top Boundary (TOP-BC)	TOPBC	1

5.1.3 Thermo-hydraulic model parameters, boundary, and initial conditions

The Opalinus Clay host rock and over- and underlying units are each represented as homogeneous layers with uniform (but possibly anisotropic) thermal-hydraulic properties. The property assignment is largely based on the new reference data sets from GDS-3.1. The relevant thermal and flow properties are described in the following. The parameter values are summarized in Tab. 5-3. The parameters of the formations, which consist of several lithostratigraphic units, are calculated as a weighted arithmetic mean for the horizontal permeability and porosity and as a weighted harmonic mean for the vertical permeability. The thickness of the borehole BEN is used for the weighting.

The sandy Keuper unit SK in the Ergholz Member is not included in the calculation of the mean value for the lower Keuper Aquifer KAL, as the proportion of this unit is not known. Instead, the parameters for SK are listed separately in the table, even if the unit does not exist as a separate unit in the base model.

The succession in the Dogger above the Opalinus Clay is not shown in the 3D base model due to the higher variability. Instead, the mean value for the Dogger unit is calculated under the assumption that three hard-beds (SCD unit) of 3 m thickness are present in the Sandy-Argillaceous Dogger SAD. For the more local 2D models, however, three hard-beds (SADHB) are modelled. Therefore, parameters for the SAD and SCD units and the weighted average are listed in the table.

The thermal parameters (mainly the heat conductivity and the specific heat) of each formation are summarized in Tab. 5-4.

The initial conditions essentially correspond to hydrostatic conditions (i.e., pressures are in hydrostatic conditions) and temperature for a geothermal gradient of 0.043 ºC/m. At the top boundary layer land-surface temperature is fixed to 10 ºC and pressures are set to constant atmosphere pressure. At the bottom boundary layer, no flow condition is assigned, and a constant heat flux of 100 mW/m^2 is assigned corresponding to the reference value of natural thermal flux from the earth (Senger et al. 2014). All lateral boundaries are assumed to be no-flow and adiabatic boundaries.

Tab. 5-3: Flow and transport properties assigned to the stack of geological formations

<table>
<tr><th>Formation / facies</th><th colspan="2">Equivalent lithostratigraphy GDS3.1</th><th colspan="2">$K_{x,y}$ [m²]</th><th colspan="2">K_z [m²]</th><th colspan="2">ϕ [-]</th></tr>
<tr><td>CRYST</td><td colspan="2">-</td><td colspan="4"></td><td colspan="2"></td></tr>
<tr><td>BUNT</td><td colspan="2">-</td><td colspan="4"></td><td colspan="2"></td></tr>
<tr><td>Dolomitic Muschelkalk (DM)</td><td colspan="2">DM</td><td colspan="4">4.54E-14</td><td colspan="2"></td></tr>
<tr><td>Anhydritic Keuper (MAK)</td><td colspan="2">MAK & DAK</td><td colspan="4">9.08E-21</td><td colspan="2">0.016</td></tr>
<tr><td>Anhydritic-Argillaceous Keuper (GIPSK)</td><td colspan="2">AAK</td><td colspan="4">9.08E-21</td><td colspan="2">0.087</td></tr>
<tr><td rowspan="2">Lower Keuper Aquifer (KAL)</td><td colspan="2">ZNO-ANK &AK1 &SK</td><td colspan="2">7.15E-20</td><td colspan="2">1.47E-20</td><td colspan="2">0.099</td></tr>
<tr><td colspan="2">SK[1]</td><td colspan="4">9.08E-15</td><td colspan="2">0.113</td></tr>
<tr><td>Upper Keuper Aquifer(KAU)</td><td colspan="2">ZNO-DSK&AK2</td><td colspan="2">5.51E-14</td><td colspan="2">4.61E-21</td><td colspan="2">0.117</td></tr>
<tr><td>Calcareous Lias, Argillaceous Keuper (KEUK)</td><td colspan="2">CL&AK3</td><td colspan="2">1.98E-20</td><td colspan="2">2.08E-21</td><td colspan="2">0.121</td></tr>
<tr><td>Argillaceous Lias (AL)</td><td colspan="2">AL</td><td colspan="2">9.08E-21</td><td colspan="2">1.82E-21</td><td colspan="2">0.107</td></tr>
<tr><td>Marly Lias ML</td><td colspan="2">ML</td><td colspan="4">4.54E-21</td><td colspan="2">0.080</td></tr>
<tr><td>Opalinus Clay (OPA)</td><td colspan="2">OPA</td><td colspan="2">4.54E-21</td><td colspan="2">9.08E-22</td><td colspan="2">0.110</td></tr>
<tr><td>Sandy-Argillaceous Dogger (DOGG)</td><td>SAD</td><td rowspan="2">SAD & SCD</td><td>9.08E-21</td><td rowspan="2">7.64E-21</td><td>1.82E-21</td><td rowspan="2">2.24E-21</td><td>0.089</td><td rowspan="2">0.078</td></tr>
<tr><td>Sandy-Calcareous Dogger (SAD-HB)</td><td>SCD</td><td>4.54E-21</td><td>4.54E-21</td><td>0.055</td></tr>
<tr><td>Argillaceous Dogger (AD)</td><td colspan="2">AD</td><td colspan="2">9.08E-21</td><td colspan="2">1.82E-21</td><td colspan="2">0.120</td></tr>
<tr><td>Marly Malm (MM)</td><td colspan="2">MM</td><td colspan="2">9.08E-20</td><td colspan="2">1.82E-20</td><td colspan="2">0.063</td></tr>
<tr><td>MALM</td><td colspan="2">CM (Malm aquifer)</td><td colspan="4">9.08E-17</td><td colspan="2"></td></tr>
<tr><td>TERT</td><td colspan="2">-</td><td colspan="4"></td><td colspan="2"></td></tr>
</table>

[1] Unit neglected in some models

Tab. 5-4: Reference values of heat conductivity and specific heat values assigned to the stack of geological formations for the ZNO model

Layer	**Formation**	**Heat conductivity** [W/m˚C]	**Specific heat** [J/kg ˚C]
00	BOTBC	2.58	995.0
01	CRYST	2.58	995.0
02	BUNT	2.58	995.0
03	MUSCH	4.021	905.5
04	MAK	4.021	905.5
05	GIPSK	2.143	995.0
06	KAL	2.143	995.0
07	KAU	2.143	995.0
08	KEUK	2.143	995.0
09	AL	2.143	995.0
10	ML	2.143	995.0
11	OPA	1.55	946.5
12	DOGG	2.203	995.0
13	AD	3.211	905.5
14	MM	3.211	905.5
15-16	MALM	3.211	905.5
17	TERT	3.0	995.0
18	TOPBC	3.0	995.0

5.2 Modelling workflow

The simulations of heat flow through the stack of geological formations presented in this section are performed using the EOS1 module of iTOUGH2 v7.1 (Finsterle et al. 2017). The modelling workflow is outlined in Section 5.3.1 and the inverse model is described in Section 5.3.2. The results from the numerical simulations are presented in Section 5.4.

5.2.1 Approach

The objective is to use temperature data in order to estimate the heat conductivity of each formation layer using an inverse modelling workflow. Note that there is no available data for boreholes for TRU2, TRU3, and RHE1, therefore only data for boreholes BEN, MAR1 and TRU1 are used (see Fig. 2-12).

The modelling workflow is set up with a forward simulation using the initial estimates of thermal conductivity presented in Tab. 5-4 to compare the simulated and measured temperature profiles at each borehole. The simulation is initiated with a linear temperature profile and runs for 1 Mio. years in order to obtain a temperature profile as close to steady-state as possible. Fig. 5-5 shows the temperature profiles associated with the three boreholes after 1 Mio. years. As can be observed the temperature profiles generated using the initial estimates of heat conductivities result in slightly different temperatures compared to the measured profiles.

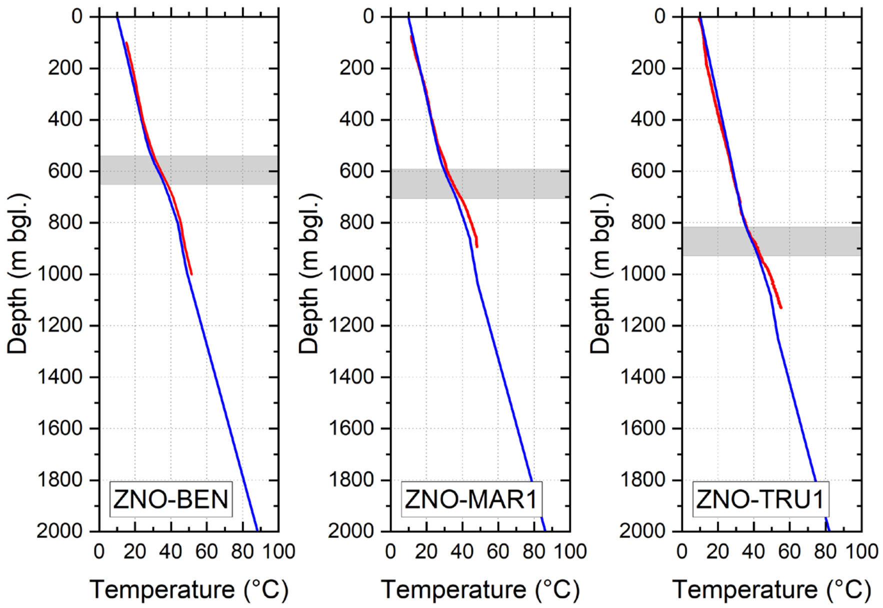

Fig. 5-5: Siting region ZNO: Comparison between measured temperatures and simulated temperatures at 1 Mio. years using the initial estimates for heat conductivities at boreholes BEN, MAR1 and TRU1, respectively

5.2.2 Inverse model

To improve the fit between simulated and measured temperature profiles, inverse computations have been performed using iTOUGH2. The inverse calculations aim to identify the optimal set of heat conductivity values that minimizes the differences between calculated and measured temperatures. The model involves 18 heat conductivity values to be estimated as shown in Tab. 5-4. To reduce the number of parameters to be estimated heat conductivity values of formations BOTBC and TOPBC are excluded from the inverse procedure. In addition, it is assumed that the sets of formations (CRYST and BUNT), (MUSCH and MAK), (GIPSK, KAL, KAU, KEUK, AL, and ML), (SADHB and DOGG) and (MALM, MM, and AD) have each the same heat conductivity value. Therefore, in total there are seven parameters to be estimated as shown in Tab. 5-5.

The key elements of an inverse modeling in iTOUGH2 are: (1) a simulation program to model flow and transport in the hydrogeologic system, here the thermal model (forward model), (2) the objective function which measures the misfit between the model output and the data, (3) the minimization algorithm which reduces the objective function by automatically updating parameter values, and (4) the error analysis which allows one to judge the quality of the estimates. The iTOUGH2 code estimates elements of a parameter vector (vector of heat conductivities of each formation) based on (temperature) observations by minimizing an objective function which is a function of the residual vector (here, the vector of squared differences between calculated and measured temperatures). The code offers a number of different minimization algorithms, the Levenberg-Marquardt modification of the Gauss-Newton algorithm is found to be a rather general and robust procedure for iteratively updating the parameter vector. By default, iTOUGH2 uses the Levenberg-Marquardt minimization algorithm, which is a modification of the Gauss-Newton algorithm.

In this report, the default minimization algorithm is used. Several preliminary test cases have been carried out in order to efficiently obtain the optimal parameters set (the best estimate set). These preliminary tests aimed to properly select the numerical parameters used by the algorithm, mainly the number of optimization iterations, the relative error, and the parameter bandwidth intervals. The numerical parameters were set to their default values.

5.3 Results

The heat conductivity values presented in Tab. 5-4 are used as initial guess for the inverse procedure. These values are also presented in Tab. 5-5 which shows also the lower and upper limits of heat conductivity of each formation. The low (resp. upper) limit of heat conductivity of each formation is assumed to be equal to the reference value minus 1.5 (resp. plus 1.5). The lower and upper limits of heat conductivity of each formation are presented in Tab. 5-5. Tab. 5-5 shows the results of the inverse calculations (column: best estimate). This best estimate set of heat conductivity values is then used as input for a forward calculation in order to obtain the temperature prediction associated with the optimal set of heat conductivity values.

5.3.1 Calibrated temperature profiles at TBO boreholes

Fig. 5-6 shows the comparison between measured and simulated temperatures associated with the 3 boreholes BUL1, STA2 and STA3, respectively, using the best estimate heat conductivity values. The figure shows that the fitted set of heat conductivity significantly improved the results.

Tab. 5-5: Initial, best estimate, lower and upper limit values of heat conductivity

Parameter number	**Layer**	**Formation**	**Initial estimate heat conductivity** [W/m˚C]	**Best estimate heat conductivity** [W/m˚C]	**Heat conductivity lower limit** [W/m˚C]	**Heat conductivity upper limit** [W/m˚C]
1	01-02	CRYST BUNT	2.58	3.32	1.08	4.08
2	03-04	MUSCH MAK	4.021	4.82	2.521	5.521
3	05-10	GIPSK KAL KAU KEUK AL ML	2.143	1.67	0.643	3.643
4	11	OPA	1.55	1.35	0.05	3.05
5	12	DOGG (incl. SADHB)	2.203	2.17	0.703	3.703
6	13-16	AD MM MALM	3.211	2.33	1.711	4.711
7	17	TERT	3.0	3.93	1.5	4.5

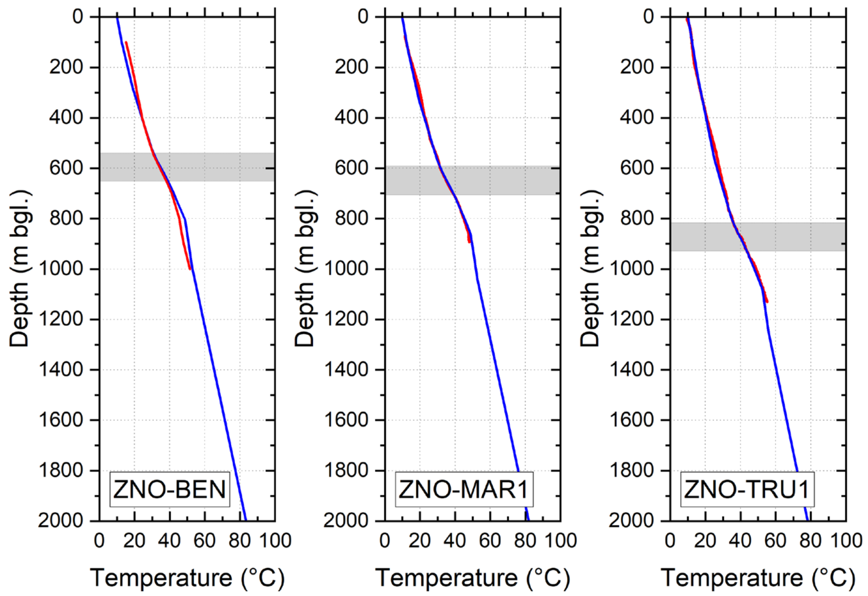

Fig. 5-6: Siting region ZNO: Comparison between measured temperatures and simulated temperatures using the best estimate heat conductivity values at boreholes BEN, MAR1 and TRU1, respectively

5.3.2 Temperature profiles through the center of HLW and L/ILW repositories

The best estimate set of heat conductivities is used to compute the 1-D temperature evolution though the center of HLW and L/ILW. Fig. 5-7 depicts the simulated temperature profile at the center of each repository area along the vertical directions. The maximal temperature at the bottom of the model reaches about 82 °C for both areas, respectively. This corresponds to a thermal gradient of about 0.036 ºC/m which is a bit different from the initial thermal gradient (i.e. 0.043 ºC/m). This is probably related to the value of basal heat flux which is for the ZNO model a bit lower than the values used for the other two models.

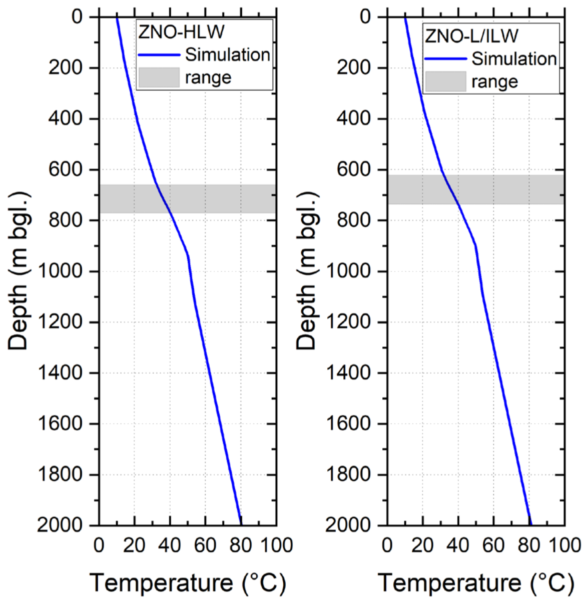

Fig. 5-7: Siting region ZNO: Temperatures profiles through the centers HLW and L/LW repositories along the vertical axis obtained using the best estimate set of heat conductivities.

Coordinates of the center of the repository, HLW (center of the HLW tunnel): 692005, 276517, -294 m asl / 724 m bg, L/ILW (center of the L/ILW cavern): 691897, 276850, -261 m asl / 678 m bg.

5.3.3 Cross-sections of temperature distributions

Fig. 5-8 and Fig. 5-9 show cross-sections of temperature distributions spanning the ZNO local model in the south-north (SN) and west-east (WE) directions, respectively. The plots show isolines spanning parallel to the surface elevation, indicating that surface morphology affects the temperature distribution even in the deeper parts of the model (i.e., 650 m below ground surface in cross-section WE). Along the SN, temperatures in the Opalinus Clay vary from 33 °C to 52 °C depending on the formation depth. Along the WE cross-section, the Opalinus Clay dips gently eastward, resulting in formation temperatures ranging between 39 °C and 40 °C.

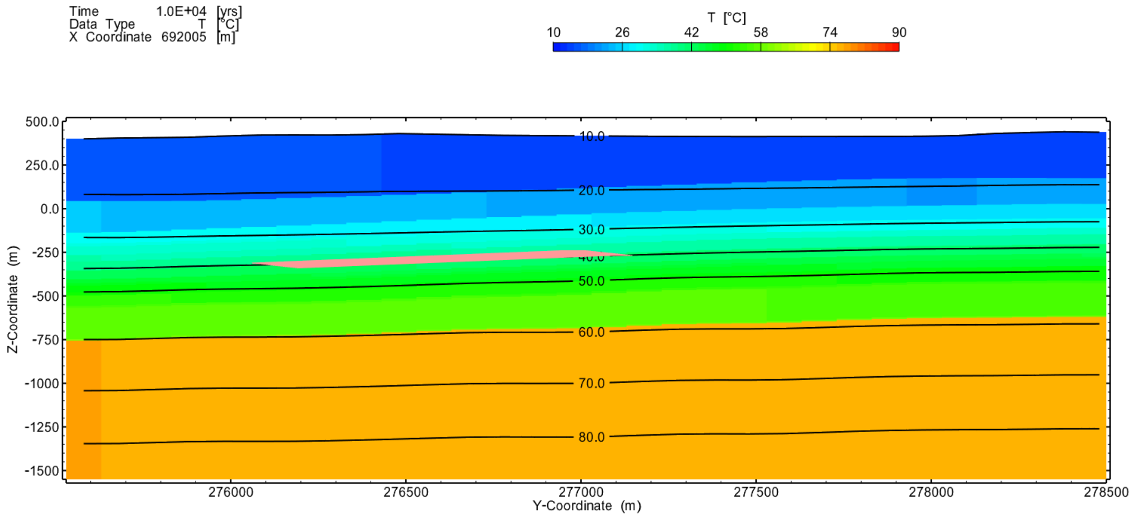

Fig. 5-8: Cross-sectional temperature distribution in the South-North (SN) direction

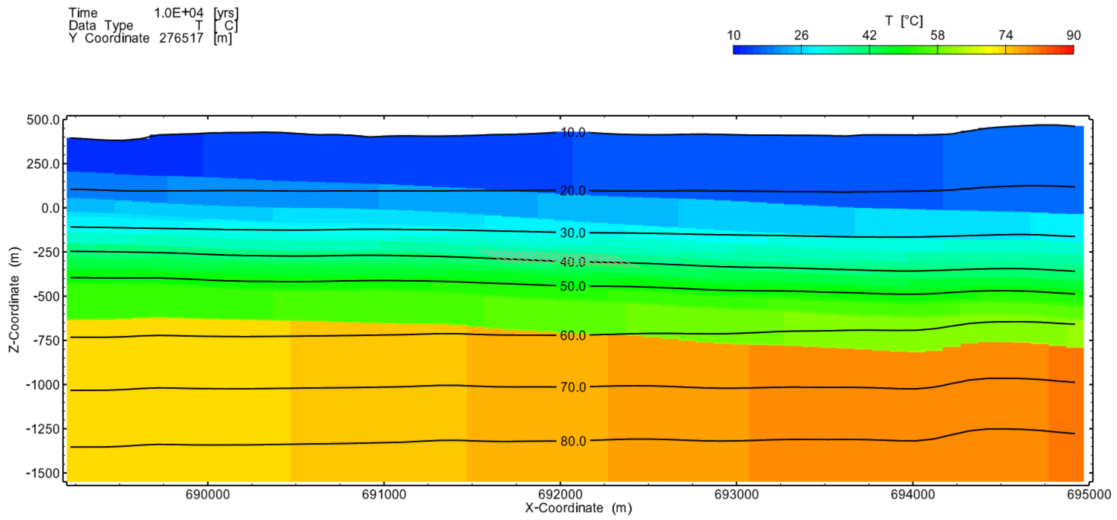

Fig. 5-9: Cross-sectional temperature distribution in the West-East (WE) direction

6 Summary and conclusions

The three candidate siting regions Jura Ost (JO), Nördlich Lägern (NL) and Zürich Nordost (ZNO) were assessed in the final Stage 3 of the Sectoral Plan for Deep Geological Repositories (SGT). The decision was taken to prepare the documents for licence application for a deep geological repository in NL. The thermal and hydraulic conditions in the three siting regions are forming an essential part of the geoscientific data base, which feeds into the site selection process. Furthermore, estimates of the undisturbed temperature distribution in the repository near-field are key input for PA/SA-related modelling for the safety case, setting the thermal initial conditions for the simulation of flow and transport processes in the vicinity of the deep geological repository for HLW and L/ILW in the siting region NL. Particularly, the modelled temperature data feed in the gas synthesis (Nagra 2024g), the consequence analysis (Nagra 2024i) and the model-based assessments for SV (Nagra 2024d) and License Application (Nagra 2024e).

A traceable workflow has been followed for the assessment of the thermal-hydraulic conditions in the candidate siting regions, comprising the compilation of available geothermal information at the regional scale, modelling of the thermo-hydraulic conditions at the repository sites and the derivation of the inputs required for the safety analyses.

7 References

BFE (2008): Sachplan Geologische Tiefenlager: Konzeptteil. BFE 2. April 2008 (Revision vom 30. November 2011). Departement für Umwelt, Verkehr, Energie und Kommunikation UVEK, Bern.

ENSI (2018): Präzisierungen der sicherheitstechnischen Vorgaben für Etappe 3 des Sachplans geologische Tiefenlager. Sachplan geologische Tiefenlager, Etappe 3. ENSI 33/649. Eidgenössisches Nuklearsicherheitsinspektorat ENSI, Brugg.

Finsterle, S., Commer, M., Edmiston, J.K., Jung, Y., Kowalsky, M.B., Pau, G., Wainwright, H.M. & Zhang, Y. (2017): iTOUGH2: A multiphysics simulation-optimization framework for analyzing subsurface systems. Computers & Geosciences 108, 8-20. DOI: 10.1016/j.cageo.2016.09.005.

Gutzeit, W., Seipold, U. & Freund, D. (1982): Eine Apparatur zur Messung der Wärmeleitfähigkeit von scheibenförmigen Gesteinsproben. Zeitschrift für angewandte Geologie 28, 92-95.

Kohl, T. (2010): Tiefe Geothermie Winterthur. BFE, Bern.

Leu, W., Mégel, T. & Schärli, U. (2006): Geothermische Eigenschaften der Schweizer Molasse (Tiefenbereich 0 – 500 m). Datenbank für Wärmeleitfähigkeit, spezifische Wärmekapazität, Gesteinsdichte und Porosität. Edited by Bundesamt für Energie (BFE).

Nagra (1989): Sondierbohrung Weiach Untersuchungsbericht: Textband + Beilagenband. Nagra Technischer Bericht NTB 88-08.

Nagra (1990): Sondierbohrung Riniken Untersuchungsbericht: Beilagenband. Nagra Technischer Bericht NTB 88-09 A & B.

Nagra (2001): Sondierbohrung Benken: Untersuchungsbericht: Textband + Beilagenband. Nagra Technischer Bericht NTB 00-01.

Nagra (2024a): Definition der Bewertungsobjekte für den sicherheitstechnischen Vergleich der Standorte in Etappe 3 des Sachplans geologische Tiefenlager. Nagra Arbeitsbericht NAB 24-01.

Nagra (2024b): Geological properties of the siting regions Jura Ost, Nördlich Lägern and Zürich Nordost for safety assessment. Nagra Arbeitsbericht NAB 24-10.

Nagra (2024c): Geosynthesis of Northern Switzerland. Nagra Technischer Bericht NTB 24-17.

Nagra (2024d): Model Supported Assessment of the Containment-Providing Rock Zone in Support of the Site Selection. Nagra Arbeitsbericht NAB 24-26.

Nagra (2024e): Model-Based Performance Assessment for a Combined Repository. Nagra Arbeitsbericht NAB 24-25.

Nagra (2024f): Post-closure safety report. Nagra Technical Report NTB 24-10.

Nagra (2024g): Production and Fate of Gases in a Combined Repository at NL. Nagra Technical Report NTB 24-23.

Nagra (2024h): Qualitative Bewertung für den sicherheitstechnischen Vergleich in Etappe 3 des Sachplans geologische Tiefenlager. Nagra Arbeitsbericht NAB 24-23.

Nagra (2024i): Radiological Consequence Analysis for a Deep Geological Repository in Northern Switzerland. Nagra Technical Report NTB 24-18.

Nagra (2024j): Synthesis of the Performance Assessment for a Combined Repository. Nagra Technical Report NTB 24-22.

Nagra (2025a): Rahmenbewilligungsgesuch für das geologische Tiefenlager – Begründung der Standortwahl. Nagra Technischer Bericht NTB 24-03.

Nagra (2025b): Rahmenbewilligungsgesuch für das geologische Tiefenlager – Sicherheitsbericht. Nagra Technischer Bericht NTB 24-01.

Papafotiou, A. & Senger, R.K. (2014): Thermo-hydraulic modelling of the temperature distribution in the siting region Jura Ost. Nagra Arbeitsbericht NAB 14-39.

Papafotiou, A., Senger, R.K. & Intera (2014): Thermo-hydraulic modelling of the temperature distribution in the siting region Nördlich Lägern. Nagra Arbeitsbericht NAB 13-56.

Schärli, U. & Kohl, T. (2002): Archivierung und Kompilation geothermischer Daten der Schweiz und angrenzender Gebiete. Geophysik 36, Beiträge zur Geologie der Schweiz: Geophysik. (36). Atelier d'impression, Université de Genève.

Schärli, U. & Rybach, L. (1991): Geothermische Detailkartierung der zentralen Nordschweiz (1:100'000). Geophysik 24, Beiträge zur Geologie der Schweiz: Geophysik. (24). Schweizerische Geophysikalische Kommission.

Schärli, U. & Rybach, L. (2001): Determination of specific heat capacity on rock fragments. Geothermics 30, 93-110.

Schill, E., Deckert, H., Geiermann, J., Koch, S., Pohl, C., Vierhuis, U., Baujard, C., Kohl, T., Ollinger, D., Schütze, C., Leven, C., Vienken, T., Eydam, D. & Munoz, G. (2011): EGS Technologie Entwicklung: Risikominimierung bei der Exploration 1.4.2008 – 31.10.2010. Wissenschaftlich technischer Schlussbericht. Institut für Geothermisches Ressourcenmanagement (IGEM), Bingen.

Seiphoori, A. (2022): Thermal conductivity, mineralogy, and pore size distribution of shallow and deep Opalinus Clay (Mont Terri / BCI, Bülach BUL1-1 and Trüllikon TRU1-1). Nagra Arbeitsbericht NAB 21-09.

Senger, R.K. & Papafotiou, A. (2013): Thermo-hydraulic modelling of the temperature distribution in the siting region Zürich Nordost and Südranden. Nagra Arbeitsbericht NAB 13-97.

Senger, R.K., Papafotiou, A. & Marschall, P. (2014): Thermo-hydraulic simulations of the near-field of a SF/HLW repository during early- and late-time post-closure period. Nagra Arbeitsbericht NAB 14-11.

App. A Measurement of thermal conductivity and specific heat capacity

Thermal conductivity is a fundamental property of materials that measures their ability to conduct heat. Rocks with high thermal conductivity, such as sandstones, efficiently transfer heat, whereas rocks with low thermal conductivities, like shales, are poor heat conductors and hence good insulators. The concept is described by Fourier's Law of heat conduction, which states that the heat flux through a material is proportional to the negative of the temperature gradient and the thermal conductivity of the material. At depth, where rocks are fully saturated, the pore fluid has a large influence on the thermal conductivity of rocks. Hence, porosity, and also permeability, have some control on thermal conductivity.

Thermal capacity, or heat capacity, is another essential physical property of matter that indicates the amount of heat required to change an object's temperature. It is an extensive property, meaning it depends on the system's size or mass. The SI unit for heat capacity is joule per kelvin (J/K). An intensive property related to this is the specific heat capacity, which is the heat capacity per unit mass of a material. It allows for the comparison of the heat-absorbing capacity of different materials irrespective of their mass.

Recently, thermal measurements on rock samples from the wells Trüllikon-1 (TRU1), Stadel-3-1 (STA3), and Bözberg-1-1 (BOZ1) were performed. A total of 90 rock samples, including 70 core samples and 20 cuttings, were selected from the three wells. The sampled formations include the Molasse layers, the entire Mesozoic from Malm to Buntsandstein, and the uppermost portions of the crystalline or Permian rocks. In total, 63% of the drilling length was cored, with 57% cored in TRU1, 65% in STA3, and 75% in BOZ1. Cuttings were taken only in the Molasse, as well as in the TRU1 drilling from 1,160 to 1,310m (from Muschelkalk to crystalline) because no cores were available. In addition, measurements from the earlier boreholes Benken (Nagra 2001), Riniken (Nagra 1990) and Weiach (Nagra 1989) are also available. Measurements in Benken were restricted to the Opalinus Clay while measurements in Riniken were only performed on samples from the permo-carboniferous trough. Samples in Weiach cover the whole stratigraphic sequence, including samples of the permo-carboniferous trough and the lowermost crystalline.

Core samples were cut into halves measuring 15 to 25 cm in length, with the cut surfaces finely ground and saturated in water under vacuum before measurements. Samples containing clay could only be kept in water until their disintegration began. Cuttings were washed, dried, and crushed in a stone crusher. A grain fraction of 0.25 – 0.2 mm was separated and then measured.

Measurement of thermal conductivity

Measurements of the thermal conductivity in the Benken borehole were performed using the divided-bar method (see Gutzeit et al. 1982). Measurements from the other boreholes were either performed using the quick thermal conductivity meter (QTM, Weiach, Riniken) or the TK04 (STA, BOZ, TRU) (see Leu et al. 2006). Both, the QTM and TK04 method, use the same measurement principles but the TK04 is also capable of measuring cuttings and is an advancement of the QTM so it is described here in more detail. The TK04 apparatus employs a line source (heating wire) for thermal conductivity measurement via the unsteady-state method. The line source is positioned at the bottom of a plexiglass cylinder, which is pressed against the flat surface of the rock sample (drill core or drill cuttings-water mixture) submerged underwater and heated for approximately 80 seconds.

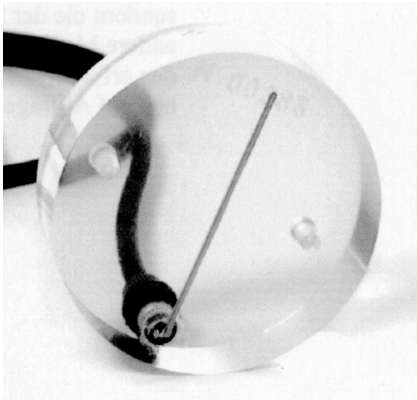 

Fig. A-1: Thermal properties of rocks, TK04 measuring device (right) with HLQ measuring probe (88 × 30 mm) with heating wire (70 × 2 mm) (left)

A thermistor measures the temperature at the surface of the rock. The heating typically results in a temperature increase of 2 to 4 Kelvin. This method places a line source at the boundary of two half-spaces: the rock sample and plexiglass. The majority of heat produced during the measurement is transferred to the rock due to the relatively low thermal conductivity of plexiglass compared to the rock. Evaluation of the measurement accounts for the probe's effect, considering that heat penetrates several millimeters into the rock. Multiple measurements are conducted at various points on the rock sample to capture any potential heterogeneity caused by different minerals with varying thermal conductivities. For samples without visible layering, the probe is placed parallel and perpendicular to the drill axis at each measurement point. For samples with visible layering, thermal conductivity can be anisotropic, with higher conductivity parallel to the bedding plane than perpendicular to it. The anisotropic thermal conductivity is defined as the ratio of conductivity parallel to the bedding plane to that perpendicular to it. To capture this anisotropy, the line source is first placed parallel, then perpendicular to the bedding lines on the flat rock surface.

For samples where only drill cuttings are available, thermal conductivity is determined on the cuttings using the same probe as for drill cores but on a two-phase mixture of drill cuttings and water. The prepared cuttings are poured into a Teflon measuring cylinder, saturated with water, and densities and weights of both phases are determined. The matrix density of the cuttings is determined by weighing the buoyancy in water. From the measured thermal conductivity of this mixture, the thermal conductivity of the rock matrix can be derived. The actual thermal conductivity of the subsurface can be determined from the matrix thermal conductivity and an estimation of the water content or effective porosity in situ.

Measurement of specific heat capacity

The process of measuring the specific heat capacity of rock samples involves a meticulous methodology based on the principle of mixing two substances, one with known (in this case water) and one with unknown heat capacity (the sample to be measured), with differing temperatures (e.g. Schärli & Rybach 1991). The approach assumes that the internal energy of both substances remains constant before and after mixing which allows the calculation of the specific heat capacity of the unknown substance. The measurement apparatus, a calorimeter, comprises of a small Dewar vessel equipped with a temperature sensor and a stirrer for efficient mixing (see Fig. A-2). Sample preparation involves drying samples in an oven before crushing and separating a specific grain fraction. For the measurement, approximately 150 g of sample material is placed into test tubes and submerged in an ice-water bath. After achieving near-zero temperatures, the samples are quickly poured into a water-filled measuring vessel. By measuring the equilibrium temperature of the mixture and taking into account that a small unknown amount of heat transfer occurs through the boundaries of the mixture system, the specific heat capacity of the unknown substance can be calculated.

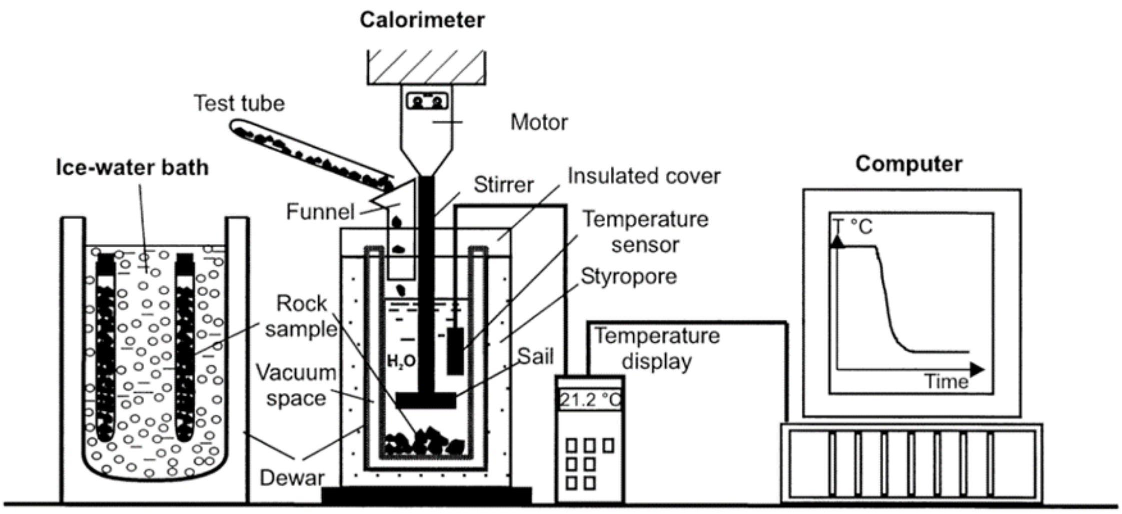

Fig. A-2: Sketch of a calorimeter

The samples are cooled to 0 °C in an ice bath and then placed into the water bath at room temperature level.

The stirrer ensures a homogeneous distribution of heat. The development of the temperature of the water bath over time is measured (from Schärli & Rybach 2001).

One notable challenge encountered during measurements involving clay-rich samples is the hydration effect, where dry clay hydrates in water, releasing heat. To mitigate this effect, measurements are conducted where the rock sample and water share the same temperature, allowing for the subtraction of temperature rise during mixing.

The measurements of both, the thermal conductivity as well as the specific heat capacity are listed in the following tables (Tab. A-1 to Tab. A-6).

Tab. A-1: Thermal conductivity and specific heat capacity of rock samples from borehole BOZ1

Geology			Thermal conductivity				spec. heat capacity
			isotropic	anisotropic		cuttings	
			λf	λsf	λpf	λm	cm
			W/m,K	W/m,K	W/m,K	W/m,K	J/g,K
OSM						2.2841	0.8527
						2.0591	0.7527
OMM						3.3408	0.7956
Malm	Villigen-Fm.					2.8453	0.8578
	Wildegg-Fm	Effinger-Mb.	1.9255				0.7689
			2.5627				0.7993
						1.7520	0.8764
Dogger	Klingnau-Fm.			1.4768	1.9860		0.8052
	Hauptrogenstein		2.2903				0.8684
	Passwang-Fm.	Humphriesi-Sch.	1.9478				0.7915
	Opalinuston			1.4327	2.4874		0.7566
				1.7279	2.4000		0.8648
				0.9072	2.4552		0.7519
Keuper	Klettgau-Fm.	Bruhalde-Mb.				1.4216	0.7019
	Bänkerjoch-Fm.			2.7137	3.0367		0.6145
				2.0398	3.4610		0.7333
Muschelkalk	Schinznach-Fm.	Stammberg-Mb.	3.9257				0.8707
		Leutschenberg+Kienberg-Mb.	3.2404				0.8432
	Zelglingen-Fm.	Dolomitzone	3.2120				0.8476
		Obere Silaftzone	4.9994				0.7393
		Untere Sulfatzone	5.1564				0.7135
	Kaiseraugst-Fm.	Wellenmergel		1.1003	2.4402		0.7837
Buntsandstein	Dinkelberg-Fm.		3.9672				0.7608
			4.2422				0.7569
Rotliegendes	Weitenau-Fm.		2.7502				0.7571
			2.8204				0.7692

Tab. A-2: Thermal conductivity and specific heat capacity of rock samples from borehole STA3

Geology			Thermal conductivity				spec. heat capacity
			isotropic	anisotropic		cuttings	
			λf	λsf	λpf	λm	cm
			W/m,K	W/m,K	W/m,K	W/m,K	J/g,K
USM	USMII					2.4871	0.7767
						2.1353	0.7964
						2.5654	0.7993
						2.4429	0.8100
	USMI					2.2326	0.8333
Malm	Felsenkalk/Massenkalk		2.8326				0.8225
			3.1988				0.7996
	Schwarzenbach-Fm.		2.2384				0.7860
	Villigen-Fm.		2.7580				0.7890
			2.5115				0.7965
			2.5382				0.8245
	Wildegg-Fm	Effinger-Mb.	1.9490				0.8426
				1.5688	1.8626		0.8540
Dogger	Herrenwis		2.5287				0.8333
	Wedelsandstein			1.2614	1.6238		0.8550
	Opalinuston			1.0206	2.5486		0.8666
				1.0280	2.4872		0.9212
				1.0348	2.3704		0.8615
Lias	Staffelegg-Fm.	Rietheim-Mb.		1.2440	2.0240		0.8713
		Schambelen-Mb.	2.3707				0.8327
Keuper	Klettgau-Fm.	Gruhalde-Mb.				1.7690	0.8315
	Bänkerjoch-Fm.		3.8028				0.7586
			2.4792				0.8264
			5.4574				0.7270
Muschelkalk	Schinznach-Fm.	Stammberg-Mb.	3.9544				0.8444
		Leutschenberg+Kienberg-Mb.	2.8609				0.8295
	Zelglingen-Fm.	Dolomitzone	3.8988				0.8355
		Obere Silaftzone	5.5242				0.7756
		Salzzone	6.0972				0.8980
	Kaiseraugst-Fm.	Wellenmergel		1.2988	2.3720		0.8645
Buntsandstein	Dinkelberg-Fm.		3.6020				0.7693
Rotliegendes	Weitenau-Fm.		2.1823				0.8052

Tab. A-3: Thermal conductivity and specific heat capacity of rock samples from borehole TRU1

Geology			Thermal conductivity				spec. heat capacity
			isotropic	anisotropic		cuttings	
			λf	λsf	λpf	λm	cm
			W/m,K	W/m,K	W/m,K	W/m,K	J/g,K
USM						2.1429	
						1.6571	0.8025
						2.1736	0.8060
						2.1178	0.8153
						1.7610	0.8147
							0.7831
Malm	Felsenkalk/Massenkalk		2.2500				0.8207
			2.8852				0.8176
	Schwarzenbach-Fm.		2.2455				0.8534
	Villigen-Fm.		2.7821				0.8485
			2.4339				0.8263
	Wildegg-Fm.	Effinger-Mb.	1.9523				0.8464
Dogger	Parkinsoni-Würtenbergica-Sch.		2.2864				0.8066
	Wedelsandstein		2.7976				0.8520
	Opalinuston			1.0805	2.3104		0.9157
				1.4683	2.4504		0.8355
				0.8925	2.2804		0.9559
Lias	Staffelegg-Fm.	Rietheim-Mb.	2.0851				0.8766
		Frick-Mb.		1.2926	2.5032		0.8772
Keuper	Klettgau-Fm.	Gruhalde-Mb.					0.8717
			1.7480				
			5.1549				0.7844
	Bänkerjoch-Fm.	Gansinger-Mb.	2.5667				
							0.7695
			4.5636				
Muschelkalk	Schinznach-Fm.		4.1231				0.8088
		Stamber-Mb.	3.3791				0.8616
	Zelglingen-Fm.	Leutschenberg+Kienberg Mb.				2.6388	0.8864
	Kaiseraugst-Fm.	Sulfatzone				1.4626	0.9016
Buntsandstein	Dinkelberg-Fm.	Wellenmergel				4.9587	0.8626
Rotliegendes	Weitenau-Fm.					2.2150	0.8468
						2.3215	0.8941
Kristallin						2.1955	0.8133
						1.6815	0.9637

Tab. A-4: Thermal conductivity and specific heat capacity of rock samples from borehole BEN

Geology		Thermal conductivity anisotropic		spec. heat capacity
		λsf	λpf	cm
		W/m,K	W/m,K	J/g,K
Dogger	Opalinus Clay	1.06	2.31	0.78
		1.47	2.45	0.72
		0.89	2.28	0.75
		1.02	2.55	0.79
		1.03	2.49	0.8
		1.03	2.37	0.77
		1.43	2.49	0.79
		1.73	2.4	0.76
		0.91	2.46	0.8
		1.79	2.23	0.79
		1.26	2.04	

Tab. A-5: Thermal conductivity and specific heat capacity of rock samples from borehole WEI

Geology		Thermal conductivity isotropic λf W/m,K	Thermal conductivity anisotropic λsf W/m,K	Thermal conductivity anisotropic λpf W/m,K	spec. heat capacity cm J/g,K
USM		2.83			775
		1.99			
		2.00			
		2.77			700
		2.00			
			1.68	2.71	783
		2.30			
		2.55			
		1.86			798
Malm	Massenkalke + Felsenkalke	3.30			
		2.62			
		3.46			
		3.56			
		2.61			
		2.29			
		2.61			
		2.78			
		2.62			
		2.34			
		2.83			
	Effingen Formation	2.55			
	Effingen Formation	1.75			
	Effingen Formation	2.12			
Dogger	Parkinsoni-Würt. Fm.	1.64			
		2.19			
		2.33			
		2.10			
		2.51			
		2.20			
	Murchisonae Oolith	2.80			
	Opalinus Clay	2.51			
Lias	Jurensis-Mergel	2.40			
			1.12	1.99	
Keuper	Arietenkalk	2.42			
	Trias, Keuper, Obere Bunte Mergel	2.76			
	Gipskeuper		2.94	4.79	
		3.81			
		4.88			
		4.59			
	Trias, Keuper, Lettenkohle	3.96			
	Trias, Keuper, Lettenkohle	4.83			
Muschelkalk	Trias, Muschelkalk, Oberer Muschelkalk, Trigonodusdolomit	3.58			
	Trias, Muschelkalk, Oberer Muschelkalk, Hauptmuschelkalk	2.54			
	Trias, Muschelkalk, Oberer Muschelkalk, Hauptmuschelkalk	3.46			
	Trias, Muschelkalk, Oberer Muschelkalk, Hauptmuschelkalk	3.31			
	Trias, Muschelkalk, Mittlerer Muschelkalk, Sulfatschichten	4.73			
	Trias, Muschelkalk, Mittlerer Muschelkalk, Sulfatschichten	4.11			
	Trias, Muschelkalk, Mittlerer Muschelkalk, Sulfatschichten		1.52	1.99	
	Trias, Muschelkalk, Unterer Muschelkalk, Wellendolomit	2.83			

Tab. A-5: Cont.

Geology		Thermal conductivity			spec. heat capacity
		isotropic	anisotropic		
		λf	λsf	λpf	cm
		W/m,K	W/m,K	W/m,K	J/g,K
Perm	Perm, Saxonien-Thuringien, Feinkörnige Rotschichten		1.31	2.35	
	Perm, Saxonien-Thuringien, Feinkörnige Rotschichten	2.66			
	Perm, Saxonien-Thuringien, Feinkörnige Rotschichten		1.31	2.35	
	Perm, Saxonien-Thuringien, Polymikte Kristallinbrekzien	3.39			
	Perm, Saxonien-Thuringien, Polymikte Kristallinbrekzien	3.22			
	Perm, Saxonien-Thuringien, Rotbraune zyklische Serie	2.72			
	Perm, Saxonien-Thuringien, Rotbraune zyklische Serie	2.92			
	Perm, Saxonien-Thuringien, Rotbraune zyklische Serie	2.71			
	Perm, Saxonien-Thuringien, Rotbraune zyklische Serie	3.33			
	Perm, Saxonien-Thuringien, Rotbraune zyklische Serie	4.11			
	Perm, Autunien, Graubraune bis grauschwarze zyklische Serie	2.88			
	Perm, Autunien, Graubraune bis grauschwarze zyklische Serie	2.89			
	Perm, Autunien, Graubraune bis grauschwarze zyklische Serie	2.68			
	Lacrustine Series	2.84			
		3.44			
		4.29			
		3.40			
		3.40			
		4.63			
	Perm, Autunien, Grobzyklische Grobsandstein-Ton-Serie	4.40			
	Perm, Autunien, Grobzyklische Grobsandstein-Ton-Serie	3.40			
	Perm, Autunien, Grobzyklische Grobsandstein-Ton-Serie	2.88			
	Perm, Autunien, Grobzyklische Grobsandstein-Ton-Serie	2.59			
	Perm, Autunien, Grobzyklische Grobsandstein-Ton-Serie	3.86			
	Perm, Autunien, Grobzyklische Grobsandstein-Ton-Serie	3.86			
Carbon	Coal Series	3.87			
		0.63			
		0.63			
		4.13			
		3.99			
		3.46			
		3.71			
		1.68			
		4.33			
	Karbon, Stephanien C+D, Mittlere kleinzyklische Sandstein-To	3.50			
	Karbon, Stephanien C+D, Mittlere kleinzyklische Sandstein-To	3.50			
	Karbon, Stephanien C+D, Mittlere kleinzyklische Sandstein-To	2.96			
	Karbon, Stephanien C+D, Mittlere kleinzyklische Sandstein-To	3.65			
	Karbon, Stephanien A+B, Feinkonglomerat. Grobsandstein-Se	4.63			
	Karbon, Stephanien A+B, Feinkonglomerat. Grobsandstein-Se	3.73			
	Karbon, Stephanien A+B, Feinkonglomerat. Grobsandstein-Se	3.27			
	Karbon, Stephanien A+B, Feinkonglomerat. Grobsandstein-Se	4.28			
	Karbon, Stephanien A+B, Feinkonglomerat. Grobsandstein-Serie		1.76	2.67	
	Karbon, Stephanien A+B, Feinkonglomerat. Grobsandstein-Se	3.86			
	Karbon, Stephanien A+B, Feinkonglomerat. Grobsandstein-Serie		1.56	2.67	
	Karbon, Stephanien A+B, Untere kleinzyklische Sandstein- Serie		1.37	2.29	

Tab. A-5: Cont.

Geology			Thermal conductivity			spec. heat capacity
			isotropic	anisotropic		
			λf	λsf	λpf	cm
			W/m,K	W/m,K	W/m,K	J/g,K
Crystalline			2.25			
				2.30	2.55	
			2.33			
			2.64			
			2.42			
			3.50			
			2.60			
				2.13	2.67	
			3.29			
			3.10			
			2.70			
			2.40			
			2.37			
			2.57			
				2.80	2.60	
			2.78			
			2.34			
			2.25			
				2.13	3.30	
			2.53			
			3.11			
			3.27			
			3.22			
			2.90			
				2.60	2.56	
				2.31	3.60	
			2.75			
			2.10			
				2.19	3.28	
			2.76			

Tab. A-6: Thermal conductivity of rock samples from borehole RIN

Geology		Thermal conductivity isotropic λf W/m,K
Perm	Rotliegendes	3.21
		3.52
		2.96
		2.62
		2.78
		3.90
		3.27
		3.25
		3.11
		3.90

App. B Thermo-hydraulic conditions in the repository nearfield (Deep Geological Repository NL)

B.1 Background and motivation

The deep geological repository model in NL is used to determine the thermal evolution of regional aquifers. The focus here is on the heating of the Malm layer located ca. 200 m above the repository. To quantify the heating of the Malm, a model with the full repository and the entire stack of geological layers is needed. The following sections provide an overview of the combined repository model setup and quantify the heating of the Malm during the post-closure phase.

B.2 Model set-up

The numerical model presented here is a 3-D representation of the stack of geological formations in NL as described in Section 4.1.2. Additionally, the model includes the full repository according to the repository layout in NL. Fig. B-1 illustrates a 3-D representation of the repository model and the stack of geological formations.

The model is initialized over a period of 10 million years with an open top boundary (const. P = 0.1 MPa, const. T = 10 °C) and closed side and bottom boundaries. At the bottom boundary, a heat source is prescribed as described in Section 4.1.3. The initialization phase is followed by multiple operation phases, in which different tunnels are ventilated and emplaced, and a post-closure phase, in which the entire repository is backfilled. It can be referred to Nagra (2024g) for more details on the implementation of the different operational phases, initial and boundary conditions, description of the two-phase flow parameters used in the model, and additional considerations (e.g., porosity scaling).

The heat and gas rates start at the emplacement of the different tunnels. The heat rates per canister used in the high-level waste tunnels, which are relevant for the quantification of the heating of the Malm, are shown in Fig. B-2. The model assumes about 2,141 canisters in total (PWR, BWR and HLW).

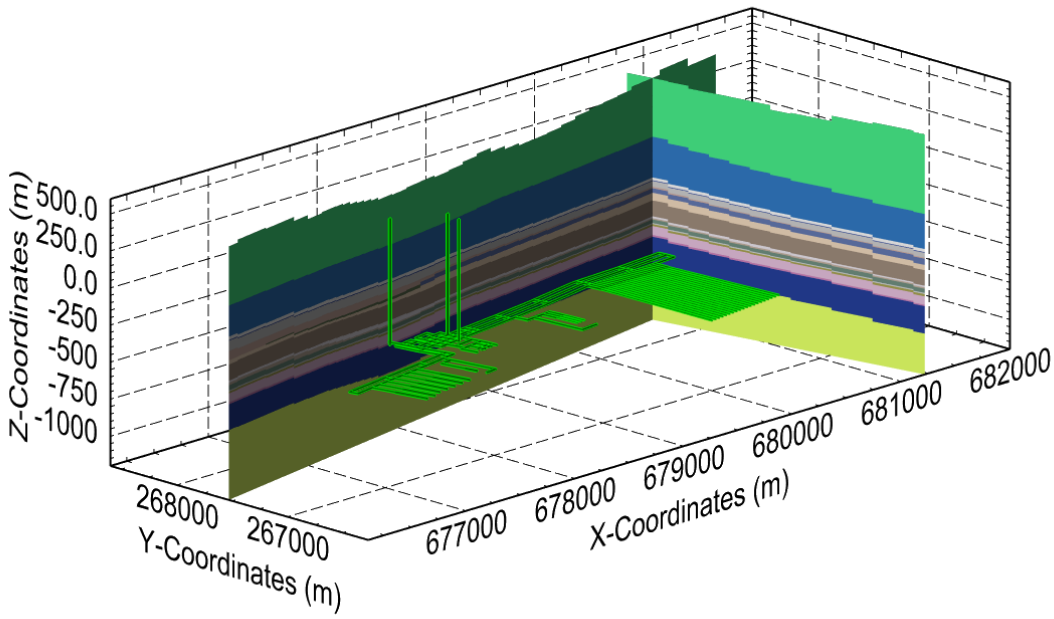

Fig. B-1: 3-D representation of the repository model and geological formations

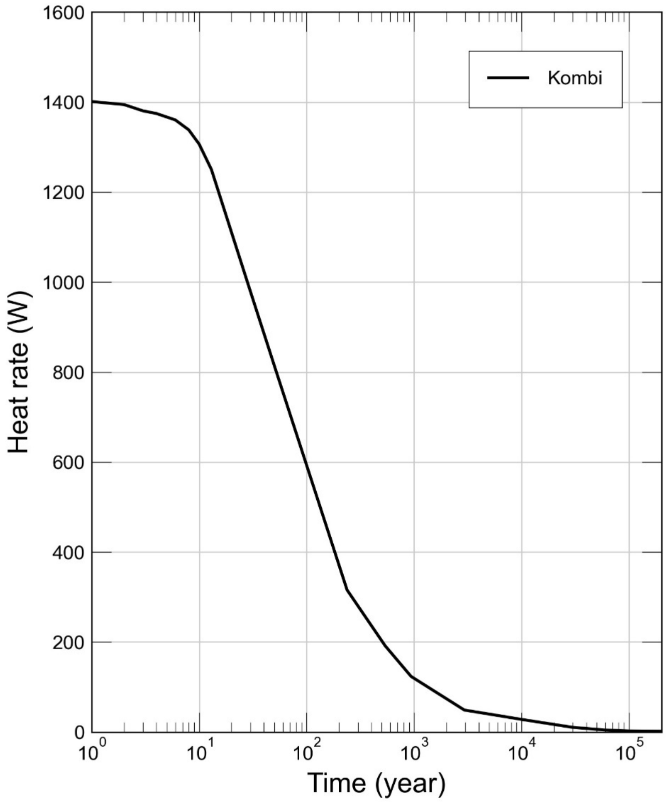

Fig. B-2: Heat rate per canister used for the repository model

B.3 Results

The temperature evolution is illustrated at the elevation of the lower Malm in Fig. B-3. The temperature is unaffected at 100 years (i.e., shortly after closure of the repository at 96 years). After 500 years, a temperature anomaly develops above the HLW repository, which gets more pronounced after 1,000 years and reaches a maximum after about 2000 years. The patch of increased temperatures has a size of about 1 km^2. At 5000 years, the temperature anomaly diminishes and has almost disappeared after 10'000 years. Figure B-4 shows the temperature on a vertical slice through the repository. The plot illustrates how the temperature pulse from the heat release in the HLW repository is conducted toward the confining layers and reaching the lower Malm at about 500 years. The temperature peak in the Malm is delayed compared to the peak reached in the repository because of the distance the heat pulse needs to travel. The temperature evolution with time in the lower, mid, and upper Malm is depicted in Fig. B-5. The peak is earliest and highest in the lower Malm (at ca. 2,000 years, ΔT = 9 °C). The peaks in the mid and upper Malm are delayed and lower in amplitude (ΔT = 6.5 °C and 4.5 °C, respectively).

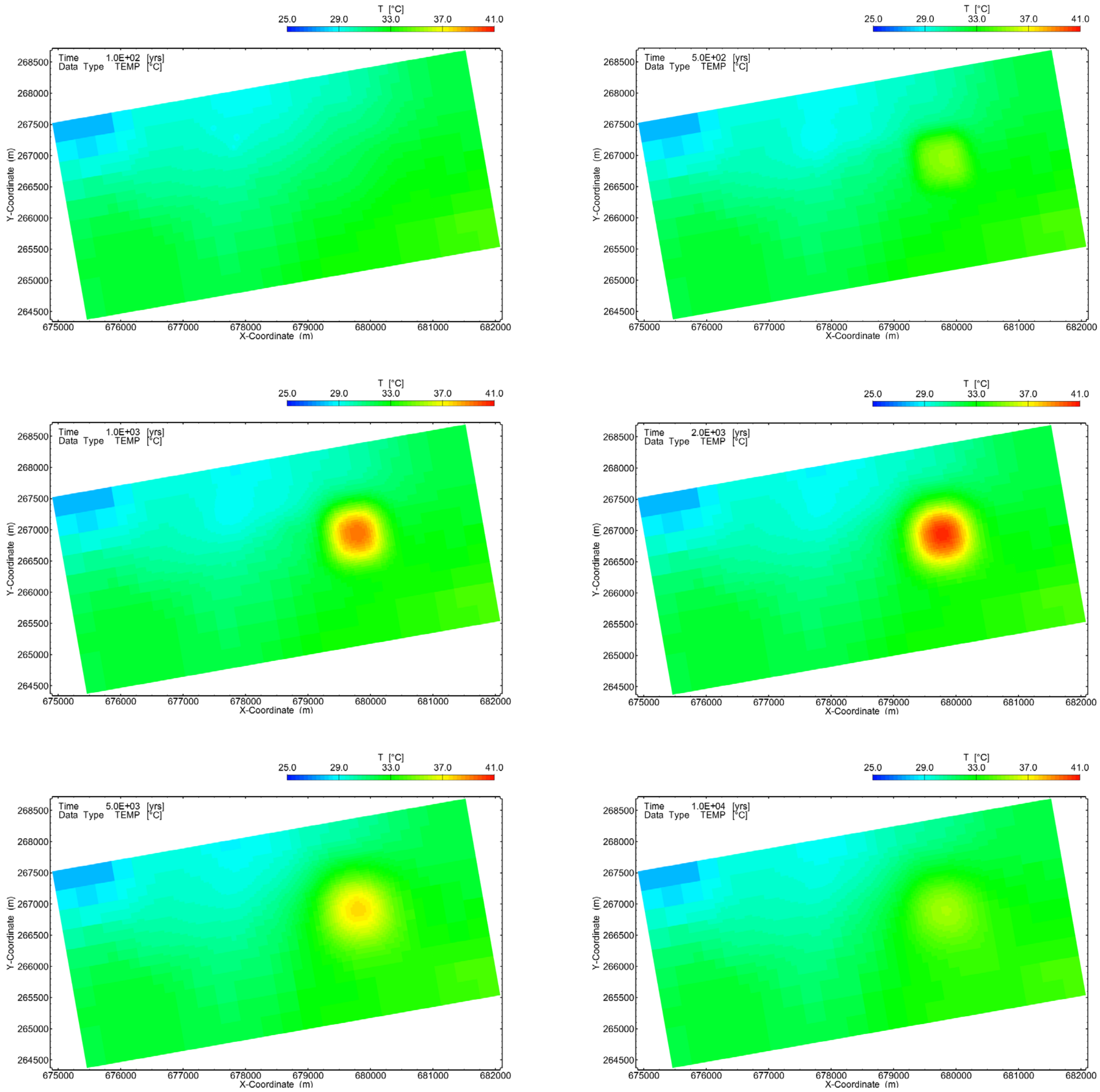

Fig. B-3: Spatial distribution of temperature at the elevation of the lower Malm after 100, 500, 1,000, 2,000, 5,000, and 10,000 years

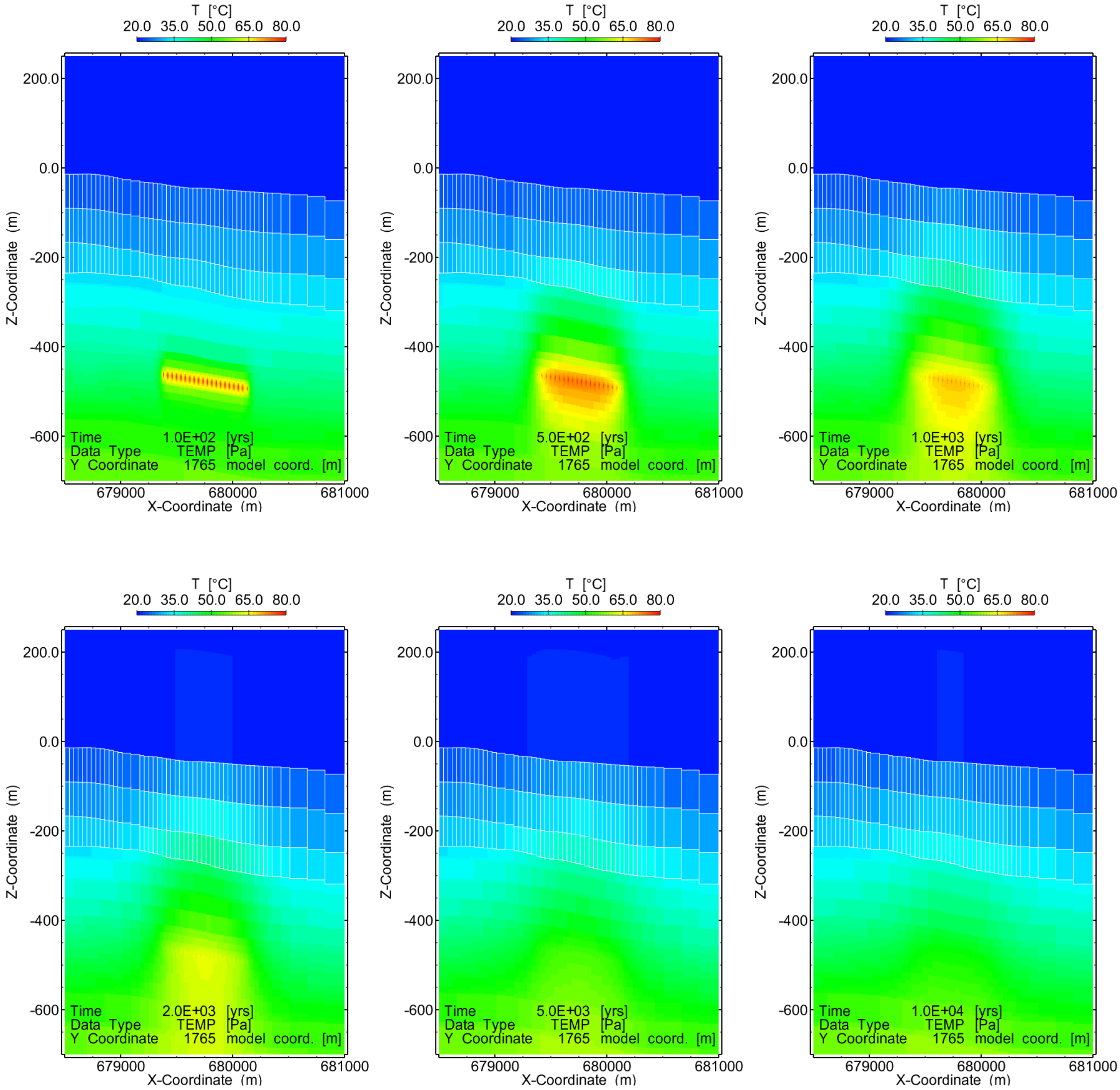

Fig. B-4: Spatial distribution of temperature at a slice through the HLW repository after 100, 500, 1,000, 2,000, 5,000, and 10’000 years

The Malm elements are highlighted in white.

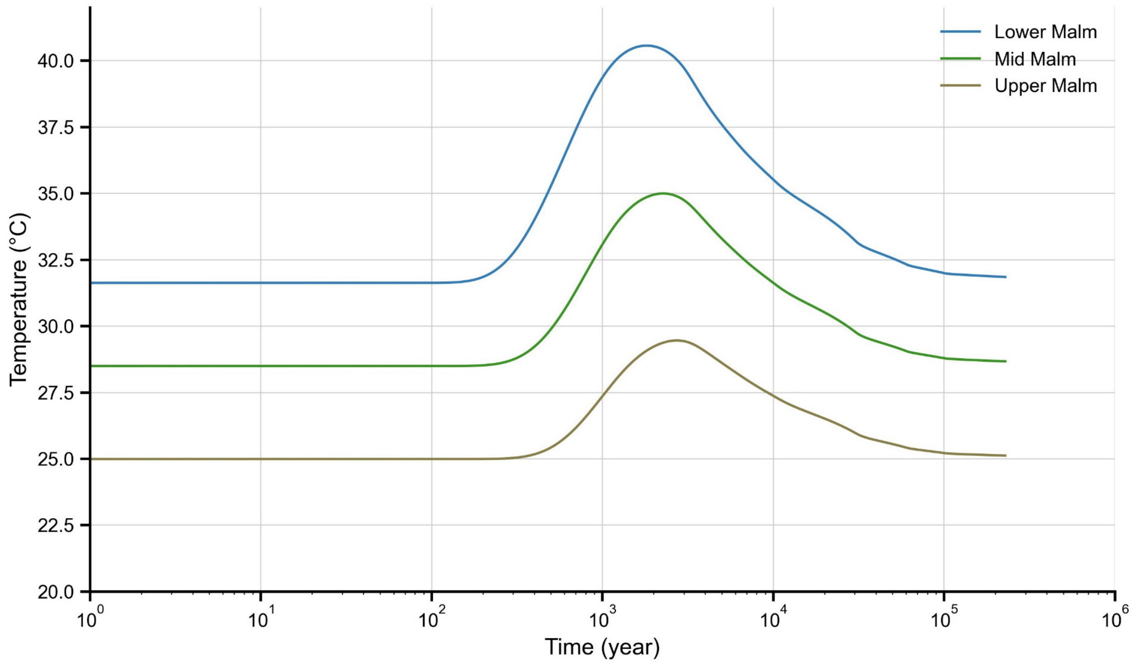

Fig. B-5: Temporal evolution of the temperature in the lower, mid and upper Malm